FUSION ENERGY HARNESSING, REACTOR TECHNOLOGY, AND SUSTAINABILITY

FLAVIO DOBRAN
GVES, New York, U.S.A

Abstract

The energy produced from the controlled thermonuclear fusion of hydrogen isotopes can replace fossil fuels and become a sustainable energy source. The fusion of deuterium and tritium has been achieved in several experimental reactors where the plasmas are confined with magnetic fields and there is high optimism that this will also be achieved with laser and ion beams. The plasma confinements and reactor

DOI: 10.1002/0471238961.0621190905121209.a01.pub2

technologies of tokamaks and stellarators are paving the way for building demonstration fusion reactors and subsequently commercial fusion power plants. Following a review of the magnetic and inertial plasma confinement concepts, the reactor technologies that implement these concepts are assessed for producing sustained plasma ignition, external plasma heating, control of plasma instabilities, developments of low-activation and high strength materials, coolants for removing fusion energy from the reactor, and breeding tritium in the blanket of the reactor for achieving fuel self-sufficiency. Sustainability of fusion energy requires the long-term availability of fusion fuels and reactor components materials, social acceptability, minimization of waste products, and safe operation of fusion power plants. These and other issues considered strongly suggest that the fusion energy will become a viable energy source for human development.

Keywords: fusion energy; fusion reactions; fusion reactor technology; magnetic confinement fusion; plasma confinement.

1. Introduction

The world's population is projected to increase from 7 billion people today to 9 billion people by the end of this century (1) and the current power demand of 12 TW is expected to double during the following decades (2). About 80% of the current energy needs are being supplied by fossil fuels (oil, gas, coal) and within 100 years this resource will be severely depleted. These energy sources currently emit some 40 $GtCO_2e$ per year of greenhouse gases into the atmosphere, warm the earth's climate system, melt glaciers and produce sea level rise, and have the potential to uproot hundreds of millions of people (3). Harvesting the required energy with solar thermal, wind, photovoltaic, and biomass energy conversion systems from the 10^5 TW of power delivered by the Sun to our planet would require the development of new energy supply technologies, overcoming security issues of energy production and distribution, and satisfying the social constraints posed by various cultures with different resources and aspirations.

The energy extracted with solar thermal, photovoltaic, wind, and biomass systems have power densities that are 10,000 times smaller than those of fossil fuels and more than 1,000,000 times smaller than those of nuclear energy systems and thus require large investments in infrastructures and constructions in some poorly secured locations to make them viable for producing the bulk of the energy needs of humanity (about 200 quads today). Harvesting of nuclear energy from the splitting of heavy nuclei (uranium, thorium, plutonium) in nuclear fission reactors can produce substantial amounts of base load power, but this energy source is also unsustainable and some products of reactions produce the publicly unacceptable long-lived (millions of years) radioactive products or spent nuclear fuel (4) that we have not yet been able to manage properly. The nuclear fission power generation can triple by 2050 and save the planet some 2 Gt of carbon emissions per year with the new Generation IV reactors that employ safer passive cooling systems (5), but even a thousand of such GW power producing reactors fall short from delivering the expected world's power need beyond 2050 and convincing the public that the accidents such as at Chernobyl and Fukushima can be avoided (6).

When the nuclei of atoms fuse or combine their total mass is reduced and this mass difference is transformed into the energies of the products of the reaction.

The amount of energy released through this process is huge as attested by the man's ability to relinquish this energy through thermonuclear bombs. In the interior of the Sun the protons of hydrogen fuse to produce helium and when the hydrogen is exhausted helium nuclei fuse to produce the next heavier element lithium and so forth. The conversion of just 0.1 g of hydrogen to energy every second is equivalent to the power of 10 TW and therefore here lies the great interest in exploiting this energy for humanity. Fusion energy can qualify as a *sustainable* energy source if it can provide most of the energy needs of the future, can be produced from natural resources that do not exceed the sustainable yield of these resources, be socially acceptable and affordable, and if its emissions do not produce environmental problems and cause public health concerns (7,8).

At the present we do not have an energy source technology that can substitute fossil fuels, but if developed the *controlled nuclear fusion* offers this possibility. Such a technology would not produce long-term radioactive waste, emissions causing global warming and health problems, and nuclear proliferation issues. There are, however, some technological problems that have to be solved before a reliable fusion power can be developed and some sustainability concerns regarding the availability of fusion materials that need to be addressed before the fusion energy can become a *sustainable* energy source.

The principles and methods for harnessing fusion energy are presented in Section 2. In the first generation fusion power reactors, fusion reactions are envisaged to be produced with magnetic and inertial plasma confinement systems. Magnetic confinement fusion employs magnetic fields to confine deuterium and tritium for a sufficient time and at high temperature to make these species interact, and the *breakeven condition* occurs when the energy supplied to achieve fusion is equal to the energy produced from fusion. Several experimental reactors have already achieved this condition. Inertial confinement fusion employs pulses of radiation, particle beams, or electric current to compress the fuel to initiate fusion reactions, but cannot yet claim the breakeven condition success, in spite of considerable investments by several governments to develop this technology to satisfy their nuclear stockpile stewardship programs. The fusion *ignition condition* is achieved when the nuclear fusion reactions become self-sustaining. Because this is more difficult to achieve than breakeven, different technologies are being developed for this purpose. The successes of research projects are crucial for building demonstration fusion reactors by the middle of this century, and if this is successful for transferring the knowledge base to the industry for building commercial fusion power plants during the second half of the twenty-first century (Section 3). Power producing fusion reactors will be technologically complex machines and in Section 4 we will address the sustainability issues of fusion in order to assess the prospects of fusion energy to become a viable energy source. We will conclude that although we do not yet possess all of the technologies for producing fusion power on a commercial scale that these technologies can be developed (and developed rapidly with adequate resources), before we run out of fossil fuels, produce irreparable damage to the environment, and place a significant burden on future generations.

2. Fusion Energy Harnessing

2.1. Fusion Reactions. Fusion of hydrogen in the Sun produces about 10^{26} W of power and for almost a century the scientists have strived to duplicate

this process on the Earth with a wide variety of different methods. The electrons in an atom are held together by the attractive *Coulomb force* between the negatively charged electrons surrounding the nucleus and positively charged protons in the nucleus, and energy is required to ionize or strip the electrons from the nucleus. Protons and neutrons in a nucleus are held together by the attractive short-range nuclear or *strong force* that overcomes the repulsive Coulomb force between the protons at the distances of the size of the nucleus ($1–10 \times 10^{-15}$ m). For fusion to occur, the reacting nuclei must have sufficient kinetic energies to come close to each other so that the attractive strong force can overcome the repulsive Coulomb force and produce a rearrangement of *nucleons* (protons and neutrons) in a *compound nucleus* with a low potential energy.

A nucleus ${}^{A}_{Z}\mathrm{M}$ (often abbreviated ${}^{A}\mathrm{M}$) is identified with its *mass number A* (number of protons and neutrons, or atomic weight rounded to the nearest whole number), *atomic number Z* (number of protons), and nuclear *rest mass M*. In addition, a nucleus is also characterized by its size, shape, binding energy, angular momentum, and (if it is unstable) *half-life*. The radius of a nucleus is much smaller than that of an atom (10^{-10} m) and the nuclei in some atoms are spherical while in others are stretched into deformed shapes.

Nuclear reactions change the elements or nuclides by altering the energy states of the nuclei. When a nuclide b is made to interact with another nuclide or subatomic particle a the product is usually another nuclide c and light particle d

$$a + b \rightarrow c + d, \tag{1}$$

where a and d may be photons, electrons, protons, neutrons, or other nuclides. Such a reaction requires that the *relativistic total energy E* (comprised of kinetic energy E_{KE} and rest mass energy Mc^2) of reactants is conserved, ie,

$$\sum_{a+b=r} Mc^2 - \sum_{c+d=p} Mc^2 = \sum_{c+d=p} E_{\mathrm{KE}} - \sum_{a+b=r} E_{\mathrm{KE}}, \tag{2}$$

where $c \sim 10^8$ m/s is the speed of light. Here, the subscripts r and p denote the reactants and products, respectively, of the nuclear reaction. The nuclear strong force holding the nucleons together is expressed in terms of the *binding energy B*, defined as

$$B = (Z\, m_{\mathrm{p}} + (A - Z)m_{\mathrm{n}} - M)c^2, \tag{3}$$

where m_{p} is the mass of the proton and m_{n} is the mass of the neutron. The binding energy is the energy required to dissociate a nucleus into its components protons and neutrons and is usually expressed in terms of the average energy per nucleon B/A. The binding energy of nuclei (Fig. 1) grow rapidly with A, reach a maximum around $A = 56$ (${}^{56}_{26}\mathrm{Fe}$) and then decreases slightly for heavier elements. The greater is the stability of a nucleus the greater is its binding energy or the smaller is its potential energy. The nuclei with low masses generally release energy and the nuclei with heavy masses require energy to achieve fusion. The heavy elements in nature are produced when massive stars undergo violent explosions or *supernova nucleosynthesis* where there is an abundance of energy.

The *Q value* of a nuclear reaction is defined as the difference between the rest mass energies of the reactants and the rest mass energies of the products of the reaction, and by equation 3 is equal to the difference between the binding energies

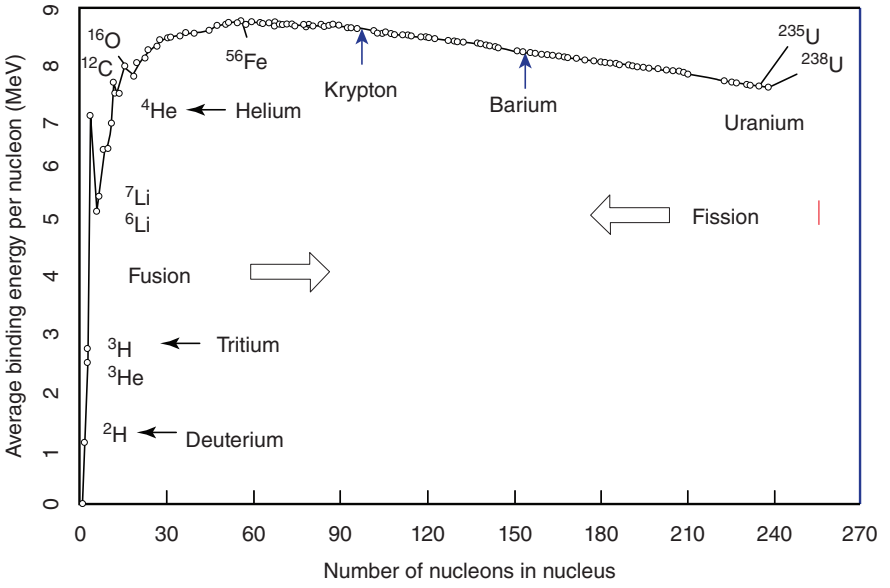

Fig. 1. Average binding energy per nucleon B/A vs the mass number A for the elements from hydrogen nucleus ($Z = 1$ and $B = 0$) to ^{238}U. (Adapted from Reference 9.)

of the products of the reaction and the binding energies of the reactants of the reaction, ie,

$$Q = \left(\sum_r M - \sum_p M\right)c^2 = \sum_p B - \sum_r B \tag{4}$$

where use was made of the conservation of nucleons A and charge Z in the reaction. Fusion reactions with low atomic mass numbers are exothermic ($Q > 0$) because the products have higher binding energies (nucleons are more tightly bound) than the reactants, or the products have a smaller mass than the reactants.

Hydrogen ${}^{A}_{Z}\mathrm{H}$ has several *isotopes* (same number of protons Z but different mass number A): ${}^{1}_{1}\mathrm{H}$ is the proton p, ${}^{2}_{1}\mathrm{H}$ (heavy hydrogen) is the *deuterium* D with one proton and one neutron, and ${}^{3}_{1}\mathrm{H}$ is the *tritium* T with one proton and two neutrons. The atoms of these isotopes have one electron to balance the charge of the one proton and thus their chemical properties are similar. The photons produced in nuclear reactions can be *γ-rays* and *X-rays*, and as an example are produced when neutrons interact with protons to produce deuterium, or when a neutron with the half-life of 12 min decays into a proton, an electron, and a neutrino. When D and T combine (Table 1), they produce an *α-particle* or helium nucleus ${}^{4}_{2}\mathrm{He}$ with a very large binding energy (Fig. 1) and one free neutron that carries most of the released energy in the form of kinetic energy. On Earth (as opposed to in the stars), we cannot convert ${}^{1}_{1}\mathrm{H}$ into energy without inexpensive proton accelerators and instead must employ deuterium and tritium at a sufficiently high temperature to make them react. The helium nucleus is a very stable and harmless byproduct. Deuterium occurs naturally in water as D_2O in one part for every 6400 parts of H_2O and is easy to separate it out (Section 4). Tritium does not occur naturally since it is an unstable isotope with the half-life of 12.3 years

Table 1. **Important Fusion Reactions and Their Q Values and Cross Sections σ at Different Center of Mass Kinetic Energies ε of Reacting Nuclei**

Reaction	Q (MeV)	σ ($\varepsilon = 10$ keV) (barn)	σ ($\varepsilon = 100$ keV) (barn)	σ_{max} (barn)	ε_{max} (keV)
Main fuels					
$D + T \rightarrow \alpha$ (3.5 MeV) + n (14.1 MeV)	17.6	2.72×10^{-2}	3.43	5.0	64
$D + D \rightarrow T$ (1.01 MeV) + p (3.03 MeV)	4.04	2.81×10^{-4}	3.3×10^{-2}	0.096	1250
$D + D \rightarrow {}^3He$ (0.82 MeV) + n (2.45 MeV)	3.27	2.78×10^{-4}	3.7×10^{-2}	0.11	1750
$T + T \rightarrow \alpha$ (1.26 MeV) + $2n$ (10.6 MeV)	11.3	7.9×10^{-4}	3.4×10^{-2}	0.16	1000
Advanced fuels					
$D + {}^3He \rightarrow \alpha$ (3.67 MeV) + p (14.67 MeV)	18.3	2.2×10^{-7}	1.0×10^{-1}	0.9	250
$p + {}^6Li \rightarrow \alpha$ (1.7 MeV) + ${}^3He$ (2.3 MeV)	4.0	6.0×10^{-10}	7.0×10^{-3}	0.22	1500
$p + {}^7Li \rightarrow 2\alpha$ (22.4 MeV)	17.3				
$p + {}^{11}B \rightarrow 3\alpha$ (8.68 MeV)	8.7	4.6×10^{-17}	3.0×10^{-4}	1.2	550
$p + p \rightarrow D + e^+ + \nu$	1.44	3.6×10^{-26}	4.4×10^{-25}		
$p + {}^{12}C \rightarrow {}^{13}N + \gamma$	1.94	1.9×10^{-26}	2.0×10^{-10}	1.0×10^{-4}	400

Source: Adapted from References 10,11.
1 barn = 10^{-28} m^2.
e^+ is the positron and ν is the neutrino. ε_{max} is the center of mass kinetic energy corresponding to σ_{max}.

and decays into ${}^3_2He$ by emitting a high energy electron and a neutrino (*β-decay*). Tritium must be therefore produced externally or internally of a fusion reactor and as we will see this presents some sustainability issues for the first-generation fusion power reactors operating with deuterium and tritium fuels. When two deuterons are used to produce fusion reactions the need for tritium disappears, but these reactions require very high kinetic energies of the reactants before undergoing fusion and are envisaged to be employed in subsequent generations of fusion power plants.

The unit of energy Joule, J, is too big to use for atoms and the more appropriate unit is the electron volt, eV, which is equal to 1.6×10^{-19} J. Molecules are typically held together with energies of 1 eV, the electron in an atom is bound to the nucleus with about 10 eV, a fusion reaction yields about 10 MeV, and a fission reaction produces typically 100 MeV. Mass can be written in *atomic mass units* (amu), which by the Einstein's mass-energy equivalence ($E = \Delta Mc^2$) can also be expressed in energy units. Thus, when a proton (1.00728 amu) and a neutron (1.00866 amu) combine to form deuterium (2.01355 amu), the missing mass of 0.00239 amu is equivalent to 2.225 MeV (931.5 MeV/amu) and is carried by the released γ-ray (photon). When, however, the heavier tritium is formed by adding a neutron to deuterium, the amount of released energy is 6.2504 MeV, and this process of binding energy per nucleon continues to grow as protons and neutrons are added to more massive nuclei until a maximum of about 8 MeV per nucleon is reached around $A = 60$ (Fig. 1). The balance between the repulsive Coulomb force between protons and the attractive strong nuclear force between nucleons sets the limit on how large a nucleus can grow.

There are many fusion reactions with $Q > 0$ and the important quantities that characterize these reactions are the fusion *cross section* σ and the *average reactivity*

$<\sigma v>$ of the reaction, where v is the relative speed between the interacting particles. The fusion cross section measures the probability of a pair of particles to fuse and can be expressed in terms of the center of mass kinetic energies of the particles. The averaged reactivity $<\sigma v>$ can then be computed by using the experimentally determined cross section σ and the distribution function *f(v)* of the species' relative velocity v. When the specie j is in thermal equilibrium with other species it has a *Maxwellian or Gaussian distribution* of velocities

$$f_j(v_j) = \left(\frac{m_j}{2\pi k_B T}\right)^{3/2} \exp\left(-\frac{m_j v_j^2}{2k_B T}\right), \tag{5}$$

where T is the temperature and k_B is the Boltzmann constant. This distribution function can be used to determine the mean kinetic energy of particles

$$E_{jav} = \frac{\int_{-\infty}^{\infty} \frac{1}{2} m_j v_j^2 f_j(v_j) \mathrm{d}v_j}{\int_{-\infty}^{\infty} f_j(v_j) \mathrm{d}v_j} = \frac{3}{2} k_B T \tag{6}$$

and since T and E are closely related it is customary in plasma physics to express the temperature in units of energy, where to $1\,\mathrm{eV} = k_B T$ corresponds the temperature of

$$T = \frac{1.6 \times 10^{-19}}{1.38 \times 10^{-23}} = 11,600\,\mathrm{K} \tag{7}$$

The Maxwellian distribution function can be used to determine the average reactivity $<\sigma v>$ of reacting species and Figure 2 illustrates both fusion cross section and reactivity of some important fusion fuels in thermal equilibrium. It

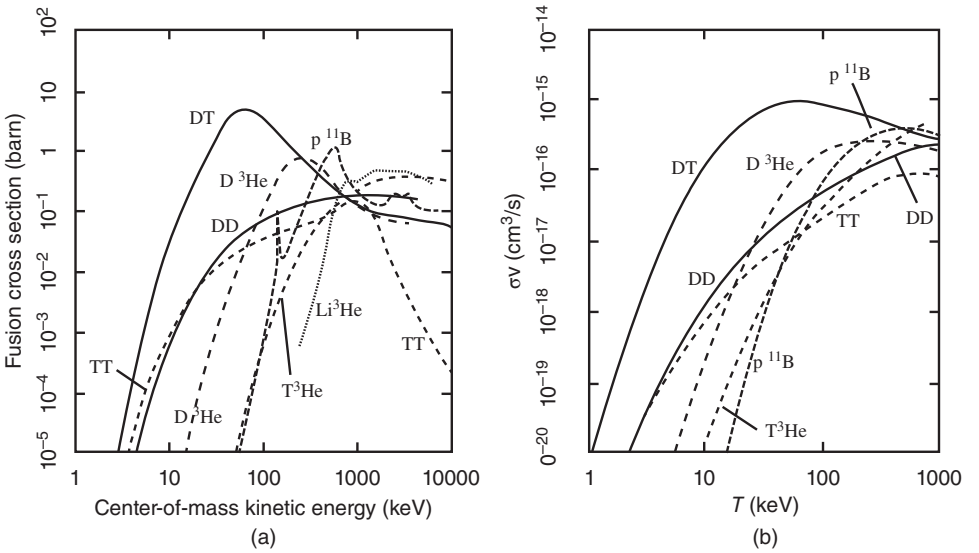

Fig. 2. (a) Fusion cross section as a function of the center of mass kinetic energy for reactions of interest to controlled fusion. The curve labeled DD accounts for the sum of the two branches of this reaction. (b) Reactivity of some fusion reactions vs the ion temperatures in keV. (Adapted from Reference 12.)

is readily apparent from these data that the reactivity of DT reaction is more than 100 times larger than that of other reactions at 50 keV. The second most probable reaction at energies below 25 keV is the DD reaction, whereas in the energy range 24–250 keV is D^3He. Above 250 keV, other reactions ($p^{11}B$, TT, T^3He) become of interest, but they are more difficult to achieve in a controlled manner. Table 1 summarizes the reaction characteristics of the main fusion fuels and some advanced fuels together with their Q values, cross sections at 10 and 100 keV, and the maximum cross sections and energies corresponding to these reactions.

The deuterium–tritium (DT) reaction has the maximum cross section of 5 barn and corresponds to the center of mass kinetic energy of about 64 keV or the ion temperature in excess of 700×10^6 K. To achieve fusion, it is not, however, necessary for particles to have this mean energy, because even at the mean kinetic energy of 10 keV (116×10^6 K) there is already a sufficient number of particles in the *tail* of the velocity distribution function with very large velocities and energies that can penetrate the Coulomb barrier and merge with the particles in the nuclei or produce many fusion reactions. For the DT reaction, the Coulomb barrier is about 400 keV (13) and the quantum mechanical tunneling helps to reduce this energy barrier. A mean energy of 10 keV produces a thermal velocity of about 10^6 m/s for deuterium and 6×10^7 m/s for electrons ($v_{th} = \sqrt{2T/m}$), and in a reactor of 10 m size these particles can be lost in about 10 μs. This would prevent fusion to occur (see below) and thus suitable methods must be found to confine these particles in the plasma for longer times. The DT reaction produces 17.6 MeV of energy with the α-particle carrying 3.5 and neutron carrying 14.1 MeV of energy. The helium nuclei are stable and if confined for sufficient time heat the plasma and can sustain fusion reactions without supplying external energy. The neutrons carry 80% of the fusion energy and their energies can be captured in the chamber wall surrounding the plasma and transformed into heat for producing electricity (Section 3). The DT reactions do not produce radioactive isotopes directly, but indirectly through the fusion neutrons interacting with the materials surrounding the plasma (fusion chamber and vacuum vessel walls, coils) and when employed to breed tritium in the wall of the chamber or *blanket* of the reactor.

Tritium is radioactive with a short half-life (12.3 years) and thus it does not exist in nature and must be produced for use in DT fusion reactors. Heavy water fission reactors currently produce most of this material (14), but this is not sufficient for fueling the commercial fusion reactors of the future, each of which requires about 10 kg of T inventory to make it functional. Tritium can, however, be produced by allowing the fusion neutrons to interact with lithium, via the reactions

$$n(\text{slow}) + {}^6\text{Li} \rightarrow \text{T} + {}^4\text{He} + 4.8\ \text{MeV} \tag{8}$$

$$n(\text{fast}) + {}^7\text{Li} \rightarrow \text{T} + {}^4\text{He} + n - 2.5\ \text{MeV} \tag{9}$$

where the first reaction with thermal neutrons is exothermic and the second reaction with fast neutrons is endothermic. The seawater contains more than 200 billion tons of lithium (15) and to produce tritium in a fusion reactor use can be made of the fusion neutrons in the blanket containing Li. But these neutrons are

not sufficient to produce the required amount of T and *neutron multiplier* materials must be employed to increase their abundance. This process of producing T is called *breeding* and requires the availabilities of Li and neutron multiplying materials such as Be or Pb. The *Tritium Breeding Ratio* (TBR) is defined as

$$\text{TBR} = \frac{\text{tritium production rate in the blanket}}{\text{tritium destruction rate in the plasma core}} \tag{10}$$

In the absence of T from other sources it is necessary to have TBR > 1 in order to compensate for tritium losses during extraction, transfer, and decay before injection into plasma. The upper limit estimates of TBR for various blanket materials range from 0.9 to 2.7 (13) and the reactions of ^{6}Li, ^{7}Li, ^{9}Be, and Pb with neutrons produce large cross sections (0.3–2 bars) (12). D, Li, Be, and Pb, are thus the principal DT fusion fuels that should be *sustainable* for long-term use.

The DD reactions (Table 1) are not completely clean, either, because they also produce neutrons, but these neutrons have an order of magnitude smaller energy than the neutrons of DT reactions and thus produce much less damage when interacting with fusion chamber materials. Since the products T and ^{3}He of DD reactions are fuels in DT and D^{3}He reactions, no radioactive ash or waste is produced in the plasma. The reactions between hydrogen isotopes and light nuclei (He, Li, B) belong to advanced fusion reactions. The D^{3}He reaction has a sizable reactivity at low temperatures and produces no neutrons, but, unfortunately, one cannot prevent deuterium from fusing with itself and produce tritium and neutrons. However, the neutrons produced are of low energy. ^{3}He does not occur naturally and a reactor that uses this fuel requires mining on the moon (16). The proton–boron p^{11}B reaction is particularly attractive because it eliminates the need for blanket shielding, tritium production and recovery, and the remote handling operations. The p^{6}Li and p^{7}Li reactions look attractive in terms of the availability of fuels, but it is very difficult to produce controlled fusion because of their very small cross-sections.

At ordinary temperatures, the atoms and molecules are neutral particles where the negatively charged electrons are bound by the electrical or Coulomb force to the positively charged nuclei. When these particles attain sufficient kinetic energies or temperature the atoms begin to ionize or the electrons and nuclei begin to form a gas of charged and neutral particles. The charged particles generate *local* concentrations of positive ions and negative electrons that generate local electric fields and currents that produce magnetic fields. These fields in turn affect the motions of particles far away and cause the mixture to exhibit a *collective behavior*. If, moreover, the dimension of the system containing these particles is much larger than the Debye distance that characterizes the local concentration of charges (1 μm–1 mm), the mixture is said to be *quasineutral* and such a mixture is technically called *plasma* (17).

2.2. Plasma Confinement. The particles in a gas at low temperatures are mostly neutral atoms and molecules whereas in a plasma most of the electrons are separated from the nuclei and both can readily respond to electric and magnetic fields. The Sun is a ball of plasma at a temperature of about 20 million degrees (except for the thin outer layer or *photosphere* where the temperature is considerably smaller) where the fusion process proceeds by the interactions of

protons through the beta-plus decay (mediated by the weak nuclear force) that produces deuterium and hence is slow and very inefficient (on average one proton fuses every billion years). The subsequent fast (seconds) reaction process involves the fusion of deuterium with another proton that produces ^{3}He (mediated by the strong nuclear force) and in several hundred years this isotope fuses with another ^{3}He and pre-existing ^{4}H to produce the helium nucleus (18). The reason that the fusion in the Sun works is that it is so big where its gravity confines the fussing particles for very long time. But on Earth we neither have the capacity to produce such a stable *gravitational confinement* nor wait for a long time before the fusion reactions can occur. Here, plasmas can be confined with magnetic fields and by irradiating fusion fuel targets with very energetic particle and laser beams, producing fusion by overcoming the strong nuclear force that binds the nucleons together. These are the *magnetic confinement fusion* (MCF) and *inertial confinement fusion* (ICF) concepts, respectively, on which we will concentrate in this work.

No known materials can resist temperatures above several thousand degrees Kelvin and a plasma that produces fusion energy for human consumption requires mean plasma temperatures on the order of 100,000,000 K (see above). The DT ions and electrons in such an environment possess very complicated motions and can be lost from the plasma environment and produce interactions with the materials of the fusion chamber surrounding the plasma. These *plasma–wall interactions* produce ablation of the chamber wall and introduce high-Z ions (plasma impurities) into the plasma, which by interacting with the electrons in the plasma emit *bremsstrahlung radiation* in the form of X-rays whose power is proportional to Z^2. This radiation cannot be confined and escapes from the plasma volume and contributes to the reduction of plasma temperature and can terminate fusion reactions. Plasma is also difficult to control because the local concentrations of charges and currents can produce highly undesirable plasma instabilities that can lead to *plasma disruptions* and plasma–wall interactions. Plasma disruptions occur due to the loss of stability and/or confinement in plasmas and the ones that are of major concern are those that cause the plasma to violently collide against the wall of the chamber and damage the in-vessel reactor components.

2.3. Magnetic Confinement Fusion

Tokamak and Stellarator. A nonrelativistic charged particle moving in an electric field **E** and a magnetic field **B** is subjected to the *Lorenz force* and the equation of motion

$$m\frac{\mathrm{d}\mathbf{v}}{\mathrm{d}t} = q(\mathbf{E} + \mathbf{v}\times\mathbf{B}), \tag{11}$$

where **v** is the velocity, q is the charge, and m is the mass of the particle. Such a particle gyrates or rotates about the magnetic field line (with a radius that is inversely proportional to the strength of the magnetic field) and at the same time moves along this line and drifts in the direction that is perpendicular to both the magnetic and electric fields. The ions and electrons gyrate in opposite directions and the particle's orbit is therefore a slanted helix with a changing pitch. This implies that any device that aims at confining charged particles cannot have magnetic field lines that are either zero or terminate on material surfaces, because these particles will be expelled from the device at these locations. This then

excludes those plasma volumes in the form of spheres and suggests those in the form of doughnut-like configurations where the magnetic field lines close on themselves and do not interact with the material wall of the reactor. Such field lines can be *toroidal*, where the magnetic field lines go around the torus the long way and encircle the hole, and *poloidal* where the field lines go around the short way and do not encircle the hole of the torus.

A toroidal magnetic field in a torus can be generated by passing the electrical current through a coil wound in the poloidal direction. This produces smaller separations of coils on the inside than on the outside of the hole of the torus and thus generates a nonuniform toroidal magnetic field that is stronger on the inside than on the outside of the torus. The charged particles in such an environment will now drift perpendicularly to the magnetic field gradient and cause positive and negative charge separations, with the ions and electrons gyrating in opposite sense and moving in opposite directions. This charge separation will produce an electrical force that will expel the plasma through the outer wall of the torus and can be mitigated by twisting the torus into the shape of *figure-eight*. Spitzer (19) named this configuration a *stellarator* and several such devices were built in 1950s in the Plasma Physics Laboratory at Princeton University. But it was not this configuration that was immediately developed to confine the plasma within the torus, but the simple doughnut-shaped schemes with improved magnetic and electric field configurations.

The first of such machines was built by Russians in the 1950s and is called *tokamak* (**to**roidalnaya **ka**mera **ma**gnitnaya **k**atushka-toroidal chamber magnetic coils). This design employs poloidal coils to produce the toroidal magnetic field and the toroidal current in the plasma to produce the poloidal magnetic field. The result is a twisting or helical magnetic field where the particles remain on nested concentric surfaces within the torus (Fig. 3a). This twisting action in the torus can also be produced without the externally generated toroidal current by the carefully shaped toroidal and poloidal coils. This is the modern stellarator concept (Fig. 3b) whose complex magnetic field must be produced with coils developed with the help of advanced computational and manufacturing techniques. But in 1950s the plasmas in the experiments using these confinement methods exhibited strong instabilities that prevented fusion reactions. Since 1960s a strong foundation of plasma physics has been developed, however, which became the cornerstone for building modern MCF machines with large plasma densities, temperatures and confinement times, and being less prone to plasma disruptions (20).

The purpose of producing helical magnetic field lines is to allow for the cancellations of vertical ion and electron drifts discussed earlier. These fields do not have to meet their own tails as they circle around the torus the long way and cannot end on material surfaces. The average number of times a field line goes the short way around a cross section for each time that it goes the long way around the torus measures the amount of twist and is called the *rotational transform*. The rotational transform has important implications for designing stable fusion energy producing machines based on the tokamak concept. As we will explain below, a particle that always remains on the same *nested magnetic surface* has a higher chance for interacting or fusing with other particles, but this is not easy to achieve because of the nature of plasma and requirements for practical operations (fuel supply and energy removal) of fusion reactors. The road to MCF is being actively

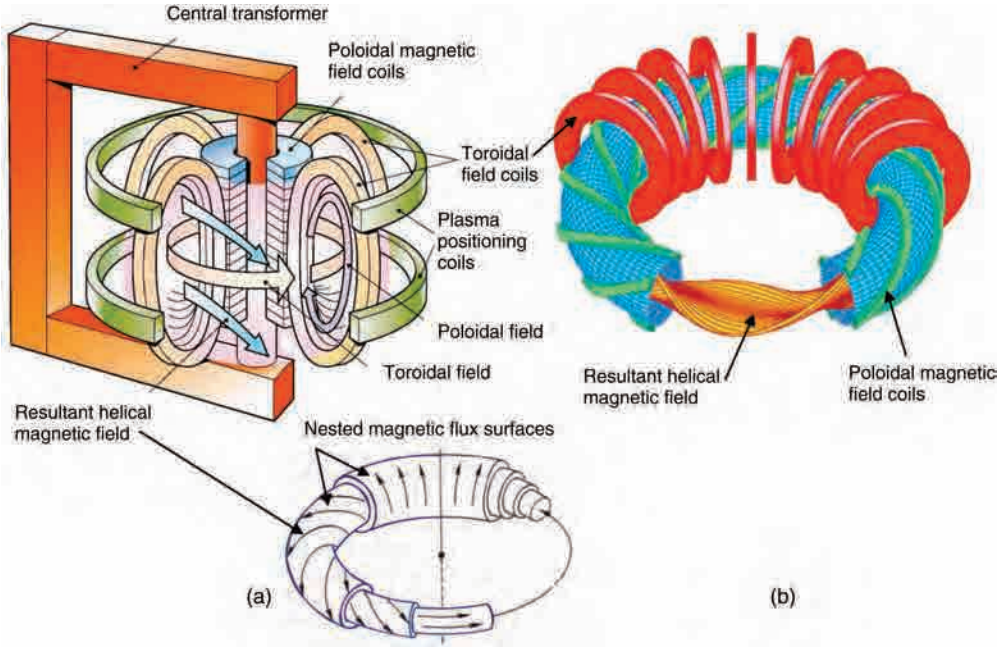

Fig. 3. (a) In a tokamak, a current in polidal coils produces a toroidal magnetic field and a toroidal current generated by the central transformer produces a poloidal magnetic field. This produces a sheared helical magnetic field. The toroidal plasma positioning coils arranged above and below the torus produce a magnetic field that stabilizes the outward expansion of plasma. (b) In a stellarator, the helical field shape is produced with carefully optimized current carrying helical and poloidal coils and there is no need to produce pulsed toroidal current with external magnets. (Courtesy of Max Planck Institut für Plasmaphysik.)

investigated in many small and large tokamaks and stellarators and some of these systems are discussed below.

Plasma Confinement Principles. An important measure of the efficiency of a fusion reactor is the *figure of merit*

$$Q_{\text{fus}} = P_{\text{fus}}/P_{\text{aux}} \tag{12}$$

P_{fus} is the fusion power produced and P_{aux} is the external power introduced into the plasma to keep its operating conditions. The *thermonuclear ignition* occurs when $P_{\text{aux}} = 0$ or Q_{fus} is infinite as in the Sun. On Earth, however, Q_{fus} should be kept sufficiently high and above $Q_{\text{fus}} = 10$, and 50 or so in a practical fusion power plant.

A *confinement parameter* specifying the product of particle density and confinement time can be derived by equating the power produced from external auxiliary heating and internal α-particle heating with the power loss from radiation (bremsstrahlung) and diffusion, ie,

$$n\tau_{\text{E}} = \frac{3k_{\text{B}}T}{\frac{1}{4}\left[(1/Q_{\text{fus}} + 1/5)\right]Q_{\text{DT}} < \sigma v > -C_{\text{b}}T^{1/2}}, \tag{13}$$

where Q_{DT} is the energy release in the DT fusion reaction. This confinement parameter is called the *Lawson Criterion* (21) and expresses the relationship between the plasma density n, confinement time of reacting particles τ_E, Q_{fus}, and ion temperature k_BT (11). The *ideal breakeven condition* for the DT fusion with $Q_{DT} = 17.6$ MeV, $Q_{fus} = 1$, and $<\sigma v>$ evaluated with $k_BT = 12$ keV (Fig. 2b) produces the *minimum* value of $n\tau_E$ of about 10^{20} s.m^{-3}. Note that this is the condition where as much fusion power is produced as heating power is absorbed. For *minimal ignition* with $Q_{fus} \geq 10$, 10% or less of the fusion power would be used to make the fusion reactions self-sustaining, which suggests that the confinement parameter should be at least an order of magnitude higher or greater than 10^{21} s.m^{-3}. For a reasonable plasma density of 10^{20} m^{-3} (9), the confinement time for breakeven is 1 s and for (minimal) ignition is 10 s.

With the plasma particle density of 10^{20} m^{-3}, it is currently impossible to track each particle's behavior and we must resort to the plasma's kinetic or fluid description. The *kinetic description* is based on the particle distribution function determined from the Boltzmann equation, whereas the *fluid description* relates the plasma's macroscopic properties (density, pressure, temperature, current, electric and magnetic fields, etc) through the transport equations obtained by taking the moments of the distribution function. We will not dwell on these models in this work but want to point out that the force balance on a small *macroscopic* portion of plasma involves the inertial effects (due to acceleration), pressure gradient, gravity, and Lorenz force, and that as a consequence the plasma equilibrium is largely maintained between the pressure gradient and electromagnetic forces, ie,

$$\nabla P = \mathbf{J} \times \mathbf{B}, \qquad \mathbf{J} = \sigma(\mathbf{E} + \mathbf{v} \times \mathbf{B}), \tag{14}$$

where $\mathbf{J}$ is the current density and σ is the electrical conductivity of plasma. If we now form the scalar product of $\mathbf{B}$ with the first equation and use the identity $\mathbf{B} \times (\mathbf{J} \times \mathbf{B}) = \mathbf{J} \times (\mathbf{B} \times \mathbf{B}) = 0$, we obtain $\mathbf{B} \times \nabla P = 0$ or that the magnetic field lies on the constant pressure surface and that the plasma is confined on concentric magnetic surfaces as depicted in Figure 3a. The current $\mathbf{J}$ and pressure P are the sources of plasma instabilities whereas the geometrical symmetry of the tokamak provides robustness in maintaining nested flux surfaces against various operating parameters.

Plasma Instabilities. A magnetic field produces a pressure that resists the destabilizing kinetic pressure P of plasma (equation 14) and in a plasma tube where the plasma is confined entirely by an axial current the associated azimuthal magnetic field is proportional to the current and inversely proportional to the radial distance from the axis of the tube. The collisions in the plasma are necessary for fusion reactions, but in the long run these collisions deteriorate the confinement on magnetic surfaces because the colliding particles temporarily disconnect from these surfaces and move or diffuse to the neighboring surfaces and thus produce inward and outward bulging ripples of the tube. These ripples are unstable and can cause the particles to leave the plasma volume. This is the *pinch instability*. A similar type of instability, called the *kink instability*, occurs in a torus when the toroidal current is sufficiently large, because the magnetic forces closer to the hole are larger than farther from the hole and tend to push the plasma

outwards. The kink is stabilized by the toroidal field and the limiting current for stable operation is called the *Kruskal-Safranov limit* and is expressed in terms of the rotational transform. The transforms smaller than one are stable to kinks and interesting things happen when the inverse of the rotational transform called *safety factor q* is a rational fraction or when the current channel joins up to itself after several trips around the torus. When the safety factor is below 2 or 3 the global kink instability can lead to plasma disruption and detrimental plasma–wall interactions.

The second process that deteriorates the confinement is caused by the charged particles, ions and electrons. This is because the charged particles can clump together and create their own electric force that can also take the particles across the magnetic field lines. Such plasma instabilities have been slowing MCF research for decades and even today there are some plasma instabilities that cannot be explained (22,23).

Ions and electrons in plasma have vastly different masses and thus velocity distributions and mean temperatures. The electrons can travel around the torus many times before interacting with ions and the plasma can behave as a superconductor. The perpendicular electric and magnetic fields produce ion and electron drifts in the direction perpendicular to these fields, but they gyrate in opposite sense. If the ions and electrons are subjected to a plasma pressure gradient perpendicular to the magnetic and electric fields as in a tokamak, these particles will drift in opposite directions and produce no charge separation as long as the plasma potential energy is minimal produced by the balance between magnetic and kinetic (plasma) pressures. A ripple on the magnetic surface will, however, disturb this balance and cause separation of negative and positive charges and generation of an electric field and an associated $\mathbf{E} \times \mathbf{B}$ related force that will cause more charge separation and growth of the ripple and exchange a plasma tube with high magnetic pressure from inside the plasma with a tube that has low magnetic pressure from farther out (like a ripple on a planar surface in normal fluid exchanging two fluid layers, with the top heavier layer exchanging place with the lower lighter layer to reduce the overall potential energy of the system). This is the *interchange instability* where the radial variation of the magnetic energy acts like gravity in the Rayleigh-Taylor instability, driving the interchange of plasma layers at different pressures. The interchange instability can be stabilized by means of the *magnetic shear* or a sheared helical magnetic field whereby the magnetic field on each magnetic surface has a different twist angle (Fig. 3a).

The magnetic field lines in a *magnetic well* are everywhere smaller than on its boundary or are convex. They have good curvature in contrast with tokamaks' mostly concave field lines with bad curvature. In a torus plasma, the radial pressure gradient competes with the curvature of magnetic field and drives interchange instabilities into the low field side of the plasma (outer-side of torus). These are called *ballooning modes* and to mitigate them modern tokamaks employ cross sections that have *D-shapes*. Such a cross section is slightly elongated, the inner surface is almost vertical, top and outer boundaries have gentle concave curvatures, and the bottom surface is reserved for the exhaust of charged particles such as alphas and unburnt DT fuel ions from the plasma volume. The special corner of D-shape is called the *divertor* and the particle exhaust is accomplished by shaping (with locally placed coils) the last closed magnetic surface in the

torus in such a way that the field lines on this surface intersect at the entrance of the divertor (called *X-point*) and thus lead the particles into the divertor (Fig. 14a).

The collisional processes can produce plasma losses through various diffusion processes. *Classical diffusion* across the magnetic field lines is computed from the random walk trajectories of charged particles using their gyration (Larmor) radii as the step-sizes of their radial displacements in collisions. This diffusion is inversely proportional to the magnetic field and temperature (13). A much faster diffusion, called the *neoclassical diffusion*, produces *banana orbits* of particles and is caused by the magnetic drifts in hot plasmas and step-sizes between collisions that are 10 times larger than the Larmor radii. A still larger diffusion rate leading to the disruption times in milliseconds is the *Bohm diffusion* across the magnetic field. This diffusion is proportional to the temperature and inversely proportional to the magnetic field (13) and is caused by the randomly fluctuating electric fields in the plasma. The excess transport above the collisional one is called *anomalous transport* and in tokamaks is assumed to be dominated by turbulence.

Plasma with a finite resistivity can also produce nonconcentric magnetic surfaces and *magnetic islands*. This comes from the tearing of magnetic field lines at $q = 2,3$, and so on, whereby the concentric magnetic surfaces break into magnetic islands with the field lines hopping from one island to the next and returning to the same islands but not to the same places. The *tearing instability* associated with this transport produces the escape rates that are faster than classical just as in banana diffusion. The locations of islands depend on the radial distribution of current, which to some extent depends on the ways the plasma is being heated with external means.

Microinstabilities in plasmas arise from nonuniformity, anisotropy, finite size of Larmor orbits, plasma density gradients, production and dissipation of turbulence energy at different scales, etc. These effects give rise to non-Maxwellian distribution functions in different regions of the plasma and can cause tearing of electrical currents into filaments, drifting of electrons and ions, wave breakup leading to the transport of plasma in blobs of density, etc. These effects produce *ion diamagnetic drift, density wave instability, convective cells* of alternate positive and negative charges that tend to transfer the plasma outwards, etc. These and other microinstabilities are a large and complex field and the reader is referred to the plasma literature for further details. They have typical frequencies of 10 kHz and wave periods of 100 μs, while the growth of turbulence takes about 1 ms. These times are much smaller than several seconds required for the attainment of quasi –steady-state plasma profiles.

Besides the toroidal and poloidal magnetic fields, a tokamak also needs a vertical magnetic field for stabilizing the outward expansion of hot plasma. The internal plasma pressure pushes the plasma outwards, tending to make the cross section flatter and expanding the ring radially. The toroidal current also produces a hoop force in the plasma that tends to expand its major radius. A vertical magnetic field, produced by toroidal coils arranged above and below the torus, can stabilize this expansion by producing an inward Lorenz force on moving charges and thus prevent the outward expansion of plasma (Fig. 3a). The plasma's vertical position needs to be controlled by the externally imposed radial fields with fast-acting feedback power supplies and feedback systems. Plasma *position instabilities* can also lead to disruptions.

Recall that the safety factor $q = 1$ represents the boundary of kink instability and that the magnetic field lines on neighboring magnetic surfaces cannot be parallel because of the required shear to stabilize the instabilities. Since $q < 1$ occurs near the center of the torus where there is no magnetic confinement and the plasma is the hottest and offers least resistance, the current in this location tends to increase, change the current distribution elsewhere, and cause severe *sawtooth oscillations* of ion and electron temperatures that eject hot plasma near the center and inject cooler plasma from more distant locations. Sawteeth can help drive the impurities out of the plasma because their interaction with electrons produces bremsstrahlung radiation that cools the plasma. This is a *self-healing* feature of tokamaks and does not appear in stellarators where the magnetic field is predefined by the external coils.

Stellarators operate with much smaller toroidal currents than tokamaks and their plasmas are thus much less sensitive to kink modes, sawtooth, and resistive tearing modes of instabilities that limit plasma performance. The toroidal magnetic field and pressure gradient produce, however, a small poloidal plasma current which, in turn, generates a toroidal current to satisfy the Maxwell's incompressibility condition ($\mathrm{div}\mathbf{J} = 0$). Heating of plasma (see below) can also produce a toroidal current, but the total current produced in stellarators is much less than in tokamaks. The plasma-terminating disruptions are therefore reduced and the stellarator operates with a larger margin of safety than the tokamak. In stellarators, as opposed to in takamaks, the plasma density is not limited by the *Greenwald limit* (24) and thus they can operate at higher densities and βs (β is the ratio of plasma pressure nk_BT to magnetic pressure $B^2/2\mu_0$), as demonstrated in the *Large Helical Device* (see below) where the plasma core density reached $n_e = 10^{21}\,\mathrm{m}^{-3}$ and $\beta = 0.05$. When comparing a stellarator to a tokamak, the macroscopic stability is better, neoclassical confinement is worse, turbulence and edge plasma performance appear comparable, and because the magnetic field is less symmetric the particle orbits are less understood (25).

When the loss of plasma stability and confinement occurs, very rapid (tens of milliseconds) plasma thermal and electromagnetic energies are released from the plasma volume and strong electromagnetic forces and large thermal loads are induced in the surrounding components. Studies of the disruptions in the JET tokamak in the United Kingdom show that their root causes were neoclassical tearing modes and human errors associated with the control of the reactor (26). Plasma disruptions are actively being investigated because of their potential to degrade the performance and utility of fusion reactors (27).

Plasma Heating. Heating of plasma has some very important and unexpected consequences. A *toroidal current* $\mathbf{J}$ in a tokamak is needed to produce the poloidal magnetic field for generating the rotational transform and to heat the plasma, but there is a limit of how much current and for how long it can be sustained. This toroidal current can also be generated through external waves that push the electrons along the magnetic field lines and by the *bootstrap current* $\mathbf{J}_b$ produced by the toroidal electron drift. Such a drift of electrons is caused by the radial plasma pressure gradient and the perpendicularly oriented poloidal magnetic field (see earlier discussion). Both the toroidal current $\mathbf{J}$ and the bootstrap current $\mathbf{J}_b$ always flow in the same direction, and it is anticipated that in commercial fusion reactors the bootstrap fraction of the current will be more than 90% (9,28). The stellarators do not need an inductive current drive.

The currently preferred method used for heating the plasma is by *neutral beam injection* (NBI). Here the hydrogen or deuterium atoms with energies 100–200 keV are injected into the plasma to heat the plasma. Similarly, *ion cyclotron resonance heating* (ICRH) and *electron cyclotron resonance heating* (ECRH) are also used to heat the plasma by affecting the gyration frequencies of ions and electrons and thus influencing the collisions of particles.

When the neutral beam heating of plasma is used with a divertor as discussed above, the plasma can achieve the *high confinement mode*, called the *H-mode*. This was first observed in the experimental ASDEX tokamak (29) when the heating power was increased and since has been observed in other toroidal machines and with different heating methods. What happens is that at the outer minor radius of plasma volume a thin (1–2 cm) transport barrier or pedestal is formed that prevents the plasma to diffuse to but not to escape readily across this barrier. This pedestal is characterized by large and sheared $\mathbf{E} \times \mathbf{B}$ drifts of particles in the toroidal direction that stabilize the microinstabilities. In the H-mode, the confinement time improves by a factor of 2 and the plasma pressure almost doubles. This improvement is very significant and forms a necessary design strategy for magnetic confinement fusion reactors. And yet, the plasma energy can also find ways to escape from the transport barrier through another instability, called *edge localized modes* (ELMs). We will describe ELMs in Section 3 where we discuss reactor designs.

Tokamak and Stellarator Optimizations. The research in 1960s demonstrated that *minimum-B* or magnetic well configurations stabilized the interchange instability, and that the plasma resistivity and magnetic shear can also increase the plasma stability. This and the oil embargo of 1973 encouraged the construction of medium-size tokamaks and by the end of the decade large tokamaks (TFTR in the United States, JET in the United Kingdom, JT60 in Japan, and T15 in the Soviet Union) (20). Auxiliary heating and H-mode came of age in early 1980s and in late 1983 Alcator C tokamak achieved $n\tau_{\mathrm{E}} = 6 \times 10^{19}$ s.m^{-3} and $T = 1.5$ keV (30), but the temperature was still an order of magnitude too low.

The safety factor q typically increases from 1 at the core to less than 10 at the periphery of the minor plasma radius and the changing degree of twist provides a shear stabilization of instabilities. Since q is an important machine design parameter all large tokamaks have been able to produce the so called *hollow current profiles* whereby the current is almost zero near the center and edge of plasma cross section and peaks in between. This produces a q that is large at the center (small twist), drops to a minimum (large twist), and then rises slowly toward the plasma edge. Such profiles decrease the plasma turbulence and increase confinement. At the locations where q is a minimum, most of the instabilities are quenched as if exists an *internal transport barrier* (ITB). These barriers have been produced in all large tokamaks in operation (ASDEX upgrade in Germany, DIII-D of General Atomics in the United States, JT-60U of Japan, JET of the European Union). ITB is able to reduce the total diffusivity to very low values in large parts of the torus (31).

The three large tokamaks TFTR, JET, and JT60 (Table 2, Fig. 4) demonstrated in the 1990s that the 200 million-degree plasma temperature and Lawson confinement parameter $n\tau_E$ for breakeven ($Q_{\mathrm{fus}} = 1$) in DT plasmas are achievable (Fig. 5). In the fall of 1997, JET reached fusion power levels of 16 MW for 1 s and

Table 2. **Operational Parameters and Achieved and Projected Fusion Progress of Recent MCF Projects**

Machine name Fuel	Country Place	Machine	Major radius (m)	Minor radius (m)	Plasma current (MA)	Coils	Toroidal magnetic field (T)	Heating power (MW)	Q_{fus} Pulse (s)	T_{ion} (keV) $n\tau T$ (keV.s.m^{-3}) β (%)	Start date End date
TFTR DT	USA Princeton	Tokamak	2.5	0.88	3		6	39	0.27 0.2	13 1.0×10^{20} AD 0.3	1982 1997
JET DT	EU/UK Abingdon	Tokamak	2.92	0.95	4		3.6	24	0.641 1	18 10×10^{20} AD —	1983 —
JT-60U DD	Japan Ibaraki	Tokamak	3.05	0.71	2.7		4.4	40	1.25	45 15×10^{20} AD 1.8	1985 2010
LHD DD	Japan Toki	Heliotron Stellarator	3.9	0.65		SC	4	42	— 3600	13 AD 0.5×10^{20} AD 5 AD	1998 —
W7-X DD	Germany Greifswald	Classical Stellarator	5.5	0.55	12	SC	3	25	— 1800	— PD — PD — PD	2015 —
ITER DT	Int/France Cadarasce	Tokamak	6.2	2.0	15	SC	5.3	50	10 1000	10 PD 5.0×10^{21} PD 1.8 PD	2025 2035

SC (superconducting coils cooled with liquid helium at 4K) (32,34–38).
AD (achieved), PD (predicted).

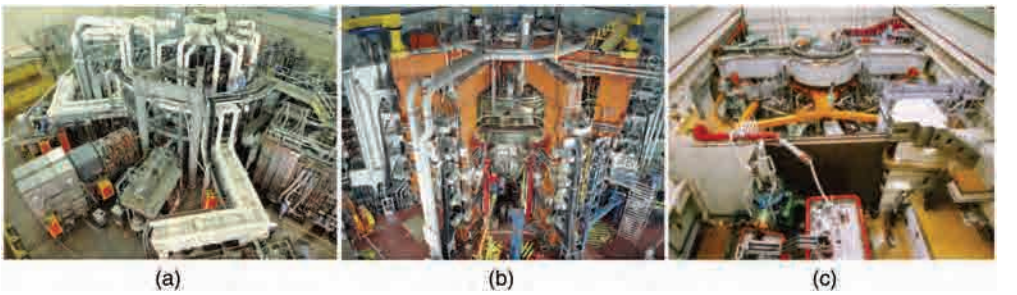

Fig. 4. In 1990s, two large tokamaks (a) TFTR and (b) JET demonstrated fusion, whereas (c) JT-60U tokamak produced the largest fusion triple product of density, temperature, and confinement time. (Courtesy of Princeton Plasma Physics Laboratory, European Fusion Development Agreement, Japan Atomic Energy Agency.)

fusion gain $Q_{fus} = 0.65$ (32,33), and made significant contributions to the complex technology of nonsuperconducting coils, plasma heating, fuel pellet injection and tritium recovery, plasma facing components, and plasma diagnostics. Because of its geometric symmetry, a tokamak provides good confinement and was selected for the next important advance of producing a significant fusion power output in International Thermonuclear Experimental Reactor (ITER) (Section 3).

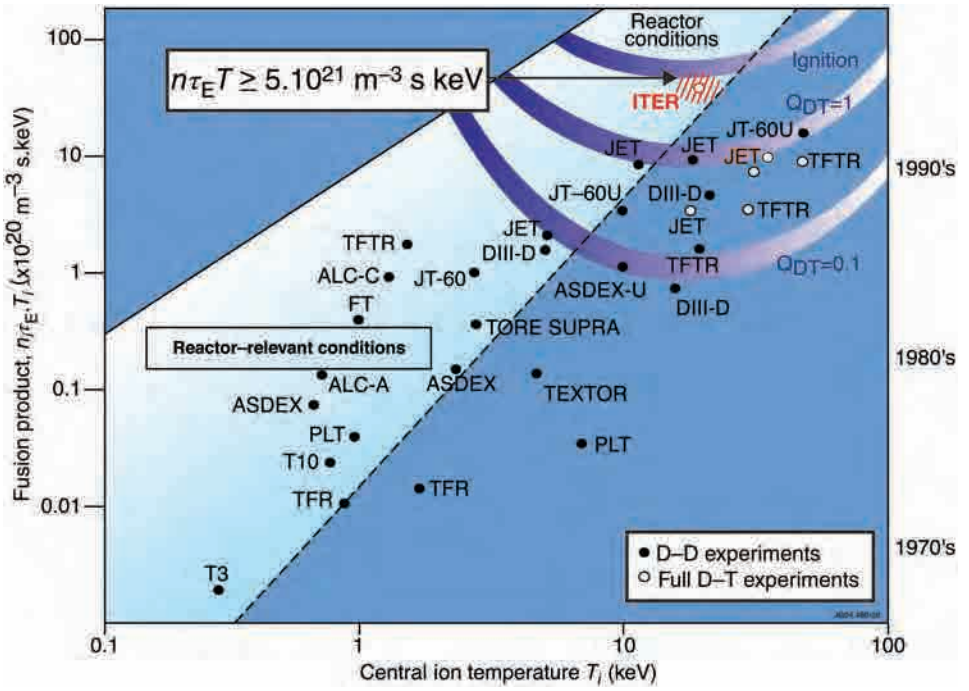

Fig. 5. Lawson diagram for magnetic confinement fusion illustrating progress over 50 years. $Q_{fus} = 1$ is the breakeven condition, whereas the reactor conditions require at least $Q_{fus} > 5$. ITER aims at achieving $Q_{fus} = 10$ (15). (Courtesy of Japan Atomic Energy Agency.)

The steady-state operation of a large fusion power plant is essential (15) and requires either a stellarator or a tokamak operating with long current pulses. A *lower-hybrid current drive* (LHCD) (39) boosts the toroidal electron motion and operates by injecting radiofrequency waves into the plasma via phased wavequide arrays, but for dense plasmas of fusion power plant reactors requires further developments (40). As demonstrated in the Japanese TRIAM-1M tokamak, LHCD can sustain currents for over 5 h (41). Steady-state tokamak operations are being actively pursued with the EAST reactor in China, JT-60SA reactor in Japan, and KSTAR reactor in Republic of Korea. Low aspect ratio tokamaks improve plasma performance and several machines have been built to study their performance gains (20,42).

The term "stellarator" is used generically to describe those toroidal devices that produce closed magnetic surfaces by means of external conductors, and there are different coil designs that employ this concept (classical stellarator, torsatron, and heliotron) (43). The Large Helical Device (LHD) is an experimental heliotron reactor located in Toki, Japan and became operational in 1998 (44). It employs two helical coils that wind around the torus and two pairs of poloidal and resonant magnetic perturbation coils that further shape the plasma in the torus (Fig. 6). The LHD's specification is provided in Table 2 and since it began operating has

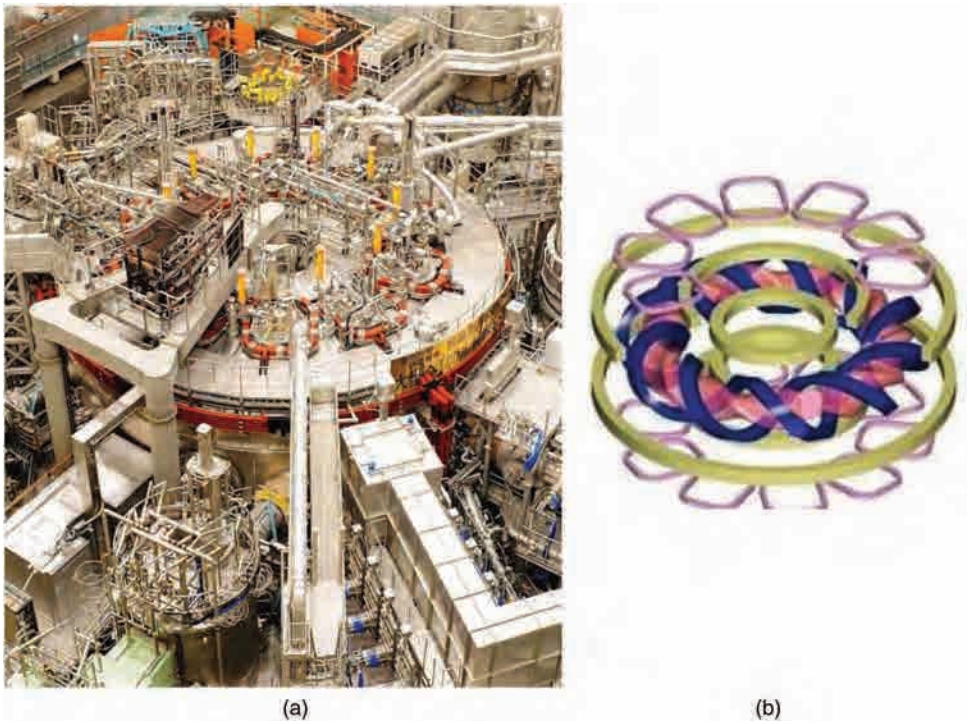

Fig. 6. (a) Large Helical Device in Toki, Japan. (b) This stellarator employs two helical coils winding around the torus and two pairs of poloidal field coils to shape the plasma. (Courtesy of Japan Atomic Energy Agency.)

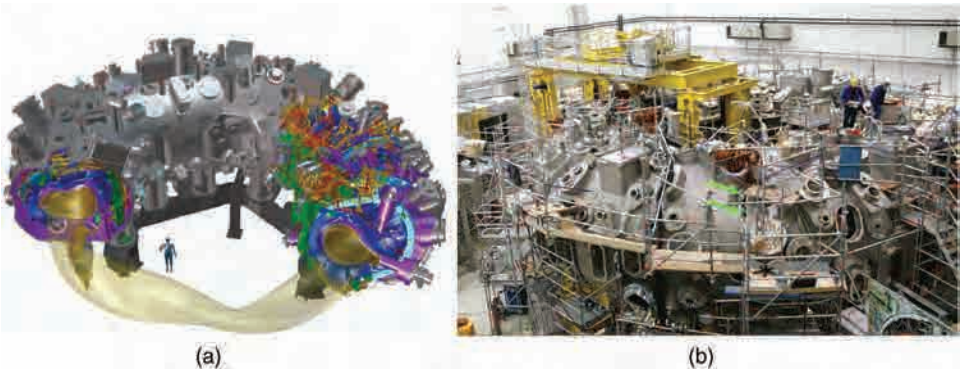

Fig. 7. (a) Cutaway drawing of W7-X with plasma (front), 70 superconducting coils (blue), central support ring (green), cryostat vessel (gray) with ports. (b) View of W7-X during construction in 2013 (38). (Courtesy of Max Planck Institut für Plasmaphysik.)

achieved (not at the same time) $\beta = 0.05$, $n = 10^{20}\,\mathrm{m}^{-3}$, ion and electron temperatures of 13 keV, and steady-state operation for 1 h (44–46). Although the LHD has so far achieved only 50% of $n_i\tau_E T_i$ required for breakeven, it has demonstrated that the vacuum chamber and high magnetic field producing coils can be manufactured to the required tolerances and that the stellarators can operate with higher βs than tokamaks.

Wendelstein 7-X (W7-X) is an experimental modular optimized stellarator that will not burn DT. It is located in Greifswald, Germany, became operational in October 2015 (47), and its specification is provided in Table 2. W7-X's coils consist of 50 nonplanar and 20 planar poloidal coils arranged in five modular units producing a pentagon shape of the torus and a helical shape of the plasma (Fig. 7). This machine was designed to operate continuously for 30 min and it employs a five-island structure divertor to control the power and particle exhaust. These targets were designed for heat fluxes up to $10\,\mathrm{MW/m^2}$ and are made of CuCrZr cooling structures and CFC tiles bonded to the target surfaces. The surface of the blanket facing the plasma is designed for heat fluxes up to $0.3\,\mathrm{MW/m^2}$ (38,48). The first operational phase started on February 2016 and produced hydrogen plasma at 80×10^6 K for 0.25 s (49).

The tokamaks JET and TFTR demonstrated that it is possible to produce controlled fusion and that long confinement times can be achieved (DD plasmas in JT-60U). The development of stellarators is, however, lacking the development of tokamaks, but this technology may ultimately prove to be the preferred choice for magnetic confinement of plasma because of its advantages to operate in steady state without plasma disruptions. The characteristics of these machines are summarized in Table 2 and the achieved plasma conditions ($n_i\tau_E T_i$ and T_i) of many tokamaks are reported in Figure 5.

The next step in tokamak development aimed at producing net fusion power output is the ITER. This reactor is currently being built in France by an international community and by 2035 aims to demonstrate ignition (Table 2) and help build MCF demonstration fusion reactors by 2050 (Section 3).

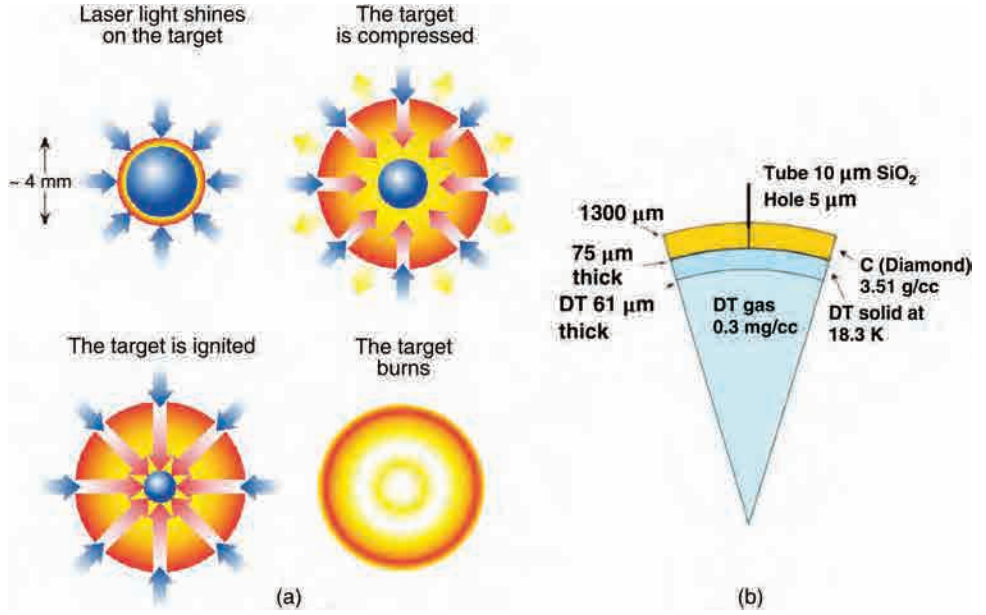

Fig. 8. (a) Inertial confinement fusion involves rapidly heating with laser or ion beams a capsule containg a fuel and employing the outwardly expanding plasma of capsule ablator to compress the fuel to high density and temperature before the capsule material flies apart. The process involves four stages: target heating, outward ablation of capsule, inward compression of fuel, and fusion burn. (b) A typical DT fuel target is surrounded by low-Z materials (carbon or beryllium) to achieve optimum shock heating and is introduced into the fusion chamber at a cryogenic temperature to achieve maximum compression (50). (Courtesy of National Academy of Sciences.)

2.4. Inertial Confinement Fusion.

Plasma Confinement Principles. Inertial confinement fusion involves no external means of confinement and relies exclusively on the mass inertia, where the high densities of 600–1000 g/cm^3 and temperatures 10^7–10^8K must be achieved in the fuel before it disassembles in 100–200 ps. This is achieved by supplying energy to a fuel target whose outer layers consist of a low-Z material and whose interior contains the (DT) fuel in both solid and gaseous forms. The ICF ignition process illustrated in Figure 8a involves four stages: (1) symmetrical and very fast (few nanoseconds) delivery of energy from a suitable source or *driver* to the outer layers of a target of several millimeters in diameter, (2) *ablation* or evaporation of the outer layers of the target causing outward expansion of the ablated material, (3) implosion of the interior of the target toward the center of the capsule causing compression of the fuel to very high mass density (10^6 kg/m^3) and core temperature (>10 keV) in a very small size (typically 10^{-5} m) to initiate thermonuclear reactions, and (4) outward propagation of the fusion burn front causing the remaining fuel to ignite before the target explodes or disassembles. The time of confinement is the time required for the shock wave at the thermodynamic conditions of the target in that moment to travel from the fuel target surface to the center of the fuel and is on the order of 100–200 ps. Fuel ignition occurs when

the rate of energy gain in the fuel exceeds the rate of energy loss and this requires implosion velocities on the order of 300 km/s (50). The ablating outer shell of the target is made of low-Z materials for the purpose of absorbing the energy efficiently, whereas the adjacent inner shell of the target contains a cryogenic solid (DT) fuel for efficiently compressing it. The (DT) fuel gas within the target serves the purpose of igniting the hot-spot at the center of the target (Fig. 8b). A near steady-state power production can be achieved through rapid and repetitive thermonuclear explosions where the energy output is limited by the capacity of the fusion energy conversion system to remove the fusion energy produced.

The *figure of merit* Q_{fus} for ICF power plant is also defined as the ratio of fusion energy produced E_{fus} to the auxiliary energy required E_{aux}. The *target energy gain* G is another useful parameter for ICF and is defined as the fusion energy released E_{fus} by one target to the energy delivered E_{d} to the target by a driver, ie,

$$G = \frac{E_{\text{fus}}}{E_{\text{d}}}. \tag{15}$$

Given the driver efficiency η_{d}, blanket efficiency η_{b}, and recycling power fraction f, the figure of merit and gain are then related as follows:

$$Q_{\text{fus}} = G\eta_{\text{d}} = \frac{1}{\eta_{\text{b}} f}. \tag{16}$$

This implies that for a 15% efficient driver, 40% efficient blanket, and 20% (large) recirculating power we need the target gain of 83 and figure of merit of 12.5. By halving the driver efficiency and keeping other parameters the same, doubles the required target gain. With $E_{\text{d}} = (2\text{–}5)$ MJ and $G = 100$, the fusion energy released is 200–500 MJ per target, and if 10 targets can be burned every second, the fusion power release would be between 2 and 5 GW. The amount of fuel contained within the fuel capsule must be limited, however, because it depends not only on the driver energy but also on the fusion energy release that the fusion chamber can safely handle. (Burning only 12 mg of a 50–50 DT mixture yields 4.2 GJ of energy, which is equivalent to the energy release of 1 ton of TNT.) Producing high gain targets and high blanket efficiencies is the key for designing viable *inertial fusion energy* (IFE) power plants.

A Lawson-type expression for the confinement parameter $n_o\tau_{\text{c}}$ can also be defined for ICF, where $n_{\text{o}} = \rho / m_{\text{f}}$ is the ion number density, ρ is the mass density, m_{f} is the average mass of fuel ions, $\tau_{\text{c}} = R_{\text{f}} / c_{\text{s}}$ is the confinement time of fuel, R_{f} is the fuel radius at the moment of maximum compression, and $c_{\text{s}} = \sqrt{2k_{\text{B}}\text{T}/m_{\text{f}}}$ is the isothermal speed of sound (11). The fuel compression can be estimated from the *burn efficiency*

$$\Phi \approx \frac{\rho R_f}{\rho R_f + H_B} \tag{17}$$

where for the DT fuel the *burn parameter* $H_{\text{B}} = 8c_s m_f / \langle\sigma v\rangle$ is between 60 and 90 kg/m^2. For $\Phi = 0.3$ and $H_{\text{B}} = 70$ kg/m^2, $\rho R_{\text{f}} = 30$ kg/m^2, and since the fuel radius R_{f} is expressible in terms of fuel density and mass of fuel ($m_{\text{f}} = 4\pi\rho R_{\text{f}}^3/3$), we obtain for $m_{\text{f}} = 10^{-3}$ g that the required density $\rho = 3 \times 10^5$ kg/m^3 for fusion is 1500 times

higher than the density of fuel before compression. The corresponding compressed core radius is $R_f = 100\,\mu m$.

This fuel compression requirement demonstrates the outstanding feature of the inertial approach to fusion that since the early 1950s could only be achieved uncontrollably with thermonuclear weapons (51). Since then both the United States and the USSR supported classified research programs to develop *controllable* thermonuclear explosions, but it was not until the development of lasers in 1960s and their continuing improvements (52–54) that the controllable inertial fusion progress took notice. Laser-driven implosions with the emission of thermonuclear neutrons were first reported in 1971 by the Lebedev Laboratory in Moscow (55) and in mid 1970s KMS Fusion and Laboratory for Laser Energetics (LLE) in Rochester followed suite. Laser fusion started to be declassified and during the ECLIM Conference in Madrid in 1988 (56) the leading scientists agreed on international collaboration. By the end of 1990s a rather complete ICF picture became available (57–59).

Large Nd-doped glass lasers were built at the Lawrence Livermore National Laboratory (LLNL) in the United States, with names like Janus, Shiva, Nova, and National Ignition Facility (NIF) in late 2000s (60). The ANTARES CO_2 laser technology at LANL was abandoned in early 1980s due to its poor efficiency, whereas the krypton-fluoride (KrF) laser, heavy-ion, and pulsed power systems have received substantial support. The United States has major ICF facilities at LLNL (lasers, NIF), Naval Research Laboratory (NRL) (lasers, NIKE), Sandia National Laboratories (SNL) (Z pulsed power system, MagLIF), Laboratory for Laser Energetics (LLE) (lasers, OMEGA), and Virtual National Laboratories (VNL) consisting of several facilities (heavy ion fusion, HIF). In Europe, High Power Energy Research (HiPER) facility is a power plant study involving 12 countries, including Russia, and European Union has a major laser fusion research facility located in France (Laser MegaJoule, LMJ). Japan has a major laser facility GEKKO XII, which is being upgraded with fast ignition system LFEX that is similar to PETAL associated with LMJ in France. China, Germany, Russia, Spain, and United Kingdom are also working separately on developing the ICF technology (50,61).

Fuel Target Energy Supply Concepts. The ICF drivers must supply energy to induce fusion reactions in fuel targets and there are different ways that this may be accomplished. Laser and ion beams and pulsed-currents are the principal methods being considered for *supplying* the energy and the direct-drive and indirect-drive are the principal methods being employed to *distribute* the energy to the fuel targets. The choice of a driver is complicated because it involves not only different physical considerations, but also the design of targets and fusion chambers, target injection and alignment tolerances, and fusion reactor safety. The driver efficiency is the ratio of "wall-plug" electrical energy E_{el} supplied to the fuel target and the energy supplied to the driver E_d. The advanced laser efficiencies do not exceed 15%, ion beam accelerators are 30% efficient, and pulsed-power systems are 60% or more efficient. The laser systems drivers are more developed than the ion beam drivers and appear to have higher prospects for being employed in first-generation IFE plants. The ion beam drivers offer, however, the efficiency and target energy delivery advantages that with further technological developments should be more beneficial for use in commercial energy production environments.

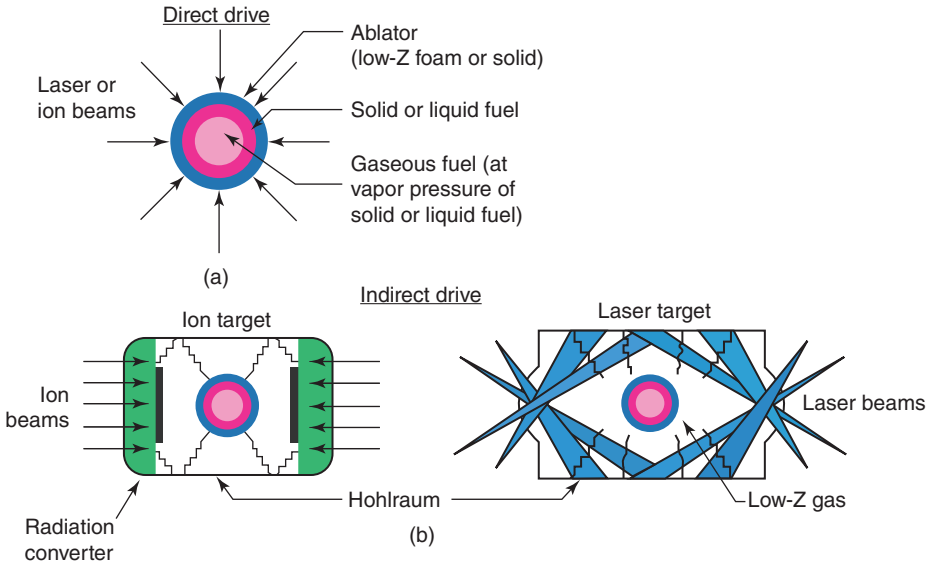

Fig. 9. (a) The direct drive involves heating the capsule directly with laser or ion beams. (b) The indirect drive involves placing a capsule with fuel within an enclosure called hohlraum and heating its inside surface to produce X-rays for uniformly illuminating the capsule and inducing fusion reactions. (Courtesy of National Academy of Sciences.)

In the *direct drive* (Fig. 9a), the energy is supplied directly to the target and to maximize the driver efficiency and achieve fusion it is necessary to illuminate the target as uniformly as possible with many highly accurate (20 μm) energy beams. The most important advantage of direct drive is the high efficiency of coupling the driver energy to the fuel target (which is reflected in the high gain) and the simplicity of the target. In the *indirect drive* (Fig. 9b) the beam alignment accuracy is less stringent (80 μm), because the energy is supplied to the inside of an enclosure called *hohlraum* in which the target is suspended (50). This enclosure consists of high-Z material that upon being struck by laser light or ion beams emits X-rays that then bath the target uniformly and drive the implosion of the fuel within the target. In a cylindrical hohlraum the main laser or ion beam is divided into two separate groups of beams that are focused onto the internal faces of the cylinder through the two small openings located on the side surfaces of the cylinder. The indirect drive has several advantages over the direct drive: the beams do not have to impinge directly on the target and thus the beam design is simpler, the target is illuminated (with X-rays) more uniformly and is less sensitive to hydrodynamic instabilities discussed below, and the target physics is largely decoupled from the driver. The disadvantage of indirect drive is that only a fraction of laser energy (about 15% at NIF (62)) is deposited and absorbed by the fusion target; the rest is lost through radiation, electrons, and heating of hohlraum. Another disadvantage is that the laser light interacting with hydrogen or helium gas in the hohlraum can cause laser–plasma interactions that degrade capsule implosion symmetry (63). Both lasers and ion-beams can be used in the direct and indirect drive mode to compress the targets.

In a *pulsed-power* system the electrical energy stored in capacitors is discharged in about 100 ns through a specially designed hohlraum (such as a cylindrical wire array) containing a fuel target. The strong axial current passing through this hohlraum produces a strong electric field, which in turn produces a strong azimuthal magnetic field and an inward radial force capable of compressing the fuel in the target to thermonuclear ignition conditions. The *Z-machine* at SNL used this Z-pinch principle with current discharges of some 30 MA to produce plasmas of several billion degrees but not the ignition of plasma (64). This technology opens the way to produce fusions of hydrogen atoms with heavier atoms such as lithium and boron without producing neutrons (Table 1).

A successful ICF mini-explosion vaporizes the target and hohlraum, and the fusion chamber must be cleared from debris before the next shot. With 250 MJ of energy liberated during each shot, a practical 1 GWe base-load inertial fusion power plant with 40% thermal efficiency and 10% power recycle would require about 10 shots each second. This is an extraordinary requirement, considering powering, discharge and possible cooling of driver, time required for introducing and aligning fuel targets within the chamber, and clearing of the chamber from the products of fusion reactions. Pulse-power drivers can liberate tens of GJ of energy during each shot and this energy must be safely and efficiently removed with minimal damage to the materials of fusion chamber.

Fuel Target Ignition. The design of fuel targets can vary, depending on the driver and method of ignition, but they are typically spherical shells containing solid and low pressure gaseous fuels (Fig. 8b). The outer shell of the target consists of an ablator, the concentric inner shell is made of a solid (DT) fuel, and within this shell is placed the gaseous (DT) fuel for initiating thermonuclear reaction. The ablator shell is made of low-Z materials (C, Be) for optimum heating and the target containing the fuel shell is introduced into the fusion chamber at a cryogenic temperature to minimize the work of compression.

The simplest method of igniting fuel in the target is through the process of *hot-spot ignition* as illustrated in Figure 8a. Hot-spot ignition requires the creation of a small central mass of fuel that is heated to the mean temperature of about 10 keV to initiate fusion for burning the rest of the fuel. The entire process takes about 100 ps. In the experiments this temperature has been achieved, but the simultaneous achievement of this temperature and density of 10^6 kg/m^3 has not yet been accomplished. Asymmetric compression produces the Rayleigh-Taylor instability and the interaction of the driver with the surrounding plasma can produce fast electrons that penetrate and preheat the target, both of which degrade the quasi-isentropic compression process (see below). The hot-spot ignition has been the main route to inertial fusion and requires compression symmetry to avoid the hydrodynamic instability. A target energy gain of $G \geq 10$ is required for demonstrating full burn propagation (50).

In addition to the hot-spot ignition, three other methods have been proposed to ignite the fuel within the target. These are the fast ignition, shock ignition, and Z-pinch or magnetic ignition. *Fast ignition* decouples target compression and hot spot formation. It still requires fuel compression to at least 30 kg/m^2 (65) to keep the ignition energy low, but it relaxes the speed of compression and compression symmetry and offers the possibility to ignite a pure deuterium fuel through a

localized DT seed. The target compression is still being accomplished by the traditional direct or indirect driver until the implosion reaches the maximum density. Then a second ultrashort (10–100 ps) laser pulse of ultrahigh petawatt power is activated that, after boring a hole in the plasma, guiding the beam through a cone inserted into the fuel target, or converting the laser or ignitor pulse into an intense electron or ion beam, provides its energy to the compressed fuel for initiating fusion (50,66). Fast ignition involves extremely high energy-density physics and picosecond petawatt lasers (67) that are becoming available in high energy laser facilities such as OMEGA, NIF, PETAL, and FIREX. The principles of fast ignition were first demonstrated at the Institute of Laser Engineering in Osaka, Japan (68). Hot-spot ignition and fast-ignition are the main ignition modes for the indirect mode (50).

Shock ignition is usually associated with the direct drive and is a method for minimizing the driver energy requirement. Here, rather than using a separate, high intensity, ultrashort-pulse laser to heat the central spot as in fast ignition, a short and high intensity "spike" is added to the end of the main drive pulse shape to launch a very strong shock into the fuel. The inward-propagating shock collides with the outward-propagating shock from the central spot, which increases the pressure and triggers ignition of the central spot. This has been demonstrated in the experiments involving the OMEGA laser at LLE (69). Shock ignition should be able to achieve gains exceeding 100 at laser energies smaller than 500 kJ (70).

Z-pinch ignition is being developed at Sandia National Laboratories (SNL) and employs pulsed-power drive integrated into the *Z*-machine (71). This machine can store some 30 MJ of energy and when discharged through Marx generator electrical circuits can produce 15–30 MA of current in 10–600 ns current pulses. When such a current is passed through a specially designed DT fuel target it can produce magnetic fields of hundreds of teslas that compress the fuel to gigabars of pressure. The Z-pinch driver can use large targets and thus has the potential to produce high gains and energy yields (400 MJ). It is more efficient than the laser driver (Table 3), can achieve very high compression temperatures (several billion degrees), and is being considered as a viable option for developing future IFE plants (72,73). The development of Z-pinch technology intensified in recent years with *magnetized linear inertial fusion* (MagLIF) concept, following the failure at NIF to produce fuel ignition with the indirect-drive laser system (74). In MagLIF, the magnetic force produced by the current discharged from the Z-machine is used to implode a gas-filled and premagnetized cylindrical target, and when the implosion of the cylinder is initiated a laser beam preionizes and preheats the gaseous fuel in the interior of the cylinder. This process was demonstrated in the laboratory with a cylindrical target containing deuterium gas

Table 3. **Reference Examples of Drivers, Targets, and Fusion Chamber Walls (50)**

Driver	Electrical efficiency (%)	Energy (MJ)/ repetition rate (Hz)	Target type	Target gain *G*	Chamber wall
DPSS laser	16	1.8–2.2/16	indirect	60–90	solid
KrF laser	7	0.5–2.0/10	direct	100–250	solid
heavy ion	25–45	1.8–3.3/5	indirect	90–130	liquid
pulsed power	20–50	33/0.1	magnetic direct	300	liquid

precompressed by the 10 T axial magnetic field. A laser of 1 TW power and the Z-machine discharging 19 MA current in 100 ns were then employed to produce 3 keV (35×10^6K) stagnation temperature and about 10^{12} DD neutrons (75).

Magneto inertial fusion (MIF) describes a class of fusion systems where the magnetic fields are first used to compress fuel targets and then lasers or particle beam are employed to further compress the targets to fusion ignition conditions. MIF is a hybrid between MCF and ICF approaches and allows a wide range of driver-target combinations, such as the direct-drive laser implosion of targets, implosion of targets with plasma jets, field reversed configuration, MagLIF discussed above, etc. MIF can access 1–1000 Mbar pressures and magnetic fields of hundreds of tesla, with plasma densities ($10^{25}\,m^{-3}$) that are intermediate between those of MCF ($10^{20}\,m^{-3}$) and ICF ($10^{31}\,m^{-3}$). In comparison to classical ICF, MIF driver power requirements and velocities of compression are reduced, compression times are increased, and with the possibility of producing GJ energy yields lower repetition rates (0.1–1 Hz) can be used (76).

All of the fuel ignition concepts considered above are supposed to ignite only a small fraction of the fuel in the center of the target to initiate fusion reactions, with the thermonuclear burn subsequently propagating into the bulk of the fuel and consuming the rest of the fuel before the target disintegrates. This process has, however, not yet been fully demonstrated in the experiments and remains today the main obstacle for claiming the scientific feasibility of controlled inertial fusion. One-dimensional modeling simulations show that there are definite energy utilization advantages of fast ignition, shock ignition, and KrF lasers (77).

The inertial confinement fusion is also prone to instabilities; to those associated with the target density nonuniformity and to those caused by laser radiation which produces *parametric instabilities*. The driver beam-target surface interaction phase determines the success of the compression stage, since the microscopic and macroscopic illumination nonuniformities can cause instabilities that render this process ineffective. Macroscopic instabilities can be controlled by using many beams, but then this makes such systems very expensive and technologically challenging. As in MCF, the Rayleigh-Taylor instability occurs when there are two different density material layers pushing against each other. In ICF, the hot ablated material of the capsule expands outwardly and pushes against the colder nonablated target material and any deviation from smoothness in either the target or laser light causes the ripples at the interface of the layers with different densities to grow and destroy the compression process. The incoming laser radiation interacts with the outgoing blown-off plasma and creates a wave whose high density on the crests reflects the incoming light and thus the incoming and reflected waves interfere constructively, leading to more incoming light reflection and weakening of energy delivery to the target. The Stimulated Raman Scattering (SRS) instability is caused by the electrons accelerated by the plasma wave (*electron plasma wave*) because these *suprathermal electrons* preheat the DT fuel and degrade the compression process. The Stimulated Brillouin Scattering (SBS) instability is produced by the ion acoustic wave generated by the acoustic vibration of the medium caused by the variation of the beam's electric field. Both SBS and SRS can produce very strong (hundreds of tesla) magnetic fields. These and other instabilities can, however, be minimized by shaping the driver pulses with ever increasing intensities and using high frequency lasers whose beams

penetrate more deeply into the collisional dense plasma. The challenge in igniting the thermonuclear fuel resides with high fuel compression and highly symmetric spherical implosion.

The ion beam targets are similar to the laser targets, with the ion range or penetration depth being a function of mass and kinetic energy. The range decreases with increasing mass and increases with kinetic energy, and since it is easier to focus ions at higher kinetic energies and with larger masses the current emphasis is on heavy-ion (Cs or Pb) fusion rather than on light-ion (Li) fusion. The primary difference between the laser and ion beam drivers lies in the physics of beam-target interaction and conversion of beam energy into radiation. Limited data show that the ion-beam indirect drive can produce gains as high as 130 at 3 MJ. The heavy-ion fast ignition requires different accelerators and is currently under study in both the United States and abroad (50,65).

Current ICF targets are made by hand and cost several thousand dollars each, and their cost for use in fusion reactors will depend on many factors (78,79). Projected target yields range between 100 MJ for laser drivers to 10 GJ for pulsed power drivers (50). The direct-drive targets are coupled to laser-driven drivers, whereas the indirect-drive targets employ hohlraums and are coupled to laser, heavy-ion, or pulsed-power drivers. The fuel capsule design must include considerations whether the hot-spot ignition, fast-ignition, shock-ignition, or Z-pinch-ignition is employed.

The products of fusion reactions do not only depend on the type of fuel used but also on the materials employed to contain the fuel. The ablating shell of the target can be made of plastic, carbon, beryllium, or some other low-Z material, whereas the hohlraum containing the target can be made of gold, lead, or other high-Z material. A variety of different ions and a radiation spectrum can be therefore produced in an inertial fusion chamber and will have to be considered when designing the chamber and its associate energy removal system. After each thermonuclear burn the chamber must be cleared from debris and Table 3 gives an indication of what types of fusion chambers may be compatible with different drivers and are discussed in Section 3.

Laser, Heavy-Ion, and Pulsed-Power Drivers. Currently, there are four main ICF drivers being considered for delivering megajoules of energy in several nanoseconds: diode-pumped-solid-state-lasers (DPSSLs), KrF gas lasers, heavy-ion beams from accelerators, and pulsed-power drivers (50). The outstanding issues remaining with these drivers are the quality, reliability, maintainability, and availability for providing some 10 shots per second for many years of operation.

High power lasers are described in the book of Injeyan and Goodno (80). Solid state and gas lasers are two classes of high power lasers suitable for ICF and they are distinguished by the laser medium used. In a solid-state laser, the medium is an insulated crystal or glass, and the impurity ions are the active or gain medium with the properties that allow the energy supplied (with flashlamps or lasers) to drive the electrons in the active medium into excited states from where they rapidly decay to one or more metastable states and remain there for a sufficient time to create a population inversion. The decay of electrons from a metastable energy level to the ground state produces the emission of a coherent (laser) light. Neodymium-glass (Nd:glass) laser lases at $\lambda = 1.06\,\mu m$ and higher harmonics, KrF

gas laser lases at $\lambda = 0.25\,\mu m$, CO_2 gas laser lases at $\lambda = 10.6\,\mu m$, and so forth. Higher frequencies produce higher energy and are more resistant to instabilities, but lower the coupling efficiency. The flashlamp-pumped Nd:glass laser working with the third harmonic (3ω) is employed at both NIF (62) and LMJ (58,81) for single-shots target studies only, because the waste heat generated in large glass disks has to be removed before reusing the disks. These two facilities are very similar in design but differ in details. The OMEGA laser system at LLE in Rochester has 60 beams and can operate up to 30 kJ of energy and 60 TW of power in the direct-drive configuration mode, but so far has not been able to achieve the breakeven condition (82).

The NIF facility at LLNL (Fig. 10) was commissioned in 2009 and during the National Ignition Campaign (NIC), ending in 2012, delivered more than 300 shots with up to 1.8 MJ of energy per shot (83). NIF's laser system consists of 192 beams that are directed on fuel targets of about 1 mm in size contained in about 1 cm-sized hohlraums. A typical hohlraum design and an experimental hohlraum before and after being irradiated with laser beams in the fusion chamber are shown in Figure 11. The fuel targets are cooled to cryogenic temperatures before being irradiated with laser beams and because the hohlraum is only 25% efficient at converting the ultraviolet beams into X-rays, the target is irradiated with only 450 kJ of energy. The NIF campaign did not achieve breakeven ($G = 1$) as projected, but it did achieve alpha heating of the targets during the compression process and yield significant advances in laser and target development and some 10^{14} neutrons at 1.4–1.6 MJ drive energy (50,62,65). The breakeven requires the production of more than 5×10^{17} neutrons (84).

The KrF gas laser contains argon, krypton, and less than 1% fluoride. It is pumped by electron beams and is suitable to illuminate direct-drive targets because of its ultraviolet wavelength of $\lambda = 0.248\,\mu m$. It has a low efficiency (about 8% compared to 10% for 3ω DPSSLs) and thus requires high gains of more than 140 and direct-drive energy of 2.4 MJ. This energy can be reduced by employing the

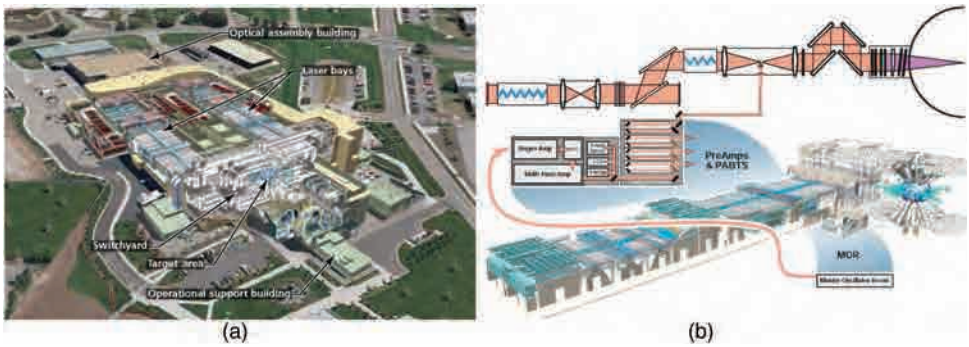

Fig. 10. (a) The National Ignition Facility showing two laser bays, switchyard, target chamber area, operational support building, and optics assembly building (62). The facility's optics consists of some 40,000 pieces and 60,000 points controlled by two million lines of software (84). (b) NIF's laser system consists of flash lamps for powering the Nd:glass lasers, amplifiers, and optics for focusing 192 beams on fuel target (85). (Courtesy of Lawrence Livermore National Laboratory.)

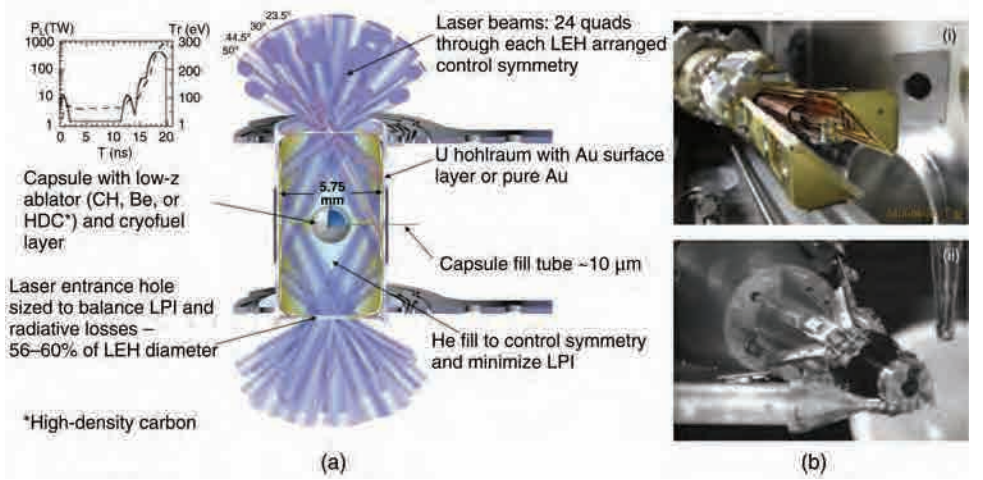

Fig. 11. (a) NIF's fuel target design (62). (b) Cryogenic layered target shot on September 29, 2010 before and after being shot in the NIF target chamber (84). (Courtesy of Lawrence Livermore National Laboratory.)

laser with shock ignition, or with fast ignition where the driver energy can be reduced from the conventional direct-drive of 2 MJ to 400 kJ. The heat generated in KrF laser can be removed by a circulating coolant and appears to have large advantages when used with both fast ignition and shock ignition targets. The KrF lasers developed at NRL have operated continuously for 10 h at 2.5 Hz (86) and it is projected that a 500 kJ KrF laser system can be built with laser modules of 20 kJ and attain the driver efficiency of 7% with repetition of 5–10 Hz (50).

The DPSSLs can be used for sustaining high repetition rates at high efficiencies. An example of DPSSL is the Nd:YAG laser that can be used with frequency doubling ($\lambda = 0.532\,\mu m$) or quadrupling ($\lambda = 0.263\,\mu m$) and can operate close to 20% efficiency (50). DPSSLs can be employed to drive either the direct-drive or indirect-drive targets, and when integrated into laser modules have been proposed to drive the Laser Inertial Fusion Energy (LIFE) plant (79). China, Japan, and Russia are pursuing similar laser developments, including the Yb:YAG ceramic lasers (50,87). IFE power plants call for robust laser drives with modular architectures and the diode laser arrays are being evaluated to fulfill this requirement. The projected operational lifetimes of such arrays exceed 35 years at the 10 Hz repetition rate (88).

Heavy-Ion Fusion (HIF) drivers are the accelerators of particles and there are many design options, but the most promising for fusion are induction and radio-frequency (RF) accelerators. Russia and Germany are building HIF facilities and the United States is planning to resume the development of this technology. Heavy ions can deliver tens of MJ (and higher) of energy that can not only penetrate the fast ignition targets and their hohlraums but also the liquid films protecting the fusion chamber walls. Heavy ion beam driver accelerators have energy efficiency of 30–40% (89) but the current fusion ion beam drivers are less than half as efficient as these. Heavy ion beams possess high pulse rate, high reliability, integration with diverse target ignition options, beam energy of 100 kJ, and are thus

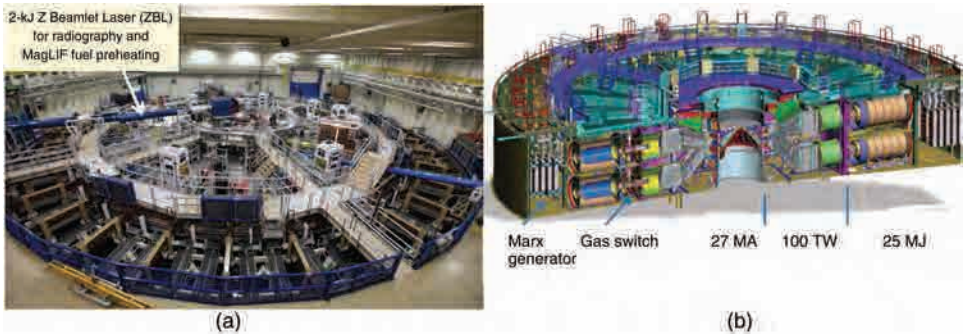

Fig. 12. (a) The Z-machine at Sandia National Laboratories with the Beamlet Laser for preheating fuel targets. (b) Cross section of Z-facility showing the constituent parts (92). (Courtesy of Sandia National Laboratories.)

considered as viable candidates for future IFE power plants. It is anticipated that the HIF progress will lead in two decades to the construction of a 2–3 MJ HIF ignition test facility with 5 Hz driver (90).

The *pulsed–power* approach to IFE intends to utilize currents in excess of 50 MA to generate high magnetic pressures to compress and heat magnetized and preionized DT fuel contained in cylindrical targets of about 1 cm in size. The Z-machine at SNL (Fig. 12) was developed for this purpose and is capable to store 22 MJ of energy and discharge 27 MA of current in 100–200 ns pulses, producing 1000–5000 T magnetic fields and 1–100 Mbar pressures. It is envisaged that the pulsed-power will have relatively low cost and high efficiency and it promises to be scalable for use in IFE plants where the anticipated fuel and power delivery to the fuel is by the Recyclable Transmission Line (RTL) (50). The performance of this line and of thick-liquid-wall protecting the metal wall of reactor chamber from fusion reaction products have not yet been adequately investigated (73,91).

There are thus different approaches to ICF, involving different combinations of drivers, targets, and fusion chamber walls (Section 3). The driver-target can be integrated into the direct-drive, indirect-drive, and magnetized-drive configurations, and the chamber can be constructed from solid- and liquid-protected walls facing the products of fusion reactions. Which of these combinations are technologically and economically feasible remains, however, to be seen and will likely take several decades before an IFE demonstration plant can be built.

3. Fusion Reactor Technology

3.1. Roadmaps to Fusion Energy. Roadmaps to fusion energy suggest further research on plasma confinement issues and the development of fusion reactor technologies leading to the design and construction of *demonstration reactors* (DEMOs). The near-term research phase requires achieving ignition and the development of technologies for tritium breeding and energy exhaust from the reactor. ITER is the most visible intermediate tokamak machine scheduled to produce net fusion power output by 2035, and the Wendelsten-7X is the

most visible stellarator machine scheduled to produce nonburning plasma conditions during the same time frame. Z-pinch, NIF, LMJ, and similar intermediate inertial confinement plasma projects are still striving to demonstrate fusion breakeven. The International Fusion Materials Irradiation Facility (IFMIF) was initially scheduled to be built in Japan to develop and test materials for withstanding high heat and neutron fluxes typical of DEMOs and commercial reactor environments (93,94), but currently only a prototype of this facility, called IFMIF EVEDA (Engineering Validation and Engineering Design Activities), is being built in this country.

DEMOs will be the scaled versions of commercial fusion reactors and several countries have active research programs dealing with the design and development of these technologies. The tokamaks are the European DEMOs A,B,C,D,1,2, American ARIES-AT, Chinese Fusion Engineering Test Reactor (CFETR), Korean K-DEMO, and Japanese DEMO-CREST (95). The stellarators are Japanese Force Free Helical Reactor (FFHR2) based on LHD, German HELIAS based on W7-X, and American ARIES-CS. Table 4 summarizes the available design and operational parameters of these reactors aimed at building large-scale Fusion Power Plants (FPP) and are further discussed below.

A similar roadmap leading to the development of ICF technologies was commissioned by the U.S. Department of Energy before committing to any specific DEMO. This would require the demonstration of ignition, gain >10, driver life with $>10^7$ pulses, automation of target fabrication, and the development of chamber design, including neutron shielding, tritium breeding, and materials survival, for laser, heavy-ion, and pulsed-power systems (50). Following the integrated research experiments, there would be two additional major facilities: a Fusion Test Facility (FTF) for demonstrating repetitive DT target shots exceeding 10^5 per year and a DEMO that would bring the ICF to the prototype demonstration level. The goal is to focus on the development of a single DEMO. Table 5 provides the design parameters of some ICF power reactors that are also discussed below.

The fastest path to plasma ignition favors magnetic confinement fusion because it leads the inertial confinement fusion development. The tokamak reactor concept is ahead of the stellarator concept, but the latter offers steady-state operation and may be the best choice for commercial fusion power plants. Direct and magnetized target ignitions appear to offer the best chances leading to IFE power plants. But there still remain some outstanding physics issues of plasma confinement and engineering solutions for reliable superconducting coils and the associated cryogenic systems, vacuum systems, materials for plasma facing components, multi-MW auxiliary heating systems, plasma fueling systems, remote handling of activated components, plasma energy conversion systems, precision targeting of ICF fuel targets, etc. We will first discuss ITER and materials and coolants for blankets and divertors and then follow with magnetic and inertial confinement fusion reactor technologies.

3.2. International Thermonuclear Experimental Reactor. In 1987, the European Union, Japan, Soviet Union, and the United States agreed to build a large fusion energy facility that became known as the ITER (36,96). After many design modifications and negotiations where to construct such a facility it was decided to build the reactor in Cadarache, Southern France. The IFMIF was

Table 4. **Parameters of Some Tokamak and Stellarator Demonstration Reactors**

Parameter	ITER	DEMO A	DEMO B	DEMO C	DEMO D	DEMO 1	DEMO 2	ARIES-AT	CFETR	KDEMO	HSR5/22	FFHR2	ARIES-CS
Reactor concept	Tokamak	Tokamak	Tokamak	Tokamak	Tokamak	Tokamak	Tokamak	Tokamak	Tokamak	Tokamak	Stellarator	Stellarator	Stellarator
electrical power (GWe)	0.15	1.55	1.33	1.45	1.53	0.5		1.00	0.1	0.7	1.62		
fusion power (GW)	0.5	5.00	3.6	3.41	2.53	1.8	3.25	1.7	0.2	3	3	3	2.44
Q_{fus}	10	20	13.5	30	35	36	25	47	2	20	32	30	1.15
plasma volume (m^3)	837					2502	2217				1407	1744	444
pulse length (s)	1000					5400	steady		612	300	steady	steady	steady
major radius (m)	6.2	9.55	8.6	7.5	6.1	9.0	7.5	5.2	5.7	6.8	22	16	7.75
minor radius (m)	2.0	3.18	2.8	2.5	2.03	3.0		1.3	1.6	2.1	1.8	2.35	1.7
toroidal field on axis (T)	5.3	7.0	6.9	6.0	5.6	5.24	5.6	5.8	5	7.5	5	5	5.7
average beta β (%)	1.8					2.6	3.8		2		4	2	6
plasma current (MA)	15	30.5	28.0	20.1	14.1	20.0	22	13	10	12	11		
ion temperature (keV)	10	22	20	16	12	27.4	34.7	18		20	16	18	6.6
plasma density (10^{20} m^{-3})	1.0	1.1	1.2	1.2	1.4	0.8	1.22	1.0			3	5	4
neutron load (MW/m^2)	0.8	2.2	2.0	2.2	2.4	0.9	1.9	3.3	0.5	2.9	1.7	1.5	5
neutron damage (dpa)	2					20	20						
neutron fluence (MWy/m^2)	0.07												
first wall heat flux (MW/m^2)	0.3	0.6	0.5	0.45	0.5	0.5	0.5	0.45			0.4		0.6
divertor heat load (MW/m^2)	<10	15	10	10	5	20	20	5	10	10	10	2.3	10
plant efficiency (%)	30	31	37	42	60			59			46		
blanket coolant	H_2O	H_2O	He	Li-Pb/He	Li-Pb	He/H_2O/LiPb	He/H_2O/LiPb	LiPb	H_2O	H_2O			LiPb/He
T_{in}/T_{out} (°C/°C)	100/150	285/325	300/500	480/700 300/480	700/1100			700/1100	300/500		610/		500/710 368/486
divertor coolant	H_2O	H_2O	He	He	Li-Pb			Li-Pb	H_2O	H_2O	—	flibe	He
T_{in}/T_{out} (°C/°C)	100/150	140/167	540/720	540/720	600/990			700/1000		290/315	—		580/730
breeder	—	Li-Pb	Li_4SiO_4	Li-Pb	Li-Pb			Li-Pb	Li_4SiO_4	Li_4SiO_4	Li-Pb	flibe	Li-Pb
tritium breeding ratio	—	1.06	1.12	1.15	1.12	1.1	1.1	1.1	1.2	1.2	1.1	1.1	1.1
blanket struct/coolant liner	SS	SS	SS	SS/SiC	SS/SiC	RAFM/		SS/SiC	RAFM	RAFM	V5Cr5Ti	FS	FS
divertor struct/coolant liner	SS	SS	SS	SS	SS/SiC	RAFM/		SS/SiC			V5Cr5Ti		
divertor armor material	W	W	W	W	W			W			—		W
power conversion	—	Rankine	Rankine	Brayton	Brayton			Brayton			Brayton		Brayton

European Union: ITER is a reference tokamak design (36,96,97); DEMO A,B,C (98), DEMO 1 is ITER-like and DEMO 2 is advanced steady-state tokamak (99–101). Germany: HSR5/22 is based on W7-X (102,103). Japan: FFHR2 is based on LHD (104). Republic of Korea: K-DEMO (105,106). China: CFETR is similar to ITER but can produce tritium (107,108). The United States: ARIES-AT and ARIES-CS (109,110).

Table 5. **Parameters of Some Inertial Fusion Power Plant Designs**

Parameter	Sombrero	HAPL	LIFE	Osiris	KOYO-F	HYLIFE-II	Z-IFE
driver							
type	KrF	DPSSL/KrF laser	DPSSL laser	HI	Yb-YAG laser	HI induction linac	Z-pinch
beams	60			12	32	12	—
energy (MJ)	3.4	5	2.2	5	1.1	5	100
pulse (Hz)	6.7		16	4.6	16	6.4	0.1
efficiency (%)	7.5		18	28	11.4	33	60
target							
type of drive	direct	direct	indirect	indirect	direct FI	indirect	indirect
gain	118		64	86	165	70	100
yield (MJ)	400	370	125	432	200	353	20,000
chamber design							
type	dry-wall	dry-wall	dry-wall	thin-liquid-wall	thin-liquid-wall	thick-liquid-wall	thick-liquid-wall
first wall material	C/C composite	SiC/SiC_f composite	ODS-FS	woven C fabric	SiC	304 stainless steel	C/C composite
first wall protection	Xe gas at 0.5 torr	magnetic	Xe gas	flibe	Li-Pb	flibe jet array	flibe jet
first wall radius (m)	6.5	4.5	6	3.5	3	3.3	6
first wall life (fpy)	5			1.8			40
first wall coolant	Li_2O granules	LiPb	Li	flibe	Li-Pb	flibe	flibe
blanket structure	C/C composite		ODS-FS	C/C composite	SiC	stainless steel	C/C composite
blanket coolant	Li_2O+0.2 MPa He		Li	flibe	Li-Pb	flibe jet array	flibe
breeding material	Li_2O granules	LiPb	Li	flibe	Li-Pb	flibe	flibe
tritium breeding ratio	1.25	1.2	1.3	1.24	1.3	1.17	1.1
neutron FW load (MW/m^2)			3	9	5.6		
vacuum vessel	C/C composite			C/C composite		stainless steel	
power system							
type	Rankine	Brayton	Rankine	Rankine	Rankine		Rankine
intermediate coolant	Pb	flibe with Be	—	Pb	—	—	—
secondary coolant	water/steam	He	water/steam	water/Steam	water/steam	water/steam	water/steam
fusion power (MW)	2677		1970	1987		2245	2000
thermal power (MW)	2891		2570	2504	3664	2675	
gross electric power (MW)	1359		1250	1127	1519	1150	
net electric power (MW)	1000		1000	1000	1200	1000	
plant thermal efficiency (%)	47		49	45	41.5	43	

Osiris and Sombrero (111), HAPL (112), HYLIFE-II (113,114), KOYO-F (115,116), LIFE (79), Z-IFE (73,117).
FI: fast ignition.

projected to be built in Japan (97), but as noted above only a prototype of this facility IFMIF EVEDA is currently being built (93). The current ITER partners (China, the European Union, India, Japan, Republic of Korea, Russian Federation, the United States) are providing reactor components and the construction of the reactor was projected to be completed by 2025 (118). It is projected that by 2035 ITER will achieve ignition by burning deuterium and tritium plasmas (99).

The plasma volume of ITER is 10 times larger than that of JET, which will improve the magnetic confinement and make available more α-particle energy for heating the plasma. Recall that the neutrons in DT reactions carry 80% of the fusion energy that cannot be used to heat the plasma, whereas the remaining energy carried by α-particles can because the ions can be confined by the magnetic field. This requires a Q_{fus} greater than five for the fusion heating power to be greater than the external heating power, and a Q_{fus} of 10–20 when taking into consideration heating power and electrical system efficiencies and power recirculation fractions of less than 20%. ITER was designed to operate with $Q_{\text{fus}} \geq 10$ and aims to produce 500 MW of fusion power during 300–1000s of continuous operations. The cutaway views of the reactor, showing the locations of poloidal, vertical, and toroidal magnetic field coils, blanket, divertor, vacuum vessel, and various ports for plasma heating, fuel injection, and diagnostics, are shown in Figure 13. The design parameters of ITER are summarized in the first column of Table 4 for comparison with fusion power reactors discussed below.

The control of impurities in ITER and other tokamaks will be achieved by employing open magnetic field lines residing on the outer edge of the plasma volume. These lines intersect at an X-point and belong to the *scrape-off-layer* (SOL) of plasma volume whereby all of the ions contained in this layer are routed to the divertor where they deposit their energies (Fig. 14a). The main function of the diverter is to remove α-particles, unburnt D and T ions, and impurities originating from plasma–wall interactions. The blanket and associated shields have the threefold purpose of removing the energy of neutrons and plasma ions crossing

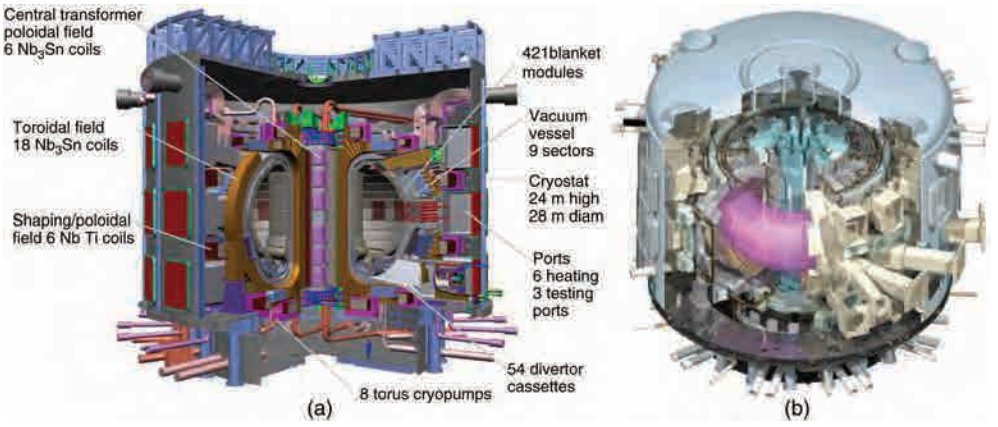

Fig. 13. (a) Cutaway of ITER showing the size relative to a human and the magnets surrounding the reactor chamber. The D-shaped cross section of plasma chamber with the divertor at the bottom, shaping poloidal field coils, vertical stabilization coils, and central solenoid coils, are clearly visible (36,96). (b) ITER's confinement structure. (Courtesy of ITER Organization.)

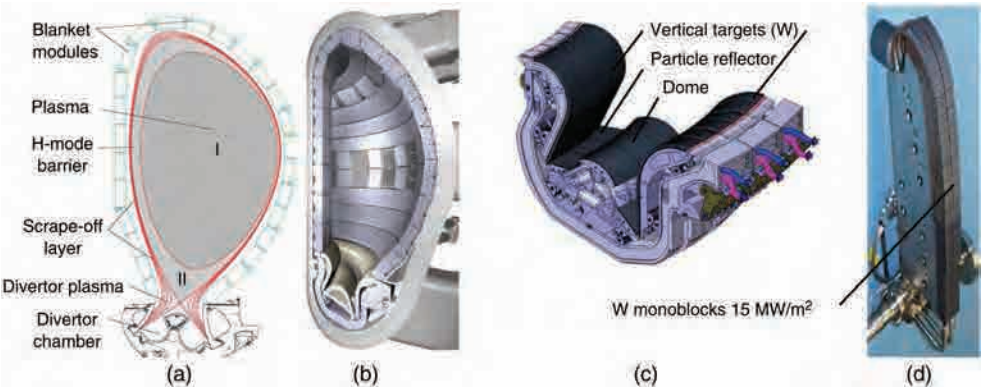

Fig. 14. (a) ITER's four principal regions where dominant physics differ. The separatrix forms the boundary between regions II and III and possesses a point of null poloidal field strength where it has the X crossing. The four regions are the core, edge pedestal region just inside the separatrix, scrape-off layer plasma just outside the separatrix, and the divertor chamber plasma region. (b) ITER's fusion chamber consists of 420 blanket and 54 divertor modules, which can be periodically replaced. The first wall is built from Be and Cu-alloy heat sink panels and the blanket modules are cooled with water at 150°C. (c) The divertor's first wall is protected with tungsten and the cassette modules are cooled with water or helium jets at high pressure. (d) The divertor cassette armors employ tungsten mounted on monoblocks (36,96,123). (Courtesy of ITER Organization.)

the surface of the plasma volume and converting this energy into useful forms, breeding tritium in several breeding blanket modules to test different blanket designs, and protecting the superconducting magnets and personnel from neutrons and radiation (119–122). ITER requires an external supply of tritium and its plasma facing components will be cooled with water at about 150°C.

The D-shaped cross section of ITER's reaction chamber with the divertor located on the bottom of the chamber is shown in Figure 14b. The side and upper parts of the chamber are made of 420 *blanket modules* and the divertor is constructed from 54 *divertor cassettes*. These are the *plasma facing components* (PFCs) of the reactor whose sides exposed to plasma incorporate protective armors, called the *first wall* of the reactor. During the normal operation of the reactor the blanket modules absorb the energies of about 97% of fusion neutrons, radiation, and some ions escaping from the plasma volume. For ITER, the maximum anticipated neutron and heat fluxes on the first wall of the blanket are less than $1\,MW/m^2$, whereas the heat flux on the divertor surfaces can be as high as $10\,MW/m^2$. The DEMOs are expected to operate with neutron fluxes of up to $2\,MW/m^2$ and heat fluxes in the divertor up to $20\,MW/m^2$ during the steady-state and $100\,GW/m^2$ during millisecond plasma disruptions. These loads require advanced materials and solutions for PFCs.

The ITER's typical blanket module is constructed from 15 cm thick front panel consisting of 1 cm Be armor protection, 1 cm Cu to diffuse heat load, and about 10 cm thick back steel structure. The first wall panels will be damaged by heat and neutron fluxes and will require frequent replacement. Beryllium has the advantage of being a good thermal conductor and a low-Z material that is nonreactive with hydrogenic isotopes escaping from the plasma volume, but is

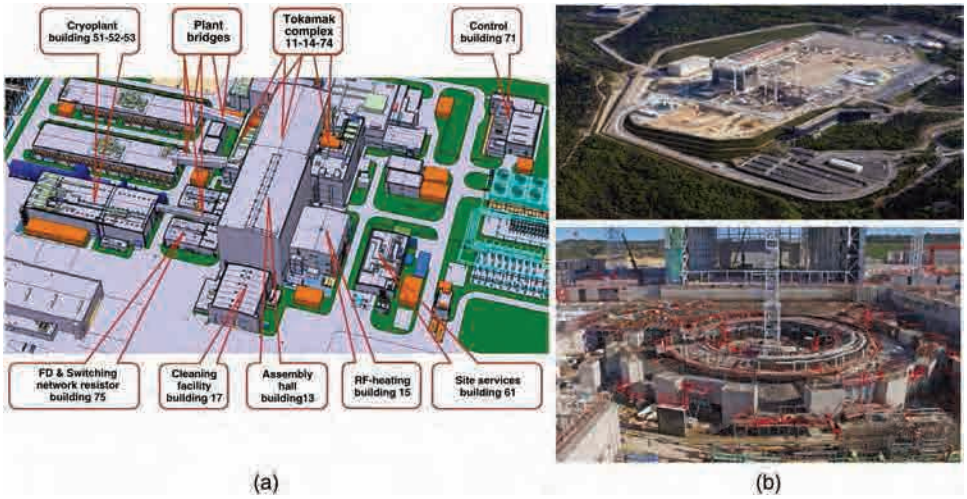

Fig. 15. (a) Planned layout of the ITER site in Cadarasche, France. (b) View of the construction site and reactor's foundation in April, 2016. (Courtesy of ITER Organization.)

toxic and easily sputters. The current ITER design of divertor cassettes (Fig. 14c) will support armor built from the high thermal conductivity tungsten mounted on monoblocks (Fig. 14d) where the peak heating locations exist. CFCs are not employed in this design because they deteriorate substantially under neutron irradiation and carbon reacts chemically with tritium and readily absorbs this fuel. Both C and W are employed for their good thermal shock and fatigue resistances. The structures of both the blanket and the divertor are made from the austenitic stainless steel and are cooled by water. Only about 1% of tritium will be burned in the reactor and the rest will be exhausted and recycled, and it is anticipated that some of the fusion energy produced will be employed to power the magnets, neutral particle injectors, and other auxiliary systems.

The mission of ITER is to improve plasma confinement and spur the development of technology for building demonstration reactors, and because the plasma instabilities can produce *plasma disruptions* with high heat loadings (124), the ITER campaign aims to find the best way to avoid disruptions by operating the reactor within the plasma stability limits. The instabilities called *edge-localized modes* (ELMs) and *resistive-wall modes* (RWMs) tend to dump plasma in preferred locations and are planned to be controlled in ITER by placing coils in strategic locations inside the chamber. The construction of ITER started with the preparation of site in 2007 and 10 years later several key buildings and reactor's foundation have been built (Fig. 15).

3.3. Materials and Coolants for Blankets and Divertors. Fusion power reactors will have to be designed for the neutron loads up to $2\,MW/m^2$ and heat loads up to $5\,MW/m^2$ on the first walls of blankets and heat loads up to $20\,MW/m^2$ on the divertors' plasma facing surfaces, while also managing millisecond energy releases from ELMs and maintaining the structural integrity from electromagnetic forces. When neutrons interact with the atoms of materials they produce atomic rearrangements or microstructural defects in the form of edge

dislocations, voids, vacancies, impurity substitutions, etc, that distort the lattice structure. These distortions lead to chemical, physical, mechanical, and geometrical changes of the materials that affect the material capacity to conduct heat, sustain mechanical and electromagnetic forces required for structural stability, and resist corrosive coolants and tritium breeding materials.

The effect of atomic collisions is measured in terms of the *displacements per atom* (dpa), or the number of times that, on average, each atom in the material is displaced from lattice by atomic collision processes. This damage increases with the service life of the material and during the operational life of ITER is not expected to exceed 5 dpa, whereas in a demonstration fusion reactor this damage in steels is estimated to be about 150 dpa for 5 *full power years* (fpy) of service when operating at temperatures 500–1000°C (125). The neutron damage to materials decreases rapidly from the first wall surfaces, such that in a steel blanket and 1 m from the first wall the neutron flux and nuclear power generation are already reduced by several orders of magnitude (126).

High energy neutrons can produce helium and hydrogen atoms that can coalesce into gas bubbles that grow and produce voids, swelling, and embrittlement of materials. In addition, neutrons can be absorbed by the atoms and produce transmutations or impurities that are radioactive. Transmutations are measured in *atomic parts per million* (appm) and they severely limit the life of some key elements commonly used for producing high quality structural materials (127). Cyclic loadings as in ICF and from ELMs can cause material fatigue and loss of ductility and strength and thus render the materials less resistant to mechanical, thermal, electromagnetic, and nuclear loads (128,129).

Future fusion power plants will have to incorporate low-activation and low tritium retention, good shock and thermal fatigue resistance over a wide temperature range, coolant corrosion tolerant, and high strength materials. Be and Pb can be used for neutron multiplication and the liquids Li, Li–Pb, Li–Sn, flibe and flinabe, and solids Li_2O, Li_4SiO_4, Li_2TiO_3, and Li_2ZrO_3 as tritium breeders, while the blanket coolants can be gases such as high pressure He and CO_2 and liquids H_2O, Li, Li–Pb, Li–Sn, flibe, and flinabe. The candidate structural materials for blankets are the reduced-activation ferritic/martensitic steels (RAFMs) in which Ta and W are alloyed to replace Nb and Mo in conventional steels, vanadium and niobium base alloys, and silicon carbide with silicon carbide fibres reinforced (SiC/SiC_f) composites. The blanket and shields must transform most (>95%) of the incident fusion energy into heat and shield the superconducting magnets from neutrons. The divertors are not envisaged to breed tritium and can employ similar structural materials and similar coolants as the blankets, but because their surfaces will be exposed to more intense and sustained fluxes of ions and impurities than those of the blankets they require special armor of refractory metals and ceramics to minimize wall erosion and tritium retention (130).

It is necessary that the exposure of materials to temperature is maintained above the metal's *ductile-to-brittle transition temperature* (DBTT) and below the *high temperature recrystallization* (RCT) regime whenever a stress is applied. The vital elements for building high strength steels are low-activation elements C, Cr, Fe, Si, Ta, V, and W used to produce RAFM steels and SiC/SiC_f composites. RAFMs such as EUROFER97and F82H can be used within the limited operating temperature window of 350 and 550°C, whereas the W- and V-base alloys Ta-8W-2Hf and

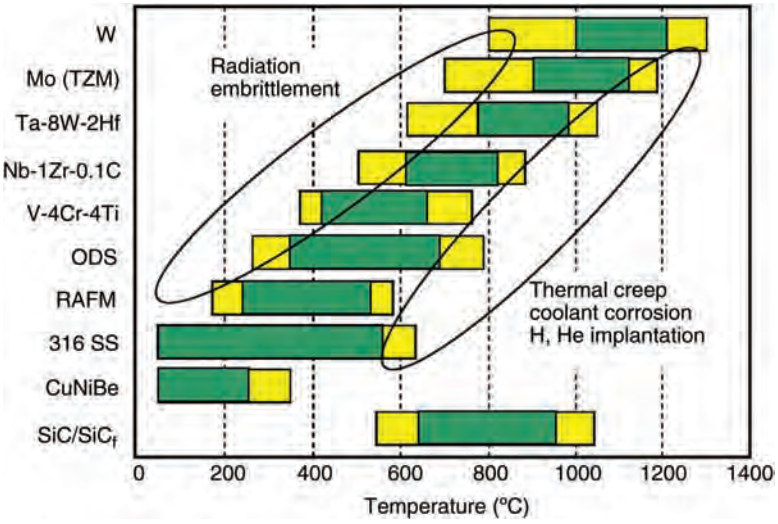

Fig. 16. Operating temperature windows of some fusion reactor materials with neutron-induced damage from 10 and 50 dpa. The minimum and maximum allowable operating temperature limits of these materials are delineated by embrittlement and thermal creep regimes. Green areas indicate safe and yellow areas marginal operating ranges. (Adapted from Reference 130.)

V-4Cr-4Ti can be employed below 1000°C. The oxide-dispersion-strengthened (ODS) ferritic steels (containing Ti-, Y-, and O-rich nanoclusters) provide significant strength and creep resistance to 700°C and more and can thus significantly improve the operating temperatures of steels (128,129,131,132). With the exception of V-alloys, even the refractories require additional improvements to reduce the accumulations of H, He, and radioactivity.

Figure 16 summarizes the operating temperature windows of materials capable of sustaining neutron irradiation levels up to 50 dpa. The material radiation embrittlement regime defines the lower temperature limits, whereas the thermal creep, coolant corrosion, and H and He implantation regime defines the upper temperature limits. Increasing neutron exposures of materials increase DBTT limits at low temperatures and decrease the upper operating temperature limits, while the irradiation creep and transmutation produce a significant decrease of thermal conductivity and thus the operating temperature window of SiC/SiC_f composites above about 10 MWy/m^2. The neutron displacements tolerances of materials do not necessarily correspond to their tolerances of H and He transmutations and radiation doses (130).

The RAFM steels and in particular the ODS steels and vanadium-base alloys are the candidate structural materials for future fusion reactors because they are resistant to helium embrittlement at high temperatures and suitable for a variety of coolant and tritium breeding options. The ferritic/martensitic steels are chemically compatible with He/Li–Pb, H_2O/Li–Pb, He/Li ceramic, and flibe/flinabe coolants/breeders, whereas the vanadium alloys can be used with Li/Li coolants/breeders. The refractory alloys are compatible with the liquid metals and salts, with the impurities in the coolants being of major concern for corrosion. The

chemical compatibility data of Li–Pb and Li–Sn mixtures with other potential structural materials appear to be lacking, but the promising candidates for Li–Sn cooled systems are V alloys and SiC/SiC_f composites (133). The SiC/SiC_f composites have significant safety and waste disposal issues, but can be employed with He/Li–Pb, He/Li ceramic, and flibe/flinabe coolants/breeders (134) operating at temperatures below about 1050°C (128).

The refractory metals Cr, Ti, V, and W and their alloys with Hf, Nb, Ta, and Zr are suitable for PFCs and are highly resistant to creep at high temperatures. Of these, tungsten has the highest melting point temperature (3422°C) and low physical sputtering yield, no chemical sputtering in hydrogen plasma, does not codeposit with hydrogen isotopes, possesses high thermal and shock resistant capacities, and is the preferred choice for the first wall and divertor target surfaces. Its shortcomings are that it loses ductility with temperature cycling from below and above DBTT and under neutron irradiation it suffers from H and He bubble formations that cause material swelling. Carbon has a good power handling and thermal shock resistance and preserves its shape under extreme temperature excursions, but its physical and mechanical properties degrade significantly under neutron irradiation. Fibre reinforcement improves its strength and was considered as the material of choice in ITER for the strike zone of the separatrix in the divertor (135), but was recently replaced with tungsten as noted above. The SiC/SiC_f composites have high thermal conductivities, but their high H and He generation rates and tritium absorption raise concerns for applications in neutron-intensive and tritium handling environments (136).

In very intensive radiation and particle environments such as IFE chambers, liquid metals lithium, gallium, tin, and their compounds flowing along the plasma facing metal walls can remove large heat loads (50 MW/m^2), but their high evaporation rates (especially Li) at high temperatures, high corrosion, adverse MHD effects, and safety considerations degrade their practicality. Liquid metals are affected by He bubble formation from alpha ions that may lead to liquid surface erosion and splashing and may damage the metal surface being protected. Plasma disruptions crossing the SOL layer and reaching the liquid metal surface can also disrupt the efficiency of fusion energy removal, whereas the first walls made of capillary porous systems with Li flowing within Mo, stainless steel, and W meshes could mitigate the effects of these disruptions (137).

The useful materials for neutron multiplication and tritium breeding are Be, Pb, and its compounds for the former and Li, Li–Pb, Li–Sn, and Li-base ceramic materials (Li_2O, Li_4SiO_4, etc) for the latter. These substances produce, however, copious amounts of H and He isotopes and cause large MHD pressure drops when used as the coolants. Tritium can diffuse rapidly through most materials and coolants, and thus its containment is difficult at elevated temperatures. Most of tritium (99% in ITER and 80% in DEMOs) in the plasma volume will not burn, however, and will be exhausted through the divertor and will have to be recovered.

The blanket modules of ITER are being built from beryllium, Cu–Cr–Zr alloy, and austenitic stainless steel (316 SS), because these materials are compatible with water for heat removal and able to resist modest neutron fluxes. The armor tiles of divertor are built from W to mitigate the effects of high ion fluxes and minimize tritium retention, whereas its substructure is built from the austenitic stainless steel (138). The coolant tubes are built from Cu–Cr–Zr alloy. Beryllium

has a low risk of plasma contamination, but its physical sputtering yield is high, is toxic, codeposits with tritium, and the neutron irradiation causes brittleness. The eroded carbon also codeposits with tritium and when it enters the plasma volume reduces the plasma quality. The materials of blanket and divertor depend on both their years of service and on their locations in the chamber (127).

Fusion reactor coolants should be compatible with tritium breeding in the blanket, removal of large steady-state and transient neutron and ion-generated heat loads in the blanket and divertor, remain compatible with structural materials of the reactor's chamber, produce minimal pumping powers, possess high thermal capacities, operate at high temperatures for maximizing the power plant efficiency, and satisfy the operational safety and practicability limits. The coolants being considered are water, helium at high pressures, and lithium-based liquid metals and molten salts. When judged in terms of material, functional, thermodynamic, and safety requirements, each of these coolants has positive characteristics and shortcomings. A high operating temperature of the coolant produces a high energy conversion efficiency, which implies a lower fuel cost and less generation of waste per unit of energy produced. This also demands more advanced materials for PFCs, blankets, and divertors than are currently available.

Water should be used whenever possible because of its good heat transfer characteristics, practicality, tolerable pumping power requirements, and nonreactivity with stainless steels, but it cannot be used with the low-activation refractory materials which require elevated operating temperatures (above 700°C for W) to avoid embrittlement. Vanadium- and niobium-base alloys may also produce substantial levels of corrosion in water, titanium alloys are not suitable because of hydrogen embrittlement, whereas the high nickel-base alloys are acceptable. The extraction of tritium from water is also difficult when it leaks into the coolant system (136). Water is very reactive with liquid metals and poses safety concerns in the event of blanket rupture.

Helium is inert and transparent to neutrons and integrates well with ceramic and liquid tritium breeders, but at low pressures requires large pumping powers and manifolds for effective heat removal. Much smaller pumping powers of He are required at high pressures (10–20 MPa) (139) and temperatures (500–1000°C) and can be used in Brayton cycles with low reactivity refractory metals and ceramics to obtain high thermal conversion efficiencies (50–60%). Helium is also compatible with stainless steels and titanium and high nickel-base alloys (<650°C), but with trace impurities (H_2, H_2O, CO, CO_2, CH_4, N_2, O_2) can lead to corrosion-embrittlement of vanadium, niobium, and molybdenum alloys (136). Use of He at high temperatures requires that tritium breeding is compatible with refractory metal alloys and SiC/SiC_f composites (140).

Li and Li–Pb are typical liquid metals considered for fusion reactor cooling because of their excellent heat transfer and neutron absorption qualities, tritium breeding potential, and low melting and high boiling temperatures at low vapor pressures. Li–Sn (eutectic mixture of 25 mol% Li and 75 mol% Sn) tritium breeding potential is significantly lower than that of Li or Li–Pb. Liquid metals easily react with oxygen, are difficult to handle, corrode structural materials, and can produce large MHD pressure drops. Austenitic stainless steels (such as 316 SS) corrode in lithium above 400–450°C, ferritic steels are more corrosion resistant, and both high nickel and titanium alloys are unsuitable because of high solubility of alloying

elements in lithium. Vanadium and niobium alloys have good corrosion resistance to lithium up to 800°C (136).

Molten salts do not exhibit relevant MHD pressure drops as liquid metals and come as nitrate, sulphate, and carbonate salts containing oxygen. The chloride salts are corrosive and become neutron activated, and are therefore unsuitable. The fluoride salts flibe ($LiF–BeF_2$) and flinabe ($LiF–NaF–BeF_2$) are chemically stable at high temperatures, and can be employed for the dual purpose as reactor coolants and tritium breeders when used in conjunction with Be as the neutron multiplier. The constituents of fluorides react with Cr, Fe, Mo, and Ni and produce corrosion, but they do not react with SiC composites. The transmutation of lithium in flibe and flinabe produces very corrosive tritium fluoride species that can rapidly degrade the structural materials of the reactor (141,142).

3.4. Magnetic Confinement Fusion Reactors. More than 60 large-scale conceptual power plant designs have been considered (143) based on tokamak, stellarator, spherical torus, reversed-field pinch, spheromak, field-reversed configuration, tandem mirror, and other concepts. A typical configuration of an MCF power plant is illustrated in Figure 17. Here the tritium-breeding blanket is surrounded by the fusion plasma, radiation shields, vacuum vessel, and coils, and its first wall intercepts radiation and ions and in its interior the fusion neutrons deposit their energies and are used to breed tritium. Most of the fusion energy is removed with the primary coolant and the tritium is recovered with either a stationary or fluid circulating Tritium Processing System (TPS) or Isotope Separation System (ISS). The rest of fusion energy is removed by the shield and vacuum vessel coolants (not shown). As discussed earlier, both liquid and gaseous coolants and different tritium breeding media can be employed. Lithium and deuterium are supplied to the reactor from external sources whereas the tritium is supplied by

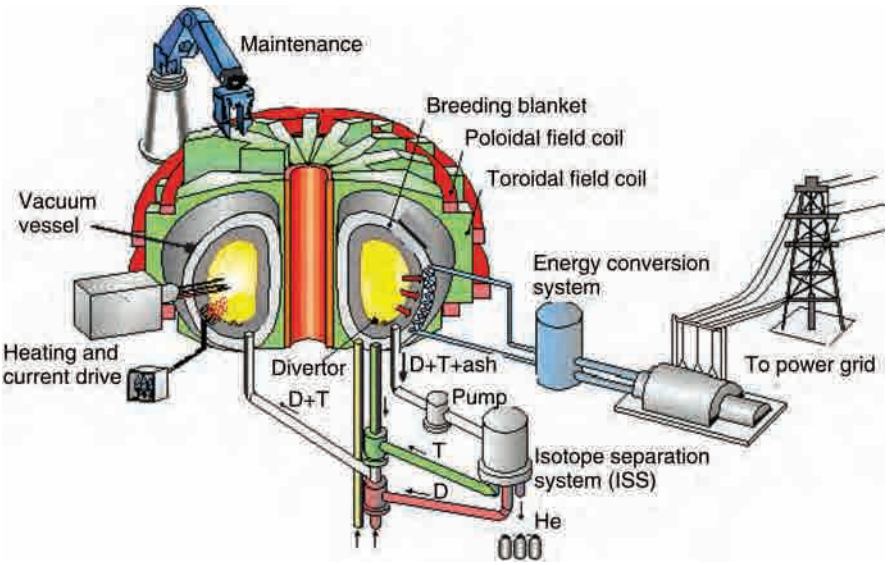

Fig. 17. Schematic of a tokamak fusion power station. Adapted from Reference 144. (Courtesy of European Fusion Development Agreement.)

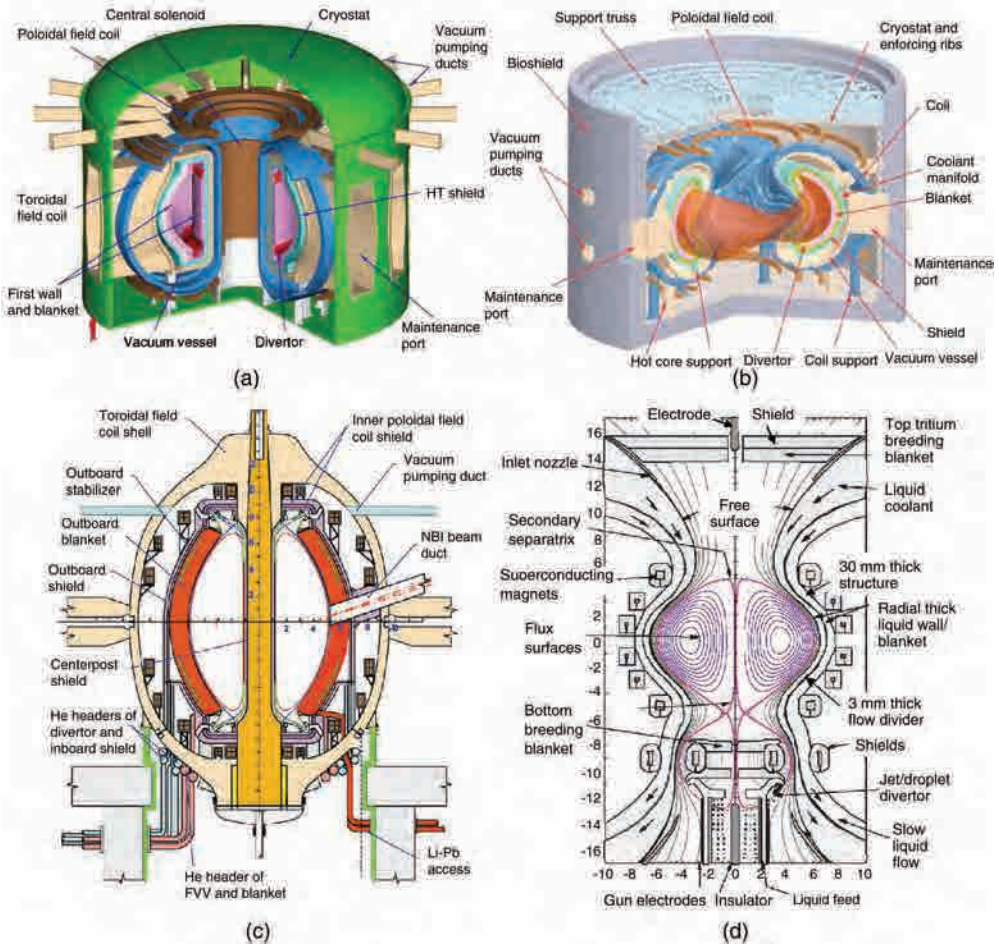

Fig. 18. Representative fusion chamber designs of MFE plants. (a) ARIES-AT advanced tokamak (109). (b) ARIES-CS compact stellarator (110). (c) ARIES-ST spherical torus (145). (d) A spheromak has no hole in the chamber and the toroidal and poloidal magnetic fields are generated through the self-organization of plasma (146,147). (Courtesy of U.S. Department of Energy.)

TPS. Various systems of the reactor must be monitored continuously to assure safe operation in normal and off-normal conditions and loss of coolant flow to the blanket. Table 4 summarizes the design parameters of some proposed fusion power reactors and Figure 18 illustrates four representative fusion chamber designs.

The reactor's breeding and energy removal functions require the operation of external auxiliary systems that remove and recycle tritium and transfer energy to secondary energy conversion system for producing electricity. The choice and design of the blanket are therefore crucial for the operation of the entire fusion power plant and it has a long history of development by China, the European Union, Japan, Korea, Russia, and the United States (130,148). The Test Blanket Module (TBM) programme of ITER will offer the possibility to test some of the blanket modules for future DEMOs in three of its equatorial ports with the aim to

gain operational experience and information on their behavior in an integrated fusion environment.

The tokamak and stellarator DEMOs that are currently being evaluated are about three times larger than ITER and are designed to operate with two to three times larger ion temperatures, remove large heat fluxes from the divertor (up to 20 MW/m^2) and neutron fluxes from the first wall (up to 2 MW/m^2), breed tritium in the blankets with TBRs greater than 1.1, and operate with high thermal cycle efficiencies (Table 4). These machines will also have to operate with minimal or no plasma disruptions and with the advanced materials without frequent replacements of blanket and divertor modules, and other critical components. High reliability of a fusion reactor requires a long service life (preferably 30–50 years) of its components and much simpler and more reliable fusion energy conversion schemes that are currently being evaluated (130). This calls for the reactor's performance level that is significantly higher than being achieved in current tokamaks.

The European Union's Power Plant Conceptual Study (PPCS) (98,144) examined four fusion reactor designs (A, B, C, D) as possible candidates for DEMOs (Table 4). Models A and B are based on the extrapolation of ITER performance, whereas models C and D assume progressive improvements in plasma performance, use of advanced materials and coolants for neutron moderation and reactor cooling, and operation at high temperatures for producing high thermal efficiencies. All designs assume 1.5 GWe delivered to the grid and to meet this demand the fusion power decreases from 5 GW for Model A to 2.5 GW for Model D (98). Model A employs water at 300°C to cool the blanket and divertor, and liquid Li–Pb (17 mol% Li and 83 mol% Pb) for breeding tritium. Model B employs helium at 8 MPa and temperature of 300–700°C for blanket and divertor cooling, and alternate layers of solid pebbles of Li_4SiO_4 and Be for breeding tritium and neutron multiplication, respectively. Model C employs a dual-coolant configuration for cooling the blanket, where He is used to cool the blanket structure and Li–Pb for removing neutron-generated heat from the breeding zone of the blanket. Model D employs Li–Pb for cooling both the blanket and the divertor and for breeding tritium in the former.

The current European DEMO effort involves DEMO1 and DEMO2 designs. DEMO1 is a conservative baseline design with its blanket required to resist the neutron damage of at least 20 dpa. The blanket sectors fit between the toroidal field coils and each sector is divided into several segments and each segment into several blanket modules (149). Tritium will be produced in the blanket with the ceramic breeder and beryllium multiplier or with the Li–Pb breeder and multiplier. It is anticipated that this demonstration reactor will be built in about 20 years from now. DEMO2 is a more advanced and higher performance steady-state fusion reactor that is based on the less mature physics and technology. Its fusion power of 3.25 GW will be produced with a smaller volume than DEMO1 and is expected to have comparable neutron and heat loadings on the blanket and divertor surfaces. DEMO2 will utilize Li–Pb for both breeding and neutron multiplication, and both reactors will produce tritium in the blankets with TBR > 1.1.

ARIES-AT (Fig. 18a) is an advanced 1000 MWe tokamak fusion power plant design developed in the United States. This reactor employs liquid metal Li–Pb at

about 1000°C for cooling the blanket and divertor and for tritium breeding in the former. The liquid metal loop is coupled to a high pressure helium loop for producing electricity or hydrogen. Li–Pb flows through the channels with silicon carbide liners to reduce MHD pressure drop. A movement to reduce the large aspect ratios of Wendelsteins has resulted in the shrinking of the major radius and aspect ratio of stellarators well below 10. These are the compact stellarators of which the National Compact Stellarator Experiment was supposed to be an experiment and ARIES-CS a power plant design (Table 4, Fig. 18b).

The Spherical Torus (ST) reactor (Fig. 18c) has a low aspect ratio that is skinny radially and tall with a central hole to accommodate the inner legs of toroidal field coils and their shielding. The plasma in this machine is different from the D-shaped plasmas of tokamaks and because its magnetic field is 2–3 times smaller it does not require superconducting magnets. This produces large resistive losses and thus requires large recirculating powers.

The Spheromak reactor (Fig. 18d) employs a torioidal plasma in a chamber with no hole in the middle and thus there cannot be any coils going through the hole to generate a toroidal magnetic field. Once the plasma with embedded fields is injected into the chamber from external sources it self-organizes into a toroidal shape with both toroidal and poloidal magnetic field components. The external coils help maintain this self-organization and remove plasma ash through the top and/or bottom of the fusion chamber. Shown in the figure is a design with molten salt liquid walls being maintained by the centrifugal force and the breeding blanket situated on the top and bottom of the chamber. The seed magnetic field is introduced into the chamber at the bottom with "plasma guns." The self-organization issues of spheromaks makes them, however, unlikely candidates for fusion reactors.

The Reversed Field Pinch (RFP) configuration is similar to a tokamak concept except for an order of magnitude weaker toroidal magnetic field and its directional reversal at a certain radial position. This has positive attributes of high mass power density, compact design, easy maintenance, normal coils, and favorable economics. An intense neutron flux is a negative attribute of this TITAN power plant design (150). RFP suffers from magnetic fluctuations caused by tearing mode instabilities and self-organization and is thus not considered as a good candidate for fusion reactors.

The blanket is a complex part of the reactor and is envisaged to be constructed from meter-size modules for easy manufacturing, safety, and remote maintenance. The Tritium Breeding Blanket (TBB) is a key component of DT MFE plant because it manages about 85% of the total power (151). TBB has two key functions: (1) produce tritium used in the reactor, and (2) absorb the fusion energy and deliver it to an energy conversion system for producing heat/electricity. For this purpose, a wide variety of TBB technologies have been proposed during the past decades for both MFE and IFE, but the near-term focus has been the development of TBB mock-ups or test blanket modules (TBMs) for testing in ITER. TBB concepts for IFE tend to be different from MFE because of different operating conditions and constraints. The expectations of both concepts include safe operation at both steady-state and off-normal conditions, operations at high temperatures for producing high thermal efficiencies, high reliability, easy maintenance, and low environmental impacts from radioactive waste streams.

ITER will be equipped with three ports for evaluating TBMs for the eventual use in DEMOs. The designs of these modules are based on the materials and coolants identified above and our purpose here is to summarize some salient features of these designs. Some of these MCF energy conversion and tritium breeding components may also prove useful for the designs of ICF reactor blankets, but the radiation and ion fluxes in these reactors will be different and more severe than in MCF reactors.

Within the European Power Plant Physics and Technology (PPPT) programme there are six blanket module prototypes being evaluated for cooling the blankets of DEMOs (100,126,149). These modules are: Helium Cooled Pebble Bed (HCPB) – European design with solid pebble beds Li_4SiO_4 or Li_2TiO_3 as tritium breeder, Be as neutron multiplier, and He as coolant at 300/500°C; Helium Cooled Lithium Lead (HCLL) – European design with liquid metal Li–Pb as tritium breeder and neutron multiplier, and He as coolant at 300/500°C; Water Cooled Ceramic Breeder (WCCB) – Japanese design with solid pebble beds Li_2TiO_3 as tritium breeder, Be as neutron multiplier, and H_2O as coolant at 280/325°C; Dual Coolant Lithium Lead (DCLL) – American and Korean design with liquid metal Li–Pb as breeder, neutron multiplier and coolant, and He as coolant of the structure at 300/500°C; Helium Cooled Ceramic Breeder (HCCB) – Chinese design with pebble beds Li_4SiO_4 as tritium breeder, Be as neutron multiplier, and He as coolant; Lithium Lead Ceramic Breeder (LLCB) – Indian and Russian design with pebble beds of Li_2TiO_3 and Li–Pb as breeders, He as coolant for FW, and liquid Li–Pb as coolant for pebble beds at 300/500°C. The dimensions of these blanket modules are typically 1–2 m long (poloidal), 0.5 m wide (toroidal), and 0.50–0.70 m deep (radial), and their structures are made of EUROFER or equivalent steel for operations below 550°C.

Three of these module designs (HCPB, HCLL, DCLL) are illustrated in Figure 19. The solid breeder concept HCPB employs the ternary Li-ceramics in a "bier-box" concept with two tritium breeder boxes in each row and several boxes in each column, with the stiffening steel grid holding the boxes in place. The newest design employs, however, a "sandwich" design with only one box per row, which has the possibility to increase TBR to 1.2 (149). As shown schematically with the drawing on the right of Figure 19a, low pressure helium gas is slowly circulated through the breeding boxes for removing tritium and high pressure helium is used as the coolant of the module. Instead of employing a solid breeder, the HCLL concept (Fig. 19b) employs the eutectic of Pb and 15.8 atom percent Li enriched to 90% ^6Li as the breeder material. Li–Pb slowly circulates through the module to avoid a large MHD pressure drop and for removing tritium. The typical "bier-box" design shown in this illustration has also the potential of producing TBR of 1.2. The large heat carrying capacity of Li can be taken to advantage for both tritium breeding and removing fusion energy and this is employed in the DCLL module concept shown in Figure 19c. Here the Li–Pb eutectic is used for both of these purposes and He at high pressure to cool the structure of the module. To reduce large MHD pressure drop, Li–Pb flows through the SiC/SiC_f insulating flow channel inserts spaced by the He carrying RAFM channels. The fusion energy absorbed by both Li–Pb and He is transferred to a secondary coolant in either Rankine or Brayton cycle of the fusion plant energy conversion system. The energy conversion with He can be significantly

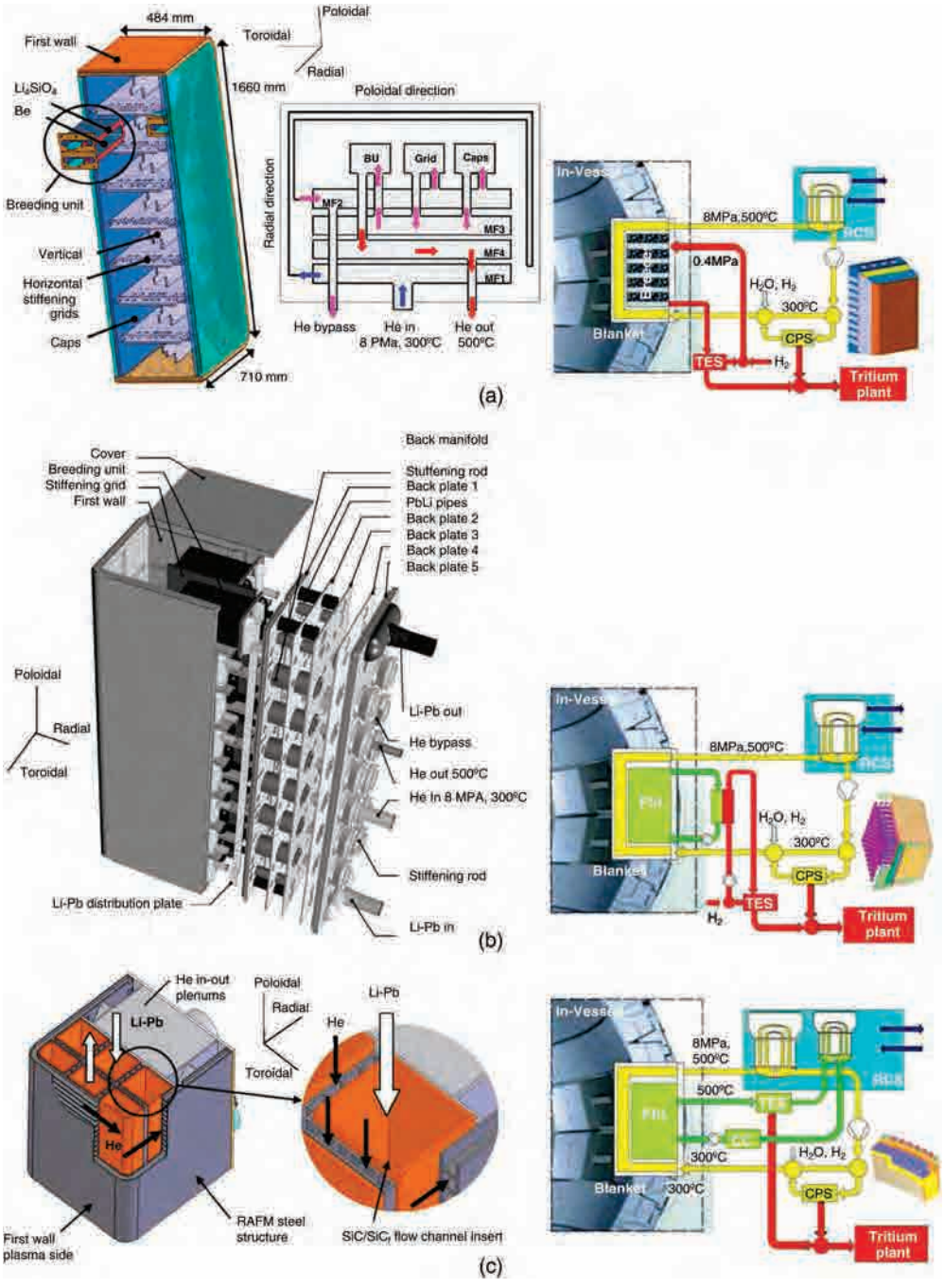

Fig. 19. (a) HCPB, (b) HCLL, and (c) DCLL test blanket modules designs for testing in ITER and possible use in DEMOs. (Adapted from Reference 130.)

improved with heat transfer enhancement techniques and operation at high pressure (8 MPa).

Tritium Management. Tritium must be produced in fusion reactors in sufficient quantities to compensate for its losses through unavoidable permeations through blanket materials and TPS and through its radioactive decay. A sufficient inventory of tritium must also be produced to start the reactor, run the reactor at high power, and (preferably) to provide initial fueling of one or more reactors. A TBR of 1.1 or 10% margin of safety is most likely unacceptable, because only few percent of tritium injected into the plasma actually fuses with deuterium, and since a large number of tritium ions are ejected through the divertor and not immediately recycled, it can take many years to produce tritium self-sufficiency. Since it will require some 10 kg of T just to get started a DEMO it is of great urgency to develop breeding blankets with high TBRs (9,152).

HCLL, WCLL, and DCLL breeder blanket concepts employ liquid metal Li–Pb loops that must be heated at all times above the melting temperature of Li–Pb, carry tritium produced within the blanket to ISS on the outside of the vacuum vessel, control the Li–Pb chemistry by separating hydrogen isotopes and helium and removing impurities produced by corrosion, ensure gravitational draining of liquid metal, and in the case of DCLL blanket transfer a large amount of fusion energy to a secondary energy conversion system. The Li–Pb loops must function within the Tritium Fuel Cycle (TFC) that must also process the plasma from scrape-off layers through the ISS. TFC must necessarily involve tritium waste treatment and storage management. The fueling system recovers tritium from the storage or external sources and then injects frozen pellets of tritium and deuterium into the center of the plasma. There is no necessity to recover deuterium because it is harmless and easy to produce, but is necessary to process all water and air in the plant environment through a detritiation system to recover tritium. The tritium containment is well developed within the nuclear fission industry, but the fusion industry will have to deal with orders of magnitude larger quantities of this material and this experience is currently lacking.

Some of these issues are currently being addressed within the EUROfusion DEMO blanket studies where it is noted that the tritium extraction can be performed with several technologies, but that the control of tritium migration and permeation into the steel structures and flow channel inserts of DCLL blanket concept still pose significant challenges (149). A detailed DEMO design is supposed to start after 2020, when the critical issues of MFE technology have been resolved.

3.5. Inertial Confinement Fusion Reactors. There are over 50 conceptual designs of inertial fusion power plants (143) and herein we will discuss some representative concepts. A typical IFE power plant (Fig. 20) employs a laser or an ion beam driver to compress DT targets managed by the target factory and injector system, TPS system, power conversion system that manages the fusion energy produced, and fusion chamber whose design depends on the driver, fusion reaction products, safety, energy conversion efficiency, and breeding potential. Since we already discussed drivers and tritium management, our discussion here will be limited to fusion chambers and DT target management.

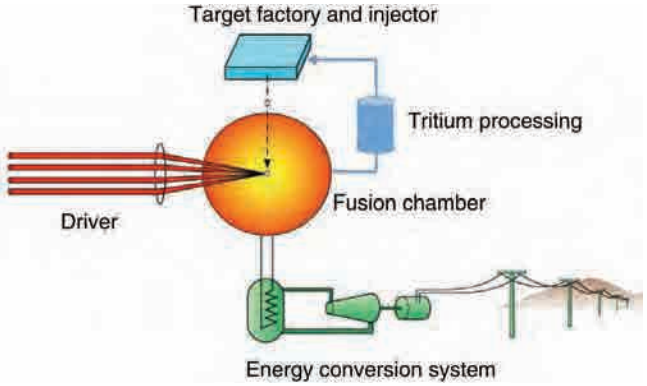

Fig. 20. Schematic of IFE power plant. Reference 153. (Courtesy of U.S. Department of Energy.)

An inertial confinement fusion chamber should be designed for repeated (5–10 Hz) supply and burn of DT fuel targets with laser or ion beams, repeated clearing of fusion reaction products from the chamber following each microexplosion, protection of PFCs from ions, radiation, and fusion reaction products, capturing and transferring of fusion energy to energy conversion system, breeding tritium, operation at high temperature for efficient energy conversion, easy maintenance, safe operation, and minimal environmental impact. The threats to chamber components depend on the driver (laser and ion beams) and on the target type design (direct and indirect illumination of DT capsules), because the direct illumination produces more ions and the indirect more X-rays. The ion beams are generally more energetic than laser beams and thus their potential for damaging PFCs is significantly greater and requires protection to increase the lifetimes of these components.

As a consequence, three different chamber first walls have been considered for IFE power plants. These are the dry-walls where the blankets are protected with high-Z gases, magnetic fields, or specially engineered surfaces, thin-liquid-walls where the blankets are protected with thin layers of liquid metals Li, Li–Pb, flibe, or flinabe, and thick-liquid-walls where the blankets are protected with thick layers of liquid metals Li, Li–Pb, flibe, or flinabe flowing along the plasma facing surfaces of blankets. Thick-liquid-walls have the advantage of lowering the costs of replacing blankets and developing low-activation materials, but their stabilities in fusion environments are poorly understood. Table 5 lists the drivers, targets, and chamber wall characteristics of some representatives IFE power plant studies and Figure 21 illustrates some fusion chamber designs.

Osiris (Fig. 21a) is a 1 GWe power plant design that employs the indirect driver consisting of 12 Xe ion beams operating at the repetition rate of 4.6 Hz with hot-spot ignition. Its fusion chamber blanket employs porous low-activation carbon-fabric filled with flibe and thin liquid layer of flibe flowing along the inner chamber wall to protect the structure from X-rays and debris. The evaporated flibe is condensed with 500°C jets at the bottom of the chamber where the 650°C hot flibe is collected for delivery to the intermediate Pb coolant loop containing steam generators. The 12-unit design of FW can be easily replaced after draining flibe from the chamber, whereas the recovery of tritium is carried out with a TPS. Both the blanket structure and vacuum vessel walls are constructed from the carbon/carbon composite (C/C) structures. The energy conversion efficiency of this design is 45% (111).

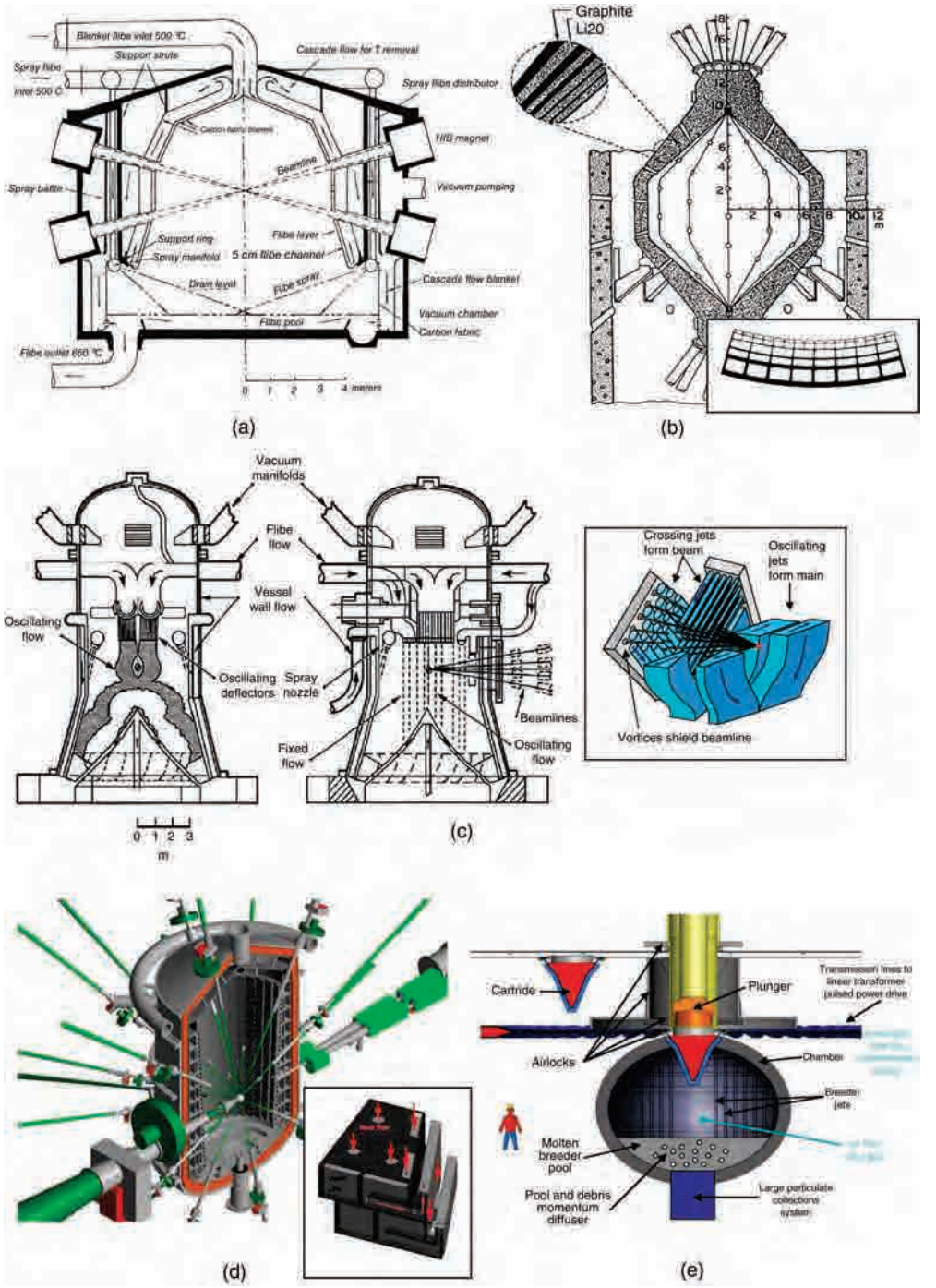

Fig. 21. IFE plants fusion chambers of (a) Osiris, (b) Sombrero, (c) HYLIFE-II, (d) KOYO-F, and (e) Z-IFE. See Fig. 21 caption on the following page for more detailed explanation.

Sombrero (Fig. 21b) is also a 1 GWe power plant design that employs a 60-beam KrF laser driver operating at 6.5 Hz with hot-spot ignition. The chamber's first wall is protected from X-rays and debris by Xe gas at 0.5 torr and the blanket is cooled with mm-size Li_2O granules. Low pressure He is used to circulate granules through the blanket and intermediate Pb heat exchanges and for removing tritium from the breeding granules. The chamber is constructed from 12 FW and blanket modules made of C/C composites that require replacement every 5 years. Sombrero's vacuum vessel walls are also made of C/C composites and because of its final focusing optics it requires a large (110 m diameter) reactor building. Both Sombrero and Osiris designs require the development of appropriate target injection and tracking systems (111).

HYLIFE-II (Fig. 21c) is a power plant concept where its chamber wall is protected with a thick-liquid-wall of flibe and its DT targets are illuminated indirectly with either a heavy-ion driver operating with hot-spot ignition or a laser driver operating with fast ignition. The liquid wall of about 0.8 m thickness is produced by the stationary and oscillating liquid flibe jets (Fig. 21c inset) which are much more effective than thin-liquid-walls in absorbing shocks from the energies of ions, neutrons, and radiation. Such a design is compatible with high yield targets and allows for a compact design of the chamber, but at the expense of the complicated arrangement of the jets and the driver beams that have to penetrate through the jets to reach the targets at the center of the chamber. Flibe from the jets is collected at the bottom of the chamber and from there is pumped through a vacuum disengager to remove tritium and transfer heat in steam generators. Since flibe does not react with water there is no need for an intermediate heat transfer loop and its high temperature of 650°C produces high energy conversion efficiency. This power plant concept has the untested technologies of managing targets, jets, and tritium, jets interacting with ions, neutrons, and radiation, and clearing of the chamber after each microexplosion (113).

KOYO-F (Fig. 21d) is a Japanese design of an IFE power plant that employs Yb-YAG lasers for illuminating direct fast ignition DT targets. Its fusion chamber allows for the penetration of 32 beams and its porous first wall is cooled with a thin-liquid cascading film of Li—Pb, which is mixed with the cooler blanket coolant Li–Pb as it flows downwards along the inner surface of the chamber (Fig. 21d inset). The blanket coolant at 500°C is collected at the bottom of the fusion chamber and is pumped through the steam generators to produce electrical energy. This design has the critical issues associated with fast ignition target fabrication and plasma ignition, first wall surface ablation, and tritium management (116).

Fig. 21. Representative fusion chamber designs of IFE plants. (a) The fusion chamber of Osiris features a porous carbon-fabric blanket filled with flibe and a thin layer of liquid flibe protecting the first wall from X-rays and debris (111). (b) The chamber of Sombrero features carbon/carbon composite first wall and blanket structure and LiO_2 as the breeder and coolant (111). (c) In the HYLIFE-II energy plant heavy-ion beams ignite DT targets indirectly from two sides and the wall of the chamber is protected with thick curtains of liquid flibe jets (inset) (113,114). (d) KOYO-F fusion chamber employs 32 beams for compression and one heating beam. Shown in the inset are first wall cooling channels (115). (e) Schematic of the Z-IFE fusion power plant concept showing the pulse power driver and recyclable transmission line that provide ignition of fuel targets. Flibe jets serve the purpose for breeding tritium, wall protection, and fusion energy removal (73,117).

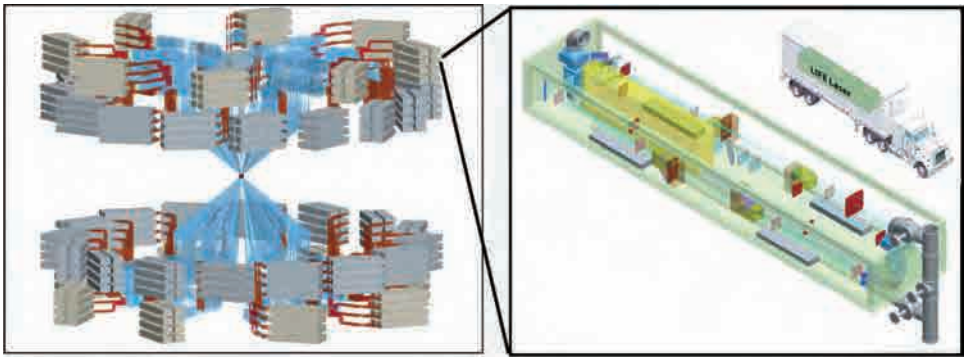

Fig. 22. Laser driver of LIFE' plant. The driver is composed of 384 DPSSL laser modules, with each module (right) having the dimensions $10.5 \times 2.2 \times 1.4\ m^3$ and rated at 100 kW (50). (Courtesy of Lawrence Livermore National Laboratory.)

The Z-pinch (Fig. 21e) inertial fusion concept offers some unique advantages that have been built into several Z-IFE plant configurations with different number of chambers and fusion power outputs (73,117). Laser and heavy-ion plants require vacuum conditions in chambers to produce unobstructed paths to targets whereas the Z-pinch driven plants do not because the targets and power sources (drivers) are managed at single locations with Recyclable Transmission Lines (RTLs). RTL connects the target to the driver where a significant portion of it is destroyed during each shot and the rest can be recycled. When flibe is used for the chamber wall protection and as a coolant for the blanket, the RTL cartridge containing the target can be made of ferritic steel and frozen flibe, with the former requiring a significant amount of energy to remanufacture. This power plant concept allows for different protections of chamber walls, such as with liquid flibe or tin flowing along the wall to remove the fusion energy released in the chamber. The 600°C coolant is collected at the bottom of the chamber, processed for solids and tritium, and subsequently circulated through the steam generators.

The Laser Inertial Fusion Energy (LIFE) power plant employs DPSSL lasers as the drivers for hot spot ignition of indirectly illuminated DT targets. LIFE beamlines are configured into 384 boxes and arranged into an annual array to allow offsite manufacturing (Fig. 22). Xe gas is used to protect the first wall of the chamber and the liquid lithium is employed for both cooling of the first wall and interior of the blanket and for breeding tritium (154). The chamber consists of eight identical sections with openings for laser beams and its first wall is constructed from horizontal pipes and the blanket interior from vertical trapezoidal cooling channels (Fig. 23). The fusion chamber is enclosed within a larger vacuum vessel and both are constructed from ODS ferritic steel. It is projected that this power plant will utilize about one million targets per day and that the targets will be produced by a target production system that has been under development at LLNL for some time. Without demonstrating ignition at NIF in 2012, the planned operation of LIFE (155) was postponed (156).

The European High Power laser Energy Research (HiPER) facility was supposed to follow-up on NIF's ignition and develop commercial power production by employing the direct instead of the indirect laser drivers to eliminate complex targets and X-rays (157). The current strategy is to use LMJ facility to investigate the physics of direct drive shock (and possibly fast) ignition of DT targets and

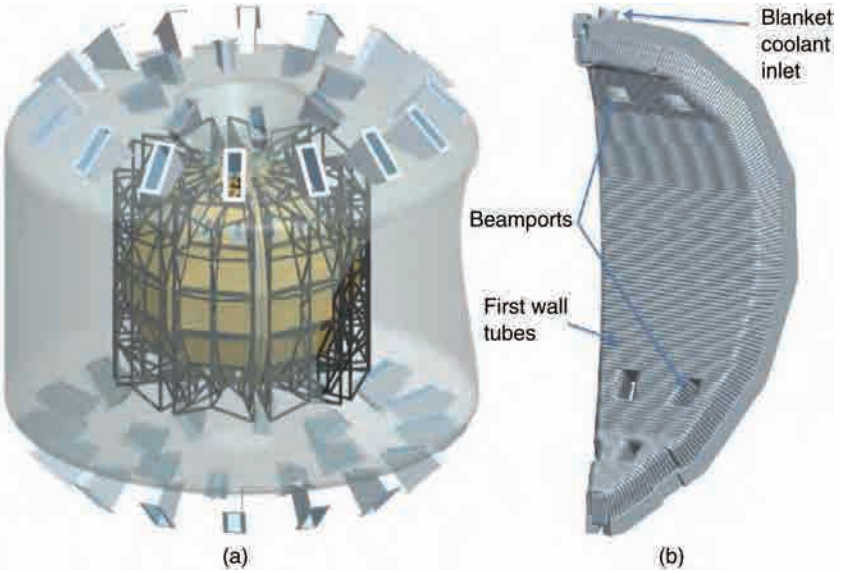

Fig. 23. LIFE's fusion chamber consists of eight identical modules cooled by lithium. The first wall and blanket cooling passages consist of horizontal tubes and vertical trapezoidal channels, respectively (154). (Courtesy of Lawrence Livermore National Laboratory.)

employ this scheme in the HiPER power producing reactor that should begin operation by 2050 (158). Its laser driver would operate at 10–20 Hz with a yield of at least 100 MJ and the power produced would be 1–3 GW. The design of fusion chamber and the rest of plant components have not yet been finalized.

Whether the thin-liquid-wall IFE power plant concepts (such as Osiris and KOYO-F), thick-liquid-wall concepts (such as HYLIFE-II and Z-IFE), or some other designs will produce the best IFE option remains to be seen. Thick-liquid-wall chamber designs reduce the need for expensive testing facilities to produce low-activation materials, produce compact chamber geometries, reduce plant capital cost, improve heat removal and tritium management, and increase the plant availability. Their disadvantages are that for high driver repetition rates the debris clearing rates will prove to be too low, heavy-ion driver beams may not be able to penetrate to the targets, and when the laser drivers are used the ablated liquid will condense on the transparent windows of the chamber and block the penetration of laser light to the targets (159).

4. Sustainability of Fusion Energy

Sustainability of fusion energy should represent a concept where the introduction of fusion energy by humanity will sustain its development without threatening the exchange processes between the humanity and the natural environment in which the humanity is expected to survive for an indefinite time. We can then assign values to this concept, such as: (1) the fusion energy produced from natural resources should not exceed the sustainable yield of these resources, (2) the fusion energy produced should be socially acceptable, (3) releases of waste products and

pollutants from operations of fusion energy plants into the environment should be limited and not cause health problems, and (4) the fusion energy produced should be affordable for promoting sustainable development. More specifically, we should be able to answer the following questions: Can controlled and sustained plasma ignition be produced in fusion reactors without frequent shutdowns? Do sufficient resources of materials exist to build and run fusion energy plants? Can appropriate fusion reactor materials and high efficiency fusion energy conversion systems be developed? What are the safety and environmental issues associated with fusion energy? We have already addressed some of these issues in previous sections and in this section we will only concentrate on the availability of critical fusion energy materials and safety and environmental issues associated with fusion energy plants.

The reactions between deuterium and tritium are the easiest to achieve and will most likely power the first-generation commercial fusion power plants. Deuterium is plentiful and inexpensive to produce, while tritium must be produced from lithium (Section 2.1) and therefore the sustainability of lithium comes into question. Be and Pb are useful for neutron multiplication in the blankets and the rare earth elements Nb and He are currently necessary for building and cooling superconducting coils and removing heat from the blankets. When high energy neutrons interact with blanket materials they produce radioactive streams of materials that must be safely handled during reactor maintenance and managed once they have been removed from the reactors. Accidents in coolant supply and tritium management systems can also pose serious hazards to both plant personnel and to the environment surrounding a fusion power plant. In the following, we will examine these issues more closely and refer the reader to the extensive safety and environmental studies of ITER that are reported in several studies (160).

4.1. Prospects for Achieving Fusion Ignition. As discussed above, fusion was demonstrated in the tokamaks of JET and TFTR, and the plasma densities, temperatures, and confinement times are steadily increasing with each new tokamak and stellarator machine. There is considerable optimism that LHD, W7-X, and ITER will pave the way to commercial MFE and that ICF will demonstrate DT ignition in the foreseeable future (156,161). The accomplishment of the goal of building and operating DEMOs would produce the *technological feasibility* of fusion power. But the speed of this development will be driven by our needs to replace fossil fuels with alternative energy sources and on our concerns for the future.

4.2. Sustainability of Fusion Materials. The first generation fusion power plants will need adequate supplies of deuterium and tritium for fueling the reactors and helium for cooling the blankets and divertors and maintaining the superconducting states of magnets. Deuterium will not become a problem because it is plentiful in water (1 part of D_2O for every 6400 parts of H_2O) and can be easily extracted by electrolysis of heavy water obtained via isotopic exchange (162). Tritium, however, does not occur naturally because it is radioactive with the half-life of 12.3 years, but can be produced from lithium via the reactions expressed by equations 8 and 9. The abundance of ^{6}Li is 7.5% and that of ^{7}Li is 92.5%. The tritium production from fusion neutrons and lithium in the blanket of a fusion

reactor is, however, insufficient for powering reactors and for this purpose the neutron producing materials such as Be and Pb can be used (Section 2.1). Beryllium is normally used in solid breeders and lead in liquid breeders and coolants (Section 3.3). Unless extracted from the seawater, adequate supply of Li could be problematic if it is also used in lithium-ion batteries, Be is significantly rarer and is a potential problem, and Pb resources are in the gigaton range and thus not critical. In the DT fusion cycle, D, ^{6}Li, Be, and Pb are actually the fusion fuels. It is anticipated that He at high temperatures will be used extensively in energy conversion systems of fusion reactors, while He at cryogenic temperatures will be employed to maintain the magnetic field coils of these reactors superconducting. Let us look more closely at the availabilities of these materials.

The U.S. Geological Survey estimates that the world's Li reserves and resources in the crust are about 13 and 40 Mt, respectively, and can be extracted economically. Lithium concentration in seawater is on average 0.17 ppm or some 230,000 Mt. Beryllium has a crustal abundance of 2.8 ppm, its separation is expensive, and its resources are more than 80 kt. Lead fairs much better at 1.5 Gt and the crustal resources of He are some 10 Mt. Niobium is an important constituent of superconducting magnets (Nb_3Sn and/or NbTi) and its world reserves exceed 4 Mt (163).

If lithium-ion batteries are implemented on large scale for electric vehicles, it will require by 2050 some 10 Mt of Li that will significantly deplete the world's reserves but not the resources. To run 5000 power plants with each producing 2.4 GW of fusion power and employing HCPB breeding blankets would require about 1.5 kt of ^{6}Li and 19 kt of natural Li annually and take about 700 years to exhaust the lithium's 13 Mt reserves from the crust and 12 million years from the seawater. To run all power plants with fusion would require about 250 kt of natural lithium and would deplete the crust's Li resources by several percent, and significantly more if lithium-ion batteries are implemented on large scale. The use of Be in 5000 HCPB power plants would require about 500 t annually and more than 600 kt for initial loading. This would exceed considerably the resources of 80 kt and we would have to develop Li–Pb-based tritium breeding blankets (HCLL and DCLL) instead (164,165).

Helium and niobium are not fusion fuels but are required for manufacturing and cooling of superconducting magnets, and since He is being produced in DT fusion reactors it should be recoverable. Helium in the Earth is produced by the nuclear decay of uranium and thorium and when it escapes to the atmosphere it readily disappears from this environment, because the Earth's gravity cannot confine it for long. Its concentration in the atmosphere is only 5.2 ppm or 3.5 Gt. Helium's reserves of 1.3 Mt and resources of 8.5 Mt trapped by impermeable rocks can be exhausted rapidly (without being conserved) during the next 100 years with the consumption of natural gas (166). The 5000 fusion power plants above would consume the nonatmospheric He resources in about 200 years and in the longer term He in the atmosphere would have to be extracted. A DEMO reactor would require the He inventory of about 60 t and the losses could amount up to 2 t/y. With the above 5000 fusion power plants operating there would be the need for 0.3 Mt of He and it would take 210 years to exhaust the resources. ITER requires about 200 t of Nb for its coils and if this amount is used in the above 5000 fusion power plants it would require 1 Mt of niobium or a quarter of current reserves (165).

Boron B is employed in the reaction $p + {}^{11}\mathrm{B} \rightarrow 3\alpha$ (Table 1), and since only 0.19% of the reactions ${}^{11}\mathrm{B} + \alpha$ produce neutrons, B may one day be the fusion fuel of choice, especially in ICF reactors. Boron does not occur in nature in an elemental state but combines with oxygen and other elements to form boric acid or inorganic salts called borates. Boron's world-wide reserves are estimated at 210 Gt (163).

This brief overview of Li, Be, Pb, He, Nb, and B reserves and resources suggests potential sustainability issues for all of these resources except lead and boron, but it is probably only He that will become scarce during the course of this century unless more effective methods are found to produce it or substitute it with more sustainable coolants and high temperature superconductors. Pb can substitute Be for breeding tritium, high temperature superconductors may replace the need for Nb, and the lithium-ion batteries may become obsolete and thus release plenty of Li for use in fusion power plants. These resources sustainability issues will therefore continue to be relevant during this and the following centuries.

4.3. Safety and Environmental Issues. A fusion reactor will contain a small amount of fuel inventory and low level of power density following the termination of fusion reactions. No fissile materials will be produced and only tritium and neutron-activated materials will present potential radiological hazards. Fusion scientists set forth two central goals for the development of fusion technology (167,168): (1) the worst possible accident must not constitute a major hazard to populations outside the plant perimeter that might result in evacuation, and (2) radioactive waste from the operation of a fusion plant should not require long-term isolation to be a burden for future generations. These objectives should be accomplished by careful selections of plasma confinement concepts and appropriate choices of materials for power plant components. Even in a severe accident, the temperature excursions should not produce melting of reactor materials and the confinement integrity must be maintained. The neutron and radiation spectra of MFE and IFE are expected to be different because of the differences in fuel targets and chamber wall protection, but in both concepts the loss of vacuum in the chamber will rapidly terminate fusion reactions. The tritium inventory of either an MFE or an IFE power plant will be no more than several kilograms, and in both plants the tritium processing rates scale as $1-\Phi$, where Φ is the tritium burn fraction or efficiency (167). For IFE, Φ is typically 30% (equation 17) and for MFE is only a few percent. We will first discuss safety and environmental issues for MCF and ICF reactors and then the management of fusion-activated materials.

MCF Safety and Environmental Issues. The European Union sponsored several studies pertaining to safety and environmental impact of fusion and here we will summarize some of these results (168). For this purpose, six different blanket concepts were evaluated corresponding to a power plant with fusion power of 3 GW, blanket life of 5 fpy, and neutron wall load of 2.1 $\mathrm{MW/m^2}$. These are the WCLL MINERVA-W and HCLL MINERVA-H blankets that have been under development for many years and the blanket Models 1–4 of more advanced designs that have not yet been fully developed. The plasma-facing surfaces of these blankets and divertors are covered with Be or W armors, except for $\mathrm{SiC/SiC_f}$ blankets of Models 5 and 6 that do not employ such a protection. The shields, vacuum vessel, and coil casings of each design are built from steel and the cryostat

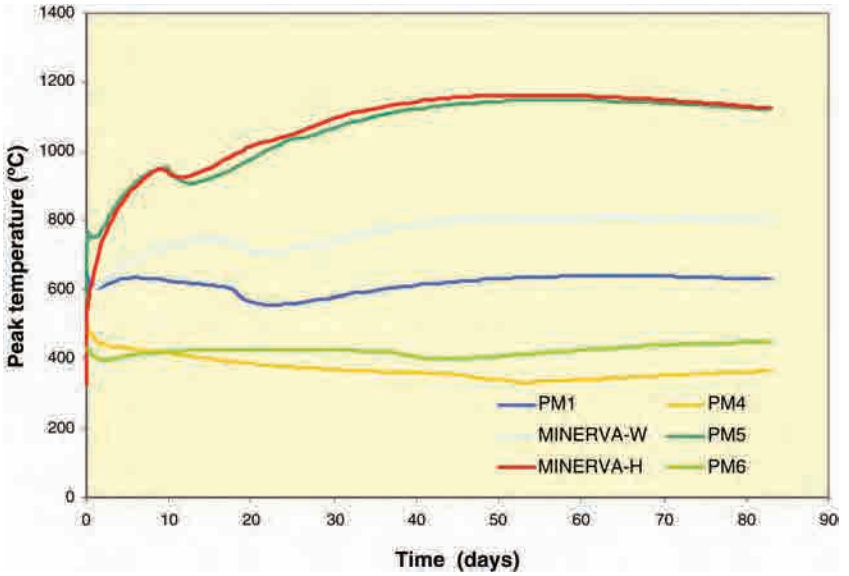

Fig. 24. Peak temperatures for the six SEAFP blanket studies (168). (Courtesy of European Fusion Development Agreement.)

vessel surrounding the magnet and vacuum vessel is built of reinforced concrete with an inner liner of steel. This first confinement structure is situated within a second confinement structure that houses the primary coolant loops of blanket and divertor and the steam generators. Both of these structures are equipped with rupture disks and stack scrubber for managing overpressures produced from the reactor's loss of coolant flow. Once the supplies of D and T to the reactor are terminated, the fusion reactions will terminate within 1 min and the energy inventories will be those stored in plasma, blanket, coils, and primary coolant (1.5 TJ for MINERVA-W and 1 TJ for MINERVA-H). Accident analyses show that these energies are too small to breach the confinement.

The decay heat in the blanket is the energy released by the decay of activated materials and if this is too high it could cause temperature excursions following a loss of coolant flow through the blanket. For all blanket designs considered, the temperatures of blanket materials do not exceed 1200°C and after 50 days begin to decrease (Fig. 24). About 1 kg of tritium accumulates in the armor of Be and 50 g in the armor of W, and together with the tritium bred in the blanket and processed through TPS, the total estimated inventory of T in the reactor is about 1.5 kg. The neutronics and activation modeling of reactor components can then be used to show that the potential biological hazards to both inhalation and ingestion after a few decades fall to the levels that are 1000–10,000 times lower than those of similar materials of fission power reactors, or by a factor of 10 greater than the radiotoxicity of coal ash.

Potential hazards to the plant operators and public come from the normal operation of a fusion power plant and from plant accidents. The occupational doses from activated components during maintenance and other operations for the He-cooled blanket come to about 0.2 man-Sv/y, whereas for the H_2O-cooled blanket most of the doses of about 2 man-Sv/y come from the activated products in coolant loops. Exposures to magnetic fields above 4 T bring about detrimental effects on

health. Tritium effluents via both atmospheric and aqueous pathways can originate from cooling loops and tritium handling and processing systems, and for the fusion power plant designs considered their doses do not exceed 1 μSv/y for each pathway. Plant accidents can result from a failure of the primary coolant loop, loss of heat removal with the secondary coolant circuit, breaches of fusion chamber and vacuum vessel, loss of cryogenic helium flow through the coils, external events such as earthquakes, etc. Calculations show that the complete loss of primary coolant loops will not produce peak FW temperatures above 1400°C for He-cooled blanket and 950°C for H_2O-cooled blanket. A contact between beryllium and water can produce hydrogen and aggravate the accident situation, and needs to be evaluated when this possibility exists.

A break of the secondary heat transport loop can result in the break of steam generator tubes and of the primary coolant loop. This would cause some 10 kg of dust to be mobilized inside the vacuum vessel and less than 6 g of dust would propagate to the outermost environment through the open pathways of confinement vessels. From worst-case accidents and one kilometer from the plant, an individual would be exposed to less than 2.6 mSv/y, which is within the dose limits (1–3 mSv/y) of natural radioactivity (167). An earthquake scenario releasing 1 kg of activated material close to the plant would result to an increase of radioactivity of 0.4 Sv.

Fusion power stations will require replacements and decommissioning of their components and a study shows that the activated volumes would be similar to the corresponding volumes from fission reactors and do not require cooling (168). But as noted above, the decay heat and radioactivity of fusion materials are 100 and 1000–10,000 times lower, respectively, and the activated materials do not require cooling. This suggests that after several decades most of the activated materials can be recycled and thus do not require permanent waste storage. The potential release rates of chemically toxic elements Li, Be, V, Cr, Zr, Sn, and Pb into the atmosphere are several orders of magnitude lower than those permissible.

The worst possible MFE tokamak plant accident does not appear to constitute a major hazard to populations outside of the plant perimeter and the radioactive waste from the operation of the plant does not appear to require long-term isolation, thus satisfying the two central goals of the development of fusion energy technology stated earlier.

ICF Safety and Environmental Issues. The same conclusions regarding the safety and environmental effects of MFE plants can also be reached for the corresponding inertial fusion energy plants. In an IFE plant, the driver energy and the fuel target system are separated from the reaction chamber, and one cannot directly inject D and T into the reaction chamber as in MFE plants. The IFE fuel cycle inventories range from several hundreds grams to several kilograms, depending on the target type and filling method employed to produce targets (167). The indirect targets have high proportions (up 99% by mass) of high-Z materials whereas the direct targets have significant amounts of low-Z materials like carbon, and the exhausted debris from both types must be separated from the unburnt fuel. About 0.4 g/target will activate in indirect drive targets and this amount will keep increasing as the target material is recycled through the target factory. Taking this activated target mass, a driver with the repetition rate of 5 Hz and 1-week turn-around cycle shows that the recirculating inventory of activated

target material will be 1200 kg. The activation of IFE blankets is different from the activation of MFE blankets, because the neutron spectra of the former are softer due to significant neutron moderation within the targets and the means employed to protect FWs. This then implies that the low-activation blanket materials may last for the entire lifetime of IFE plant.

The target type and fill technology determine the time to fill targets and since a 3 GW fusion power plant consumes about 500 g of tritium per day with 30% burn efficiency, the required amount of tritium in the target factory must be at least 1.7 kg. The maximum offsite doses from tritium and activation products effluents were estimated to be in the range from 4.5 to 45 μSv/y and the major contributions to tritium effluents in IFE are expected to occur from fuel processing and cooling systems. As in MFE plants, the release of chemical effluents Li, Be, V, Cr, Zr, Sn, and Pb will have a minor impact on the overall releases.

IFE studies lack detailed maintenance assessments, but because the driver is separated from the reaction chamber most of it should not require remote maintenance, except when the driver involves heavy-ions. The reaction chamber will require remote maintenance and if the FW does not require maintenance during the lifetime of the plant the reactor may be decommissioned hands-on after several decades of repose. The exhaust from the reaction chamber will have activated products from high-Z indirect targets and will require remote maintenance, while the ISS may not. The debris of high-Z indirect targets in target factory emit γ-rays if this debris is recycled, whereas the debris from low-Z direct targets do not, which may or may not require remote maintenance, depending on whether or not low-activation materials are used or the holdup time allows decay. The primary coolant system will require remote maintenance.

For a 3 GW fusion power, 600 MJ blast, and 5 Hz repetition rate, the plant will have to withstand some 5 billion pulses during its lifetime and the FW will require protection as discussed earlier. The chamber will also require a vacuum of less than 1 kPa for the laser and ion-beam drivers in order to deliver their energies to the targets. A reactor chamber failure will prevent further fusion reactions but may suffer additional damage if the driver does not immediately terminate supplying energy. If the primary cooling system fails the fusion reactions will also terminate, because some materials will be evaporated from the FW and spoil the chamber vacuum condition. Because most IFE designs use low-activation materials that have low decay heat, their removal by conduction and radiation is of even lesser concern than in MFE plants where no active heat removal system is necessary.

Some coolants such as Li readily react with oxygen, whereas the Li–Pb eutectic, flibe, or Li_2O granules do not but are corrosive. Carbon and beryllium are also reactive. Hot liquid metal coolants and molten salts can damage the equipment during spills, but cannot endanger the public outside of the plant. The stored energy in drivers depends on the drivers. Lasers can typically store up to 50 MJ and heavy-ion beams up to 600 MJ of energy, and if the driver beams do not intercept the targets their energy could be deposited on the chamber wall where they may produce pathways for the activated materials to escape from the confinement. The detailed studies of such accidents and their inhalation and ingestion pathways are lacking for IFE plants, but some design studies claim that

the release of 100 g of tritium would produce the worse-case doses of 50 mSv, which is not sufficient for public evacuation (167).

Management of Fusion-Activated Materials. One of the key advantages of fusion is that its waste does not contain long-lived radionuclides. This eliminates the need for storing the waste for thousands of years in geological repositories and requires only the management of short-lived waste in temporary and shallow-land burials. All main fusion fuels produce neutrons and to remove neutrons from fusion reaction products requires advanced fuels (Table 1), but these reactions are much more difficult to produce than the DT reactions and may be eventually incorporated into the second- or third-generation fusion power plants.

As discussed above, and as a study of the ARIES-CS fusion power plant confirms, the recycling doses of reactor components strongly depend on the materials of these components. The FW and blanket of this reactor are made of ferritic steel and are the most intensively irradiated components that for the first 50 years or so cannot be handled without remote maintenance tools after being removed from the reactor. The shield, vacuum vessel, coils, cryostat, and the surrounding containment building (bioshield) emit reduced levels of radioactivity and can be hands-on managed after several decades. Seventy percent of the waste (FW/blanket/back wall, divertor, shield/manifolds, and Nb_3Sn coils) are classified as Class C of low level waste (LLW), whereas the remaining 30% (coil casings, cryostat, and bioshield) are classified as Class A of LLW and can be cleared (169). This example attests to the validity of the above-noted advantage of fusion and suggests that the neutron-irradiated components of first generation fusion power plants should be constructed from best low-activation materials and that the activated materials removed from the plant should be recycled after their radioactivity drops to safe handling levels.

The fusion power core of ARIES-CS comprises some 2000 m^3 of irradiated blanket, divertor, shields, vacuum vessel, coils, and bioshield materials (169), and if we assume 5000 of such plants producing about one-third of the world's power needs (12 TW) we would have to continuously manage in the future some 10 million cubic meters of waste. This volume exceeds the amount of waste currently being produced by fission reactors, but with the important difference that this inventory has a very short lifetime. The current management of nuclear waste from hospitals, laboratories, and fission reactors (90% of which is LLW) is sporadic and highly ineffective in both the United States and abroad and there is no consensus for a large-scale recycling and clearance of waste from future fusion reactors. Both the U.S. Nuclear Regulatory Commission and International Atomic Energy Agency recommend individual dose standard of 10 μSv/y for cleared nuclear material (170,171), which is very low in comparison to the natural background radiation of 2.4–3.6 mSv/y.

None of the fusion materials considered are subject to the Treaty on the Non-Proliferation of Nuclear Weapons, because the blankets surrounding plasmas use the neutrons to produce heat for powering energy conversion systems and not for producing nuclear reactions. When, however, the neutrons can be absorbed by the nuclei of some heavy elements they can split these elements and produce chain nuclear fission reactors. Nuclear fusion can then be used to produce neutrons for nuclear fission and thus change the character of nuclear waste as in fission power

reactors. In these so called *fusion-fission hybrids* being studied in the United States, Russia, and elsewhere, it is envisaged that the fusion neutrons can manage nuclear waste from nuclear stock pile and commercial fission reactors, generate fissile fuel for light water reactors, and produce energy as in the current commercial nuclear reactors (172).

5. Conclusion

We examined future energy needs and availability of fossil fuels and their consequence on global warming and discussed whether fusion energy can be harnessed and technology developed to replace the fossil fuels that are becoming increasingly problematic with the passage of time. Nuclear fusion has been achieved in deuterium and tritium plasmas confined by magnetic fields and there is high optimism that this can also be achieved with lasers and ion beams. The behavior of plasmas in tokamaks is best understood while the stellarators may offer better solutions for future fusion power plants. The experimental machines are paving the way for building demonstration fusion reactors by the middle of this century, and if this is successful for building commercial fusion power plants during the second half of this century. The development of fusion as a sustainable energy source requires achieving sustained ignition, developing materials suitable for the fusion environment, sustainability of fusion fuel and power plant materials, development of high efficiency energy conversion and fuel processing technologies, and ensuring that fusion power plants operate safely and do not pose burden to future generations. Some of these goals will be difficult to achieve and will take perseverance, but ultimately the nuclear fusion will become a sustainable energy source.

Acknowledgments

The author wishes to thank the editor of the Kirk-Othmer Encyclopedia for the invitation to contribute an article on fusion energy, and an anonymous reviewer for critical comments.

BIBLIOGRAPHY

"Fusion Energy" in *ECT* 4th ed., Vol. 12, pp. 282–298, by W. R. Ellis; published online: Dec. 4, 2000.

CITED PUBLICATIONS

1. Human Development Report 2007/2008. United Nations Development Programme, New York, 2007.
2. Annual Energy Outlook 2015 with Projections to 2040. U. S. Energy International Administration, Department of Energy, Washington, D. C., 2015.

3. IPCC Climate Change 2014: Synthesis Report. Contribution of Working Groups I, II and III to the Fifth Assessment Report of the Intergovernmental Panel on Climate Change. IPCC, Geneva, 2014.
4. J. R. Lamarsh, *Introduction to Nuclear Engineering*, Addison-Wesley Publishing Company, 1980.
5. S. Ansolabehere, J. Deutch, M. Driscoll, and co-workers, *The Future of Nuclear Power*, MIT Press, Cambridge, 2003.
6. H. Caldicott, *Crisis Without End*, The New Press, New York, 2013.
7. F. Dobran, Energy Supply Options For Climate Change Mitigation and Sustainable Development. In *XXI World Energy Congress*, Curran Associates, Montreal, www.proceedings.cpm, 2010.
8. F. Dobran, Sustainability Attributes and Their Implementation in Energy Resources Utilization. In *ASME 5th International Conference on Energy Sustainability & 9th Fuel Cell Science, Engineering and Technology Conference*. Paper ESFuelCell2011, 7–10 August 2011, Washington, D.C., 2011.
9. F. F. Chen, *An Indispensable Truth*, Springer, New York, 2011.
10. J. M. Dawson, *Advanced Fusion Reactors*. In E. Teller, ed., *Fusion* Vol. **1**, Academic Press, New York, 1981, pp. 453–501.
11. S. Atzeni and J. Meyer-Ter-Vehn, *The Physics of Inertial Fusion*, Oxford University Press, Oxford, 2009.
12. T. Nakagawa, H. Kawasaki, and K. Shibata, Curves and Tables of Neutron Cross Section in JENDL-3.3 Parts I and II. Japan Atomic Energy Research Institute, Fukushima. 2002.
13. A. A. Harms, K. F. Schoept, G. H. Miley, and D. R. Kingdon, *Principles of Fusion Energy*, World Scientific, Singapore, 2000.
14. D. G. Jacobs, Sources of Tritium and its Behaviour Upon Release to the Environment. U.S. Atomic Energy Commission, 1968.
15. M. Kikuchi, *Energies* **3**, 1741–1789 (2010).
16. F. Najmabadi, R. W. Conn, and the ARIES Team, The ARIES-III D-^{3}He Tokamak Reactor Study. IEEE Explore DOI: 10.1109/FUSION.1991.218914. In *14th Symposium on Fusion Engineering*, September 30– October 3, 1991, San Diego, 1992.
17. F. F. Chen, *Introduction to Plasma Physics and Controlled Fusion*, Springer, New York, 2016.
18. H. A. Bethe, *Phys. Rev.* **55**, 434–456 (1939).
19. L. Spitzer Jr., *Phys. Fluids* **1**, 253–264 (1958).
20. D. Meade, *Nucl. Fusion* **50**, 014004 (14pp) (2010).
21. J. D. Lawson, *Proc. Phys. Soc., Sect. B* **70**, 6–10 (1957).
22. T. C. Hender, J. C. Wesley, J. Bialek, and co-workers, *Nucl. Fusion* **47**, S128–S202 (2007).
23. Wikipedia, Plasma Stability. Available at https://en.wikipedia.org/wiki/Plasma_stability. Accessed January 15, 2017.
24. M. Greenwald, *Plasma Phys. Control. Fusion* **44**, R27–R80 (2002).
25. P. Helander, C. D Beidler, T. M. Bird, and co-workers, *Plasma Phys. Control. Fusion* **54**, 124009 (12pp) (2012).
26. P. C. De Vries, M. F. Johnson, B. Alper, and co-workers, Survey Into the Occurrence of Disruptions and Their Root Causes at JET. *23rd IAEA Fusion Energy Conference,* Daejon, Republic of Korea, 10–16 October, 2010.
27. S. A. Sabbagh, N. Commaux, N. Eidietis, and co-workers, Critical Need for Disruption Prediction, Avoidance, and Mitigation in Tokamaks. *2014 FESAC Meeting*, 9 July, Gaithersburg. Available at https://www.burningplasma.org/resources/ref/fspp/whitepapers/FESAC-SPpaperInitiatives-Sabbagh-v12.pdf. Accessed 6 January 2017, 2014.

28. M. Kikuchi, M. Azumi, S. Tsuji, and co-workers, *Nucl. Fusion* **30**, 343–355 (1990).
29. F. Wagner, G. Becker, K. Behringer, and co-workers, *Phys. Rev. Lett.* **49**, 1408–1412 (1982).
30. K. Greenwald, G. Gwinn, S. Milora, and co-workers, *Phys. Rev. Lett.* **53**, 352–355 (1984).
31. C. Gormezano, Y. F. Baranov, and C. D. Challis, *Phys. Rev. Lett.* **80**, 5544 (4pp) (1998).
32. A. Gibson, and the JET Team, *Phys. Plasmas* **5**, 1839–1847 (1998).
33. M. Watkins, and JET Team, *Nucl. Fusion* **39**, 1227–1244 (1999).
34. K. M. McGuire, C. W. Barnes, S. Baths, and co-workers, Physics of High Performance Dueterium-Tritium Plasmas in TFTR. In *Sixteenth IAEA Fusion Energy Conference*. Paper IAEA-F1-CN-64/01-2, October 7–11, Montreal, 1996.
35. A. Iiyoshi, A. Komori, A. Ejiri, and co-workers, *Nucl. Fusion* **39**, 1245. (1999).
36. Summary of the ITER Final Design. Report G A0 FDR 4 01-06-28 R 0.2. Available at http://fire.pppl.gov/iter_summary_FDR2001.pdf. Accessed April 4, 2001.
37. H. Kishimoto, S. Ishida, M. Kikuchi, and H. Ninomiya, *Nucl. Fusion*, **45**, 986–1023 (2005).
38. H.-S. Bosch, R. C. Wolf, T. Andreeva, and co-workers, *Nucl. Fusion* **53**, 126001 (2013).
39. N. J. Fisch, *Phys. Rev. Lett.* **41**, 873–876 (1978).
40. S. Ceccuzzi, E. Barbato, A. Cardinali, and co-workers., *Fusion Sci. Technol.* **64**, 748–761 (2013).
41. H. Zusci, K. Nakamura, K. Hanada, and co-workers, *Nucl. Fusion* **45**, S142–S156 (2005).
42. V. K. Gusev, N. N. Bakharev, B. Ya. Ber, and co-workers, *Plasma Phys. Control. Fusion* **58**, 014032 (6pp) (2016).
43. R. L. Miller, and R. A. Krakowski, The Modular Stellarator Fusion Reactor Concept. Los Alamos National Laboratory Report LA-8978-MS, 1981.
44. Large Helical Device Project. National Institute of Fusion Science. Available at http://www.lhd.nifs.ac.jp/en/home/lhd.html. Accessed May 20, 2016.
45. H. Yamada for LHD Experiment Group, *J. Plasma Fusion Res. Ser.* **9**, 1–6 (2010).
46. K. Ida, K. Nagaoka, S. Inagaki, and co-workers, *Nucl. Fusion* **55**, 104018 (10pp) (2015).
47. Introduction – the Wendelstein 7-X stellarator. Max Planck Institute of Plasma Physics. Available at http://www.ipp.mpg.de/16931/einfuehrung. Accessed May 20, 2016.
48. R. Stadler, A. Vorkoper, J. Boscary, and co-workers, *Fusion Eng. Des.* **84**, 305–308 (2009).
49. Wendelstein 7-X fusion device produces its first hydrogen plasma. Max Planck Institute of Plasma Physics. Available at http://www.ipp.mpg.de/4010154/02_16. Accessed May 20, 2016.
50. *An Assessment of the Prospects for Inertial Fusion Energy*, The National Research Council of the National Academies, The National Academies Press, Washington, DC, 2013.
51. *Physics Today*, (This issues contains a series of articles discussing the development of thermonuclear weapons in Soviet Union and United States.) November, 1996.
52. J. J. Duderstadt and G. A. Moses, *Inertial Confinement Fusion*, John Wiley & Sons, Inc, New York, 1982.
53. R. E. Kidder, *SPIE Proc*. **3343**, 10–33, 1998. In *High-Power Laser Ablation*, ed. C. R. Phipps. Also, Lawrence Livermore National Laboratory Report No. UCRL-BOOK-222681, July 2006.
54. The Laser at 50, Physics World, May, 2010.
55. N. G. Basov, V. A. Boiko, S. M. Zakharov, and co-workers., *JETP Lett*. **13**, 489–491 (1971).

56. G. Velarde, E. Minguez, and J. M. Parlado, Laser Interaction With Matter. *Proc. of the 19th ECLIM*, Madrid, October 3–7, 1988. World Scientific Publishers, Singapore, 1989.
57. J. Lindl, *Phys. Plasmas* **2**, 3933–4024 (1995).
58. M. L. Andrè, *Fusion Eng. Des.* **44**, 43–49 (1999).
59. J. A. Paisner, W. H. Lowdermilk, J. D. Boyes, and co-workers., *Fusion Eng. Des.* **44**, 23–33 (1999).
60. J. F. Holzrichter, Lasers and Inertial Fusion Experiments at Livermore. Lawrence Livermore Laboratory Report UCRL-BOOK-218519, 2006.
61. C. Danson, D. Hillier, N. Hopps, and co-workers, *High Power Laser Sci. Eng.* **3**, e3, 14 pp (2015).
62. NIF, Lawrence Livermore National Laboratory Web site. Available at https//lasers.llnl.gov, 2016.
63. D. J. Strozzi, D. S. Bailey, P. Michel, and co-workers, *Phys. Rev. Lett.* **118**, 025002 (2017).
64. Sandia National Laboratories, About Z. Available at http://www.sandia.gov/z-machine/about_z/. Accessed 23 January 2017, 2017.
65. *Assessment of Inertial Confinement Fusion Targets*, The National Research Council of the National Academies, The National Academies Press, Washington, D.C., 2013.
66. S. Atzeni, Inertial confinement fusion with advanced ignition schemes: Fast ignition and shock ignition. *68th Scotish University Summer-School in Physics. NATO Advanced Study Institute*. University of Strathclyde, August 14–26, Glasgow. Available at http://gaps.ing2.uniroma1.it/~atzeni/Presentations/Atzeni-SUSSP68_lectures_1and_2_rev1.pdf Accessed April 26, 2016, 2011.
67. G. A. Mourou, P. J. Barty, and M. D. Perry, Ultrahigh-Intensity Lasers: Physics of the Extreme on a Table Top, Physics Today, January, 22–28, 1998.
68. R. Kodama, H. Shiraga, K. Shigemori, and co-workers, *Nature* **418**, 933–934 (2002).
69. R. Betti, C. D. Zhou, K. S. Anderson, and co-workers, *Phys. Rev. Lett.* **98**, 155001 (2007).
70. A. J. Schmitt, J. W. Bates, S. P. Obenschain, and co-workers, *Phys. Plasmas* **17**, 042701 (14pp) (2010).
71. J. P. Chittenden, The Z-Pinch Approach to Fusion, Physics World 13, May, 2000.
72. C. Olson, G. Rochau, S. Slutz, and co-workers, *Fusion Sci. Technol.* **47**, 633–640 (2005).
73. J. T. Cook, G. E. Rochau, B. B. Cipiti, and co-workers, Z-Inertial Fusion Energy: Power Plant Final Report FY 2006, Sandia National Laboratories Report SAND206-7148, 2006.
74. The Magnetically Driven Direct Drive Approach to Ignition: Responses to Questions by Panel 1 of the FY15 ICF Program Review. Sandia National Laboratories Report SAND2015-6173R, 2015.
75. M. R. Gomez, S. A. Slutz, A. B. Sefkow, and co-workers, *Phys. Rev. Lett.* **113**, 155003 (5pp) (2014).
76. G. A. Wurden, Realizing Technologies for Magnetized Target Fusion. Presented at *20th TOFE 2012*, Nashville, 2011.
77. J. D. Sethian, J. D. Colombant, J. Giulian Jr., and co-workers, *IEEE Trans. Plasma Sci.* **38**, 690–703 (2010).
78. D. Goodin, Target Fabrication and Injection Challenges in Developing an IFE Reactor. Presented to the National Research Council of the National Academies during Review on Prospects for Inertial Confinement Fusion Energy Systems, 29 January 2011, San Ramon.
79. T. M. Anklam, M. Dunne, W. R. Meier, and co-workers, *Fusion Sci. Technol.* **60**, 66–71 (2011).

80. H. Injeyan, and G. D. Goodno, *High-Power Laser Handbook*, McGraw Hill, New York, 2011.
81. J-L. Miquel, C. Lion, and P. Viviani, *J. Phys. Conf. Ser.* **688**, 012067 (2016).
82. LLE Review Quarterly Report. University of Rochester Laboratory for Laser Energetics, Vol. 146, DOE/NA/1944-1264, 2016.
83. National Ignition Campaign Program Completion Report. Lawrence Livermore National Laboratory Report LLNL-TR-637982, September 30, 2012.
84. E. I. Moses, *Fusion Sci. Technol.* **60**, 11–16 (2011).
85. A. Bayramian, S. Aceves, T. Anklam, and co-workers, *Fusion Sci. Technol.* **60**, 28–48 (2011).
86. M. F. Wolford, J. D. Sethian, M. C. Myers, and co-workers, *Plasma Fusion Res. Regul. Articles* **8**, 3404044 (5pp) (2013).
87. K. Ueda, J. F. Bisson, H. Yagi, and co-workers, *Laser Phys*. **15**, 927–938 (2005).
88. R. Feeler, and E. Stephens, High-Density Pulsed Laser Diode Arrays for SSL Pumping. Northrop Grumman Cutting Edge Optronics Application Note #15, 2010.
89. S. Kawata, T. Karino, and A. I. Ogoyski, *Matter Radiat. Extrem.* **1**, 89–113 (2016).
90. A. Friedman, J. J. Barnard, I. Kaganovich, and co-workers, Heavy Ion Inertial Fusion Energy: Summaries of Program Elements. Lawrence Livermore National Laboratory Report LLNL-TR-471817, 2011.
91. W. Sawan, L. El-Guebaly, and P. Wilson, *Fusion Sci. Technol.* **52**, 763–770 (2007).
92. M. Cuneo, Magnetically Driven Platforms and Applications. Presented at HEDP Summer School, July 15–19, 2013.
93. International Fusion Materials Irradiation Facility, http://www.ifmif.org, 2016.
94. J. Knaster, F. Arbeilter, P. Cara, and co-workers, *Nucl. Mater. Energy* **000**, 1–9 (2016).
95. R. Hiwatari, K. Okano, Y. Asaoka, and co-workers, *Nucl. Fusion* **45**, 96–109 (2005).
96. ITER Technical Basis: ITER EDA Documentation Series No. 24. International Atomic Energy Agency, Vienna. Available at http://www.iter.org, 2002.
97. K. Ikeda, *Nucl. Fusion* **50**, 014002 (10pp) (2010).
98. D. Maisonnier, *Fusion Eng. Des.* **83**, 858–864 (2008).
99. E. Romanelli, Fusion Electricity: A Roadmap for the Realization of Fusion Energy. European Fusion Development Agreement Report EFDA, November, 2012.
100. G. Federici, R. Kemp, D. Ward, and co-workers, *Fusion Eng. Des.* **89**, 882–889 (2014).
101. G. Federici, C. Bachmann, W. Biel, and co-workers, *Fusion Eng. Des.* **109–111**, Part B, 1464–1474 (2016).
102. C. D. Beidler, E. Harmeyer, F. Hernegger, and co-workers, The Helias Reactor HSR4/18. Max Planck Institute of Plasma Physics Report IPP III/268, 2001.
103. R. C. Wolf, and the Wendelstein 7-X Team, *Fusion Eng. Des.* **83**, 990–996 (2008).
104. A. Sagara, S. Imagawa, Y. Kozaki, and co-workers, Design Integration of the LHD-Type Energy Reactor FFHR2 Toward DEMO. In *18th International Toki Conference (ITC18) on Development of Physics and Technology of Stellarators / Heliotrons en Route to DEMO*. Paper I33, December 9–12, Ceratopia Toki, 2008.
105. K. Kim, K. Im, H. C. Kim, and co-workers, *Nucl. Fusion* **55**, 053027 (9pp) (2015).
106. Design Concept of Korean Fusion Demonstration Reactor (K-DEMO). Available at https://www-amdis.iaea.org/meetings/AMPMI14/Presentations/AMPMI-2014-12-15-Talk-KKim-KDEMO-2by4.pdf. Accessed May 27, 2016.
107. H. Li, G. Li, L. Qu, and co-workers, Basic Design Consideration of CFETR Fusion Power Stations. In *IEEE International Power Modulator and High Voltage Conference (IPMHVC)*, 632–635, 1–5 June, Santa Fe, 2014.
108. L. Delong, Gaps Analysis in Strategic Research Priorities in Support of DEMO. *45th Fusion Power Coordinating Committee (FPCC)*, January 27, 2016. Available at https://www.iea.org/media/workshops/2016/fpccwebinar/Item_4_CHINA.pdf. Accessed May 27, 2016.

109. F. Najmabadi, and the ARIES Team, *Fusion Eng. Des.* **80**, 3–23 (2006). See also other articles in this ARIES-AT Special Issue of the journal.
110. F. Najmabadi, A. R. Raffray, and the ARIES-CS TEAM, *Fusion Sci. Technol.* **54**, 655–672 (2008).
111. W. R. Meier, R. L. Bieri, M. J. Monsler, and co-workers, Osiris and Sombrero Inertial Fusion Power Plant Designs. U.S. Department of Energy Report DOE/ER/54100/1, 1992.
112. A. R. Raffray, J. Blanchard, J. Latkowski, and co-workers, *Fusion Eng. Des.* **81**, 1627–1638 (2006).
113. R. W. Moir, R. L. Bieri, X. M. Chen, and co-workers, *Fusion Technol*. **25**, 5–23 (1994).
114. S. S. Yu, W. R. Meier, R. P. Abbott, and co-workers, *Fusion Sci. Technol.* **44**, 266–273 (2003).
115. T. Norimatsu, Fast Ignition Laser Fusion Reactor KOYO-F – Summary from Design Committee of FI Laser Fusion Reactor. Institute of Laser Engineering, Osaka University. Presentred at U.S.-Japan workshop on Power Plant Studies and related Advanced Technologies with EU participation. Available at http://www-ferp.ucsd.edu/LIB/MEETINGS/0601-USJ-PPS/Norimatsu.pdf. Accessed July 17, 2016, 2005.
116. T. Norimatsu, Y. Kozaki, N. Miyanaga, and co-workers, Conceptual Design of Laser Fusion Reactor KOYO-F Based on Fast Ignition Scheme. In *Proc. of 21st IAEA Conference*. Paper FT/P5-39, 16–21 October, Chengdu, 2006.
117. W. R. Meier, R. C. Schmitt, R. P. Abbott, and co-workers, *Fusion Eng. Des.* **81**, 1661–1666 (2006).
118. D. Clery and A. Cho, *Science* **352**, 636–637 (2016).
119. G. Federici, C. H. Skinner, J. N. Brooks, and co-workers, *Nucl. Fusion* **41**, 1967–2137 (2001).
120. G. Federici, H. Wuerz, G. Janeschitz, and co-workers, *Fusion Eng. Des.* **61–62**, 81–94 (2002).
121. J. Linke, *Fusion Sci. Technol.* **49**, 455–464 (2006).
122. J. Roth, E. Tsitrone, A. Loarte, and co-workers, *J. Nucl. Mater.* **390-191**, 1–9 (2009).
123. ITER, Design Review for Tungsten Divertor Shows Way Ahead. Available at http://www.iter.org/newsline/274/1639. Accessed 21 January 2017, 2013.
124. Y. Igitkhanov, B. Bazylev, and R. Fetzer, The Quantification of the Key Physics Parameters for the DEMO Fusion Power Reactor and Analysis of the Reactor Relevant Physics Issues. KIT Scientific Report KIT-SR-7661, Karlsruhe Institute of Technology, Karlsruhe, 2014.
125. Development of Radiation Resistant Reactor Core Structural Materials – NTR2007 Supplement. *51st IAEA General Conference*. International Atomic Energy Agency Report, Vienna. Available at https://www.iaea.org/About/Policy/GC/GC51/GC51InfDocuments/English/gc51inf-3-att7_en.pdf, 2007.
126. U. Fischer, C. Bachmannb, J.-C. Jaboulay, and co-workers, *Fusion Eng. Des.* **109–111**, Part B, 1458–1463 (2016).
127. M. R. Gilbert, S. L. Dudarev, S. Zheng, and co-workers, *Nucl. Fusion* **52**, 083019 (12pp) (2012).
128. S. J. Zinkle, *Phys. Plasmas* **12**, 058101, 1–8 (2005).
129. A. K. Suri, N. Krishnamurthy, and I. S. Batra, *J. Phys. Conf. Ser.* **2008**, 012001, 1–16 (2010).
130. F. Dobran, *Prog. Nucl. Energy* **60**, 89–116 (2012).
131. M. Klimiankou, R. Lindau, and A. Moslang, *J. Cryst. Growth* **249**, 381–387 (2003).
132. M. R. Gilbert, and J. Ch. Sublet, Scoping of Material Response Under DEMO Neutron Irradiation: Comparison with Fission and Influence of Nuclear Library Selection. arXiv:1604.08496v1 [cond-mat.mtrl.sci]. Accessed April 27, 2016.
133. S. J. Zinkle, and N. M. Ghoniem, *Fusion Eng. Des.* **51–52**, 55–71 (2000).

134. M. Abdou, Overview of the Principles and Challenges of Fusion Nuclear Technology. Available at http://www.fusion.ucla.edu/abdou, 2007.
135. P. Norajitra, R. Giniyatulin, T. Ihli, and co-workers, *Nucl. Fusion* **45**, 1271–1276 (2005).
136. W. M. Stacey, *Fusion: An Introduction to the Physics and Technology of Magnetic Confinement Fusion*, Wiley-VCH Verlag GmbH, Weinheim, 2010.
137. V. A. Evtikhin, I. E. Lyublinski, A. V. Vertkov, and co-workers, *Fusion Eng. Des.* **49–50**, 195–199 (2000).
138. V. Barabash, and the ITER International Team, *J. Nucl. Mater.* **367–370**, 21–32 (2007).
139. D. K. Sze, and A. Hassanein, *Fusion Eng.* **1**, 169–172 (1993).
140. C. P. C. Wong, C. B. Baxi, C. J. Hamilton, and co-workers, Helium-Cooling in Fusion Power Plants. General Atomics Report GA-A21804, 1994.
141. Molten Salt Coolants for High Temperature Reactors. Internship Report NENP-TDS/INPRO. International Atomic Energy Agency, Vienna, 2009.
142. J. C. Farmer, LIFE Materials: Overview of Fuels and Structural Materials Issues Volume 1. Lawrence Livermore National Laboratory Report LLNL-TR-407386-Rev.1. 2008,
143. L. A. El-Guebaly, in S. B. Krivit, J. H. Lehr, and T. B. Kingery, eds., *Nuclear Energy Encyclopedia: Science, Technology, and Applications*, John Wiley & Sons, Inc, New York, 2011.
144. D. Maisonnier, I. Cook, P. Sardain, and co-workers, A Conceptual Study of Commercial Fusion Power Plants. European Fusion Development Agreement Report EFDA-RP-RE-5.0. Available at http://www.efda.org/eu_fusion_programme/downloads/scientific_and_technical_publications/PPCS_overall_report_final.pdf. Accessed 22 March 2011, 2005.
145. F. Najmabadi, and the ARIES Team, *Fusion Eng. Des.* **65**, 143–164 (2003).
146. M. Katsurai, and M. Yamada, *Nucl. Fusion* **22**, 1407–1419 (1982).
147. R. W. Moir, R. H. Bulmer, T. K. Fowler, and co-workers, *Fusion Sci. Technol.* **44**, 317–326 (2003).
148. M. Abdou, N. B. Morley, S. Smolentsev, and co-workers, *Fusion Eng. Des.* **100**, 2–43 (2015).
149. L. V. Boccaccini, G. Aiello, J. Aubert, and co-workers, *Fusion Eng. Des. Part B* **109–111**, 1199–1206 (2016).
150. F. Najmabadi, N. M. Ghoniem, R. W. Conn, and co-workers, The TITAN Reversed-Field Pinch Fusion Reactor Study. University of California Los Angeles Report UCLA-PPG-1100, 1987.
151. I. Pieli, Nuclear Fusion Programme: Annual Report of the Association Karlsruhe Institute of Technology/EURATOM January 2013–December 2013, Report KIT-SR-7671. KIT Scientific Publishing, Karlsruhe, 2015.
152. M. Abdou, Challenges and Development Pathways for Fusion Nuclear Science and Technology. Seminar at Seoul National University. 25 November, Seoul, 2009.
153. Opportunities in the Fusion Energy Sciences Program. Appendix C. Office of Science of the U.S. Department of Energy, Washington, D.C., 1999.
154. J. F. Latkowski, R. P. Abott, S. Aceves, and co-workers, *Fusion Sci. Technol.* **60**, 54–60 (2011).
155. M. Dunne, E. I. Moses, P. Amendt, and co-workers, *Fusion Sci. Technol.* **60**, 19–27 (2011).
156. J. Lindl, O. Landen, J. Edwards, and co-workers, *Phys. Plasma.* **21**, 020501 (2014). (Erratum to the article: Review of the National Ignition Campaign 2009–2012. Lawrence Livermore National Laboratory Report LLNL-JRNL-664180, 11 November.)
157. D. Batani, M. Koenig, S. Baton, and co-workers, *Plasma Phys. Control. Fusion* **53**, 124041 (13pp). (2011).

158. HiPER Preparatory Phase Study. Final Report, December 1. Available at http://www.hiper-laser.org/Resources/HiPER_Preparatory_Phase_Completion_Report.pdf. Accessed July 18, 2016, 2013.
159. W. R. Meier, Liquid Wall Chambers. Lawrence Livermore National Laboratory Report LLNL-TR-471596, February 25, 2011.
160. N. Taylor, D. Baker, S. Cittaglia, and co-workers, *Fusion Eng. Des.* **86**, 619–622 (2011).
161. V. H. Reis, R. J. Hanrahan, and W. K. Levedagl, The Big Science of the Stockpile Stewardship. Physics Today, August, 47–53, 2016.
162. B. M. Andreev, *Sep. Sci. Technol.* **36**, 1949–1989 (2001).
163. Mineral Commodity Summaries 2016. U.S. Department of Interior, U.S. Geological Survey, Reston, 2016.
164. A. M. Bradshaw, B. Reuter, and T. Hamacher, *Green* **3**, 93–111 (23pp) (2013).
165. A. M. Bradshaw, B. Reuter, and T. Hamacher, *EPJ Web Conf.* **98**, 04007 (2015).
166. S. Mohr, and J. Ward, *Minerals* **4**, 130–144 (2014).
167. S. J. Piet, S. J. Brereton, J. M. Perlado, and co-workers, Overview of Safety and Environmental Issues for Inertial Fusion Energy. In IAEA Technical Committee Meeting on Developments in Fusion Safety. Paper CONF-9610240-3, Naka. Also, Idaho National Engineering Laboratory Report INEL-96/00285, 1996.
168. I. Cook, G. Marbach, L. Di Pace, and co-workers, Safety and Environmental Impact of Fusion. European Fusion Development Agreement Report EFDA-S-RE-1, 2001.
169. L. El-Guebaly, V. Massaut, K. Tobita, and L. Cadwallader, Evaluation of Recent Scenarios for Managing Fusion Activated Materials: Recycling and Clearance, Avoiding Disposal. Fusion Technology Institute University of Wisconsin Report UWFDM-1333, Madison, 2008.
170. Radiological Assessments for Clearance of Materials from Nuclear Facilities. Nuclear Regulatory Commission Report NUREG-1640. Washington, D.C. Available at http://www.nrc.gov/reading-rm/doccollections/nuregs/staff/sr1640/, 2003.
171. Application of the Concepts of Exclusion, Exemption and Clearance. Safety Standards Series, International Atomic Energy Agency Report RS-G-1.7, Vienna. Available at http://wwwpub.iaea.org/MTCD/publications/PDF/Pub1202_web.pdf, 2004.
172. Research Needs for Fusion-Fission Hybrid Systems. U.S. Department of Energy Report of the Research Needs Workshop (ReNeW), 30 September–2 October, Gaithersburg, 2009.